

AD-A100 755

COLUMBIA RADIATION LAB NEW YORK

F/G 20/14

RESEARCH INVESTIGATION DIRECTED TOWARD EXTENDING THE USEFUL RAN--ETC(U)

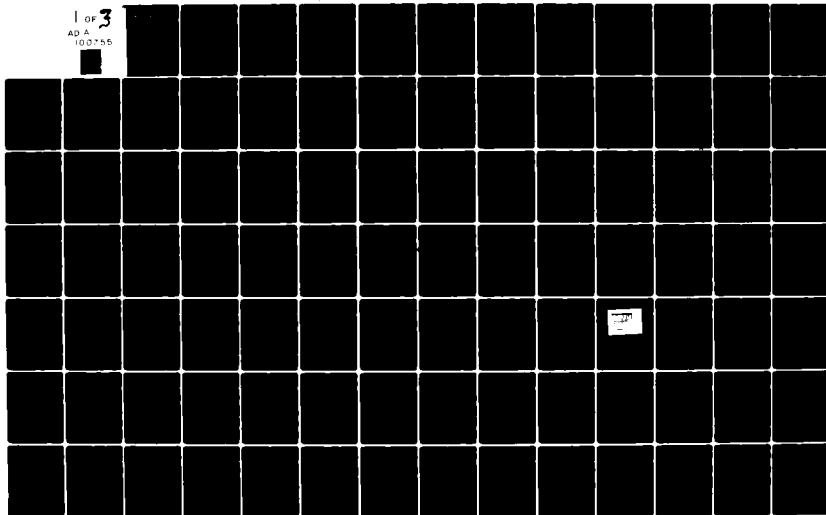
MAR 81 G W FLYNN

DAA629-79-C-0079

NL

UNCLASSIFIED

1 of 3
AD A
100755



AD A100755



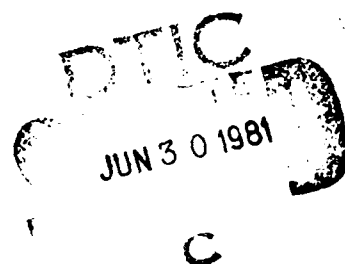
LEVEL 11

COLUMBIA UNIVERSITY

DEPARTMENTS OF PHYSICS,
CHEMISTRY, ELECTRICAL ENGINEERING

■ PROGRESS REPORT NO. 31

April 1, 1980 - March 31, 1981



CONTRACT DAAG29-79-C-0079

APPROVED FOR PUBLIC RELEASE: DISTRIBUTION UNLIMITED

To:

THE JOINT SERVICES TECHNICAL ADVISORY COMMITTEE

REPRESENTING: THE U.S. ARMY ELECTRONICS COMMAND
THE U.S. ARMY RESEARCH OFFICE
THE OFFICE OF NAVAL RESEARCH
THE AIR FORCE OFFICE OF SCIENTIFIC RESEARCH

COLUMBIA RADIATION LABORATORY, NEW YORK, NEW YORK 10027

■ March 31, 1981

DMC FILE COPY

81 06 29 119

COLUMBIA RADIATION LABORATORY

RESEARCH INVESTIGATION DIRECTED TOWARD
EXTENDING THE USEFUL RANGE OF THE
ELECTROMAGNETIC SPECTRUM

Progress Report No. 31

April 1, 1980 through March 31, 1981

Contract DAAG29-79-C-0079

Object of the Research:

Basic research in the fields of quantum electronics; electromagnetic propagation, detection and sensing; and solid state electronics.

The research reported in this document was made possible through support extended the Columbia Radiation Laboratory, Columbia University, by the Joint Services Electronics Program (U. S. Army Electronics Command and U. S. Army Research Office, Office of Naval Research, and the Air Force Office of Scientific Research) under Contract DAAG29-79-C-0079.

Submitted by: G. W. Flynn, Director

Coordinated by: P. A. Pohlman, Administrative Assistant

COLUMBIA UNIVERSITY

Division of Government-Aided Research

New York, New York 10027

March 31, 1981

Approved for public release; distribution unlimited.

The research reported in this document was made possible through support extended the Columbia Radiation Laboratory, Columbia University by the Joint Services Electronics Program (U. S. Army Electronics Command and U. S. Army Research Office, Office of Naval Research, and the Air Force Office of Scientific Research) under Contract DAAG29-79-C-0079.

Portions of this work were also supported by:

Air Force Office of Scientific Research

Grant AFOSR-77-3407B

Grant AFOSR-79-0082

Grant AFOSR-81-0009

Army Research Office

Grant DAAG29-80-C-0043

National Science Foundation

Grant NSF-CHE 77-11384

Grant NSF-CHE 77-24343

Grant NSF-ENG 78-26498

Grant NSF-ENG 78-19426

Grant NSF-CHE 79-23291

Grant NSF-DMR 80-06966

Office of Naval Research

Contract N00014-78-C-0517

Naval Air Development Center

Department of Energy

Contract DE-AS02-ER-78-S-02-4940

Contract DOE/SERI xz-φ-9226

Jet Propulsion Laboratory
California Institute of Technology

Contract 955335

Contract 955336

The support of these agencies is acknowledged in footnotes in the text.

Unclassified

SECURITY CLASSIFICATION OF THIS PAGE (When Data Entered)

REPORT DOCUMENTATION PAGE		READ INSTRUCTIONS BEFORE COMPLETING FORM
1. REPORT NUMBER Progress Report No. 31	2. GOVT ACCESSION NO. AD-A100 755	3. RECIPIENT'S CATALOG NUMBER
4. TITLE (and Subtitle) RESEARCH INVESTIGATION DIRECTED TOWARD EXTENDING THE USEFUL RANGE OF THE ELECTROMAGNETIC SPECTRUM.	5. TYPE OF REPORT & PERIOD COVERED 1 April 1980 - 31 March 1981	
7. AUTHOR(s) George W. Flynn	6. PERFORMING ORG. REPORT NUMBER 31	
9. PERFORMING ORGANIZATION NAME AND ADDRESS Columbia Radiation Laboratory Columbia University New York, New York 10027	8. CONTRACT OR GRANT NUMBER(s) DAAG29-79-C-0079	
11. CONTROLLING OFFICE NAME AND ADDRESS Department of the Army U. S. Army Research Office Research Triangle Park, NC 27709	10. PROGRAM ELEMENT, PROJECT, TASK AREA & WORK UNIT NUMBERS 1L161102BH57-03	
14. MONITORING AGENCY NAME & ADDRESS (if different from Controlling Office)	12. REPORT DATE 31 March 1981	
	13. NUMBER OF PAGES 171	
	15. SECURITY CLASS. (of this report) Unclassified	
	15a. DECLASSIFICATION/DOWNGRADING SCHEDULE	
16. DISTRIBUTION STATEMENT (of this Report) Approved for public release; distribution unlimited.		
17. DISTRIBUTION STATEMENT (of the abstract entered in Block 20, if different from Report)		
18. SUPPLEMENTARY NOTES Portions of this work were also supported by the Air Force Office of Scientific Research, the Army Research Office, the National Science Foundation, the Office of Naval Research, the Naval Air Development Center, and the Department of Energy.		
19. KEY WORDS (Continue on reverse side if necessary and identify by block number) Coherent detection Heterodyne detection Infrared detection Infrared sensing Photon counting Continued on page vii		
20. ABSTRACT (Continue on reverse side if necessary and identify by block number) We briefly review the history of heterodyne detection from the radiowave to the optical regions of the electromagnetic spectrum, and then focus on the submillimeter/far-infrared by investigating the transition from electric-field to photon-absorption detection in a simple system. The response of an isolated two-level detector to a coherent source of incident radiation is calculated for both heterodyne and video detection. When the processes of photon absorption and photon emission cannot be distinguished, the relative		

DD FORM 1 JAN 73 1473 EDITION OF 1 NOV 65 IS OBSOLETE

Unclassified
SECURITY CLASSIFICATION OF THIS PAGE (When Data Entered)

Unclassified

SECURITY CLASSIFICATION OF THIS PAGE (When Data Entered)

Block 20 continued - Abstract

detected power at double- and sum-frequencies is found to be multiplied by a coefficient, which is less than or equal to unity, and which depends on the incident photon energy and on the effective temperature of the system.

The Neyman Type A and Thomas counting distributions provide a good description for the counting of photons generated by multiplied Poisson processes, if the time course of the multiplication is short in comparison with the counting time. We have obtained analytic expressions for the probability distributions, moment generating functions, moments and variance-to-mean ratios. Sums of Neyman Type-A and Thomas random variables have been shown to retain their form under the constraint of constant multiplication parameter. The doubly stochastic Neyman Type-A, Thomas and fixed multiplicative Poisson distributions have also been considered. Applications include the photon-counting scintillation detection of nuclear particles when the particle flux is low, the photon-counting detection of weak optical signals in ionizing radiation, and the design of star-scanner spacecraft guidance systems. Conditions under which the Neyman Type-A and Thomas converge in distribution to the fixed multiplied Poisson and to the Gaussian have been determined. This latter result allows approximate solution of the related detection and estimation problems. A more exact characterization of these systems is provided by a new generalized performance parameter for systems with arbitrary counting statistics. It was shown explicitly that this parameter varies monotonically with system performance whereas the signal-to-noise ratio does not. The analysis, which utilizes normalizing transforms is also useful in the direct calculation of the Bayes risk, probability of error, and system sensitivity. A technique for evaluating system performance directly from photocounting cumulants was also derived. It is most useful in situations where exact, closed form, explicit solutions exist for the cumulants, but not for the distribution, such as in the general case of communication through atmospheric turbulence.

General expressions are obtained for the mean and variance of the number of events in a fixed but arbitrary sampling time for a nonparalyzable dead-time counter. The input is assumed to be a Poisson point process whose rate is a stochastic process, and the dead time is assumed to be small in comparison with the fluctuation time of the driving process. The mean is shown to depend only on the first-order statistics of the rate, whereas the variance is formally shown to depend on both the first- and the second-order statistics of the rate. For the particular process arising in the detection of chaotic light, an explicit expression is obtained for the dependence of the dead-time-modified variance on the power spectrum of the radiation. It is demonstrated that the variance takes on a particularly simple form for chaotic light with Lorentzian and Gaussian spectra. In the region in which our study is valid, it turns out that the dead-time dependence of the variance is contained in a multiplicative function that is essentially independent of the spectral properties of the light.

Current suppression in $\text{Al}_{0.35}\text{Ga}_{0.65}\text{As-GaAs}$ N-p heterojunctions is observed experimentally. The data are explained by examining the carrier transport modified by electron accumulation in the interface potential notch resulting from the conduction-band discontinuity. In addition, it is found that the temperature dependent I-V measurements can be used to deduce the magnitude of ΔE_c at the junction interface.

Unclassified

SECURITY CLASSIFICATION OF THIS PAGE (When Data Entered)

Block 20 continued - Abstract

A new method has been developed to form a p^+-n polycrystalline-crystalline junction at a low temperature. The technique involves the use of an E-beam evaporated polysilicon-aluminum-polysilicon multi-layer structure to obtain an Al-rich polycrystalline film by heat treatment at 600°C. Experimental evidence indicates that the current conduction is dominated by electron recombination at the interface between the polysilicon and the substrate. The best fit between a simple model and experimental data yields an effective recombination velocity of 5×10^4 cm/sec, a value consistent with carrier recombination at the grain boundaries of polycrystalline silicon.

A Schottky barrier is fabricated with a silicon-aluminum-silicon structure by the irradiation of either a pulsed or cw laser. The completed diodes have a large barrier height (1 eV) and good rectifying properties.

Thermoluminescent (the glow curve) and phosphorescent decay experiments have been performed for a range of manganese activated zinc silicate phosphors. It is observed that the phosphorescent decay time is a non-monotonic function of temperature when the light output is contributed simultaneously by two energetically adjacent traps. By representing the decay curve with exponential terms, the calculated trap depths can be correlated with the data obtained from the glow-curve experiment. Thus, the apparent contradiction between the relative insensitivity of the decay time with respect to temperature and the thermal activation of traps can be reconciled. In isolated traps, the decay time is always a monotonic function of temperature although the decay curve may not be exponential.

The dependence on the energy and electric field of Si-SiO₂ interface state capture cross sections has been measured for Al-SiO₂-nSi structures with an oxide thickness ≈ 800 Å. The capture cross section for holes, σ_p , has been observed to be several orders of magnitude larger than that for electron, σ_n , and further it has been observed to show a strong dependence on energy in the upper half of the silicon energy gap. This apparent dependence of σ_p on energy has been shown to arise primarily from a dependence on the electric field at the semiconductor surface. For the same electric field, interface states at different energies in the gap are observed to have very nearly the same magnitude of capture cross section.

The minimum dimensions of bipolar transistors with ion implanted impurity profiles for predictable device and system behavior is calculated on the basis of limitations arising from the random positions of the implanted impurities. Doubly-stochastic effects arising from uncertainty in exact implantation parameters are considered. For a chip yield of 99%, the minimum emitter size is of the order of $1 \lesssim L \lesssim 5$ μ m when a straightforward scaling theory is applied to dimensions and impurity concentrations from present device designs and a parity check on a bit word is applied.

We have determined the mechanism and rate for energy transfer between the ν_2 and ν_4 modes of COF₂. A novel relaxation behavior has been observed

Block 20 continued - Abstract

for this process. Temperature dependent relaxation rates have been determined for vibrational energy transfer in SO_2 . The overall translational-vibrational energy transfer process in oxalyl fluoride has been observed. This molecule, which has a pseudo-quasi-continuum of levels due to internal rotation, is a model for larger molecules which undergo multiquantum infrared absorption.

Collision assisted laser pumping of SF_6 has produced molecular beams with internal energies exceeding $3500 \text{ cm}^{-1}/\text{molecule}$. Such beams are particularly useful in studies of surface chemical reactions and crossed molecular beam reactions.

An excimer laser has been used to produce high velocity Cl atoms via photodissociation. Upon collision with virtually any small molecule, these fast atom fragments cause vibrational excitation of the molecule.

We have discovered several novel features of the dynamic behavior of Br_2 molecules trapped in argon, krypton, and xenon matrices at $10\text{-}30^\circ\text{K}$ when irradiated by a pulsed dye laser. Infrared emission from several electronic states is observed and evidence for $\text{Br}_2\text{-Xe}$ molecular exciplex species has been found.

We have successfully polarized Xe^{129} by spin exchange with optically pumped rubidium. The polarization was detected by adiabatic reversal of the xenon spins, as described in the preceding progress report.

We have discovered that the cesium atoms within our glass sample cells lase continuously on many transitions in the infrared spectral region, e.g. 7P to 6S at 3.095μ and 2.93μ ; 7S to 6P at 1.469μ and 1.359μ ; 7P to 5D at 1.376μ and 1.360μ . The atoms are excited with cw laser radiation at 4593\AA and 4555\AA and the lasing occurs without any feedback mirrors. We believe this is the first reported example of mirrorless cw lasing.

We have completed our studies of the newly discovered infrared absorption bands of dense alkali vapors of Cs, Rb, K and Na. All elements show very similar structure between 1μ and 2μ , structure which may be due to absorption from triplet molecules. Preliminary attempts to observe these bands in fluorescence failed to show any signal.

We have detected strong two photon excitation of rubidium according to the scheme discussed in the previous progress report. Substantial (i.e. 10% to 20%) spin polarization is also detected. However, our analysis of the data is complicated by the occurrence of strong excimer absorption which also leads to spin polarization of a comparable order of magnitude.

Extensive measurements of the magnetic circular dichroism of the CsAr excimer bands and Cs_2 dimer bands have been made during the past year. We have been able to gain for the first time unambiguous information about the angular momentum and angular momentum coupling schemes of the electronic states of excimer molecules.

Block 20 continued - Abstract

We have used spin exchange magnetic resonance spectroscopy to unambiguously identify free hydrogen atoms, free deuterium atoms and free electrons in cells containing mixtures of hydrogen or deuterium and cesium vapor which is optically pumped by the 4593\AA second resonance line of the cesium atom.

The spin destruction rates of sodium in xenon have been measured and found to be even greater than the rates of rubidium in xenon. Van der Waals molecules, NaXe, are also found to play an important role in the relaxation.

The dynamics of photodissociation of diphenyl-diazomethane and energy relaxation in the diphenylcarbene fragment are investigated using picosecond laser methods. The diphenylcarbene singlet-ground triplet equilibrium constant, free energy difference, energy separation, and a maximum value for the carbon-nitrogen bond energy in diphenyldiazomethane are obtained.

A method for determining the dynamics of intramolecular chain motion has been developed which employs the rate of exciplex formation. The kinetics of the end to end motions of the terminal donor and acceptor molecules determines the exciplex formation rate. The decay of the excited acceptor and the rise time of the exciplex emission, following picosecond laser excitation of the acceptor, is used to determine the chain dynamics. The motion is found to be exponential in nonpolar solvents for the molecule A-(CH₂)₃-DMA and is the first experimental observation of the end to end dynamics of short chain molecular motion.

Photoexcitation of extended conformers A-(CH₂)₃-D in the highly polar medium acetonitrile is followed by very rapid electron transfer yielding the solvated ion pair (7 ps). The rapid rate of ion pair formation indicates that there are no strong geometric requirements for this process and furthermore that this electron transfer process occurs directly without passing through an excited CT complex state. This is unlike the strong geometric requirements for excited CT complex formation both in polar and nonpolar media. These studies were carried out using a Nd: phosphate glass picosecond laser for excitation and a streak camera-optical multichannel analyzer for fluorescence detection.

Two-pulse photon echo experiments have been performed in Na and Li vapor which probe the sub-doppler regime of the resonance line. In Li we have made the first observation of the effects of velocity changing collisions in the asymptotic regime where the total scattering cross section obtains. A method for observing echo signals has been developed which exploits the dependence of the echo polarization on the magnetic substates which are excited. A diagrammatic method was developed to provide a simple unified procedure for analyzing coherent reordering effects in gases.

Photon Echo Nuclear Double Resonance (PENDOR) experiments on the $^1\text{D}_2$ - $^3\text{H}_4$ transition of Pr^{3+} in LaF_3 have unambiguously determined the $^3\text{H}_4$ excited state splitting parameters. Improvements in experimental techniques

Block 20 continued - Abstract

have allowed us to obtain echo modulation data for the 1D_2 - 3H_4 transition which when analyzed will provide a rather complete description of its spectroscopic and relaxation character. Initial steps are being taken to perform excited state and tri-level photon echo experiments in $Pr^{3+}:LaF_3$.

Block 19 continued - Key Words

Wave noise
Performance
Detection
Estimation
Antibunching
Dead time
Spectroscopy
Chaotic light
Optical signal processing
Heterojunction
Transport
Interface charge
Polycrystalline silicon
Rectifies
Low temperature process
Laser processed
Schottky barrier
Silicon
Phosphorescence
Thermoluminescence
Traps
Zinc silicate
Si-SiO₂ interfaces
VLSI reliability
COF₂
Relaxation
Intermode energy transfer
Relaxation
Carbon dioxide laser
Infrared
Fluorescence
SO₂
Oxalyl fluoride
Quasi-continuum
Internal rotation
Collision assisted excitation
SF₆
Molecular beam
Photofragmentation
Translation-vibration
HBr
HCl
Cl₂
ICl
Matrix
Cryostat
Br₂
Nuclear magnetic resonance gyroscopes
Mirrorless lasers

Block 19 continued - Key Words

Tunable infrared lasers
Remote sensing of magnetic fields
Excimer molecules
Photochemistry
Isotope separation
Spin polarization
Magnetometers
Diazo compounds
Carbenes
Picosecond laser
Photodissociation
Energy relaxation
Intramolecular chain motions
Electron transfer
Photon echoes
Line broadening
Echo detection
Reordering effects
Diagrammatic echo analysis
Velocity changing collisions
Echo modulation
Nuclear hyperfine relaxation
Optical linewidths

TABLE OF CONTENTS

PUBLICATIONS AND REPORTS	xi
FACTUAL DATA, CONCLUSIONS, AND PROGRAMS FOR THE NEXT INTERVAL	
I. QUANTUM DETECTION AND SENSING OF RADIATION	1
A. Coherent Detection and Sensing in the Infrared	1
B. The Effects of Wave Noise on the Absorption and Detection of Infrared and Optical Radiation	11
C. Photon Count Antibunching for Optical Communications, Radar, Imaging, and Spectroscopic Applications	23
II. PHYSICAL PROPERTIES AND EFFECTS IN ELECTRONIC MATERIALS	31
A. Carrier Transport Across Heterojunction Interface	31
B. Electronic Properties of Poly Si-Si Diodes	34
C. Laser Processed Schottky Barriers	41
D. Electron Traps in Zinc Silicate Phosphors	45
E. Energy and Electric Field Dependence of Si-SiO ₂ Interface State Parameters by Optically Activated Admittance Experiments	52
F. Statistical Fluctuations of Dopant Impurities in Ion-Implanted Bipolar Transistor Structures and the Minimum Device Dimensions for VLSI System Reliability.	62
III. ENERGY TRANSFER AND RELAXATION IN SMALL POLYATOMIC MOLECULES	70
A. Vibrational Energy Transfer in Laser Excited COF ₂ : Infrared Fluorescence from the Intermediate Mode ν_4	70
B. Temperature Dependence of SO ₂ Energy Transfer Rates	82
C. Laser Excited Infrared Fluorescence in Oxalyl Fluoride	84
D. Collision Assisted Laser Excitation of SF ₆ in a Supersonic Nozzle	93
E. Excimer Laser-Induced Photofragmentation and Vibrational Energy Disposal in Molecules	100

F.	Photophysics and Photochemistry in Low Temperature Solid Matrices	109
IV.	ENERGY TRANSFER AND RELAXATION IN ALKALI METALS	122
A.	Nuclear Spin Polarization of Xe by Optical Pumping	122
B.	Spectroscopy of the 5D State of Cesium	123
C.	Infrared Absorption of Alkali Molecules	124
D.	Ground State Polarization by Two-Photon Optical Pumping of Atomic Vapors	125
E.	Temperature and Density Variation of the Infrared Bands of CsXe: Cesium Polyxenide Bands	126
F.	Faraday Rotation and Magnetic Circular Dichroism of Alkali-Noble Gas Systems	127
G.	Particulate Formation in Cesium-Deuterium Gas Cells	128
H.	Spin Destruction in Collisions Between Cesium Atoms	129
I.	Spin Exchange and Relaxation in Na-Noble Gas Mixtures	130
V.	PICOSECOND ENERGY TRANSFER AND PHOTOFRAGMENTATION SPECTROSCOPY	131
A.	Picosecond Laser Studies of Photodissociation and Energy Relaxation in Short-Lived Fragments	131
B.	Picosecond Laser Studies of the Dynamics of Chain Relaxation	136
C.	Electronic Energy Relaxation by Charge Transfer Processes	139
VI.	GENERATION AND CONTROL OF RADIATION	
A.	Spontaneous and Induced Coherent Radiation Generation and Control in Atomic Vapors	145
B.	Relaxation and Excitation Transfer of Optically Excited States in Solids	153
	SIGNIFICANT ACCOMPLISHMENTS AND TECHNOLOGY TRANSITION REPORT	163
	PERSONNEL	166
	JSEP REPORTS DISTRIBUTION LIST	168

PUBLICATIONS AND REPORTS

Publications

- D. R. Coulter, F. R. Grabiner, L. M. Casson, G. W. Flynn and R. B. Bernstein, "Laser Pumping of SF₆ in the Collisional Region of a Nozzle Beam: Bolometric Detection of Internal Excitation," J. Chem. Phys. 73, 281 (1980). (NSF, DOE and JSEP-work units 4,5,6)
- Marsha Isack Lester and George W. Flynn, "Intermolecule Vibrational Energy Transfer Dynamics in IR Laser Pumped SO₂/18O₂ Mixtures," J. Chem. Phys. 72, 6424 (1980). (NSF and JSEP-work units 4 and 5)
- M. L. Mandich and G. W. Flynn, "Vibrational Energy Transfer Map for OCS," J. Chem. Phys. 73, 1265 (1980). (NSF and JSEP-work units 4 and 5)
- M. L. Mandich and G. W. Flynn, "Collisional Relaxation of Vibrationally Excited OCS in Rare Gas Mixtures," J. Chem. Phys. 73, 3679 (1980). (NSF and JSEP-work units 4 and 5)
- M. C. Teich, "The Physics of Heterodyne Detection in the Far-Infrared: Transition from Electric-Field to Photon-Absorption Detection in a Simple System," in Proc. International Conf. on Heterodyne Systems and Technology, edited by S. Katzburg and J. M. Hoell (NASA Conference Publication No. 2138, NASA Langley, Hampton, Virginia, 1980), pp. 1-10. (JSEP-work unit 12)
- M. C. Teich, "State-Vector Formalism for Intrapersonal, Interpersonal, and Group Interactions," Behav. Sci. 25, 297 (1980). (NIH)
- M. C. Teich and P. Diamant, "Relative Refractoriness in Visual Information Processing," Biol. Cybernetics 38, 187 (1980). (NSF)
- P. R. Prucnal and M. C. Teich, "An Increment Threshold Law for Stimuli of Arbitrary Statistics," J. Math. Psychol. 21, 168 (1980). (NSF and NIH)
- P. R. Prucnal, "Receiver Performance Evaluation Using Photocounting Cumulants with Application to Atmospheric Turbulence," Appl. Opt. 19, 3611 (1980). (NSF)
- P. R. Prucnal, "A New Generalized Performance Measure for Single-Threshold Detection Systems," Appl. Opt. 19, 3606 (1980). (NSF)
- N. D. Bhaskar, M. Hou, M. Ligare, B. Suleman, and W. Happer, "Role of Na-Xe Molecules in Spin Relaxation of Optically Pumped Na in Xe Gas," Phys. Rev. A 22, 2710 (1980). (AFOSR)
- A. Vasilakis, N. D. Bhaskar, and W. Happer, "New Infrared Absorption Bands of Sodium Vapor," J. Chem. Phys. 73, 1490 (1980). (AROD and AFOSR)

- N. D. Bhaskar, J. Pietras, J. Camparo, J. Liran and W. Happer, "Spin Destruction in Collisions Between Cesium Atoms," *Phys. Rev. Lett.* 44, 930 (1980). (NSF and AFOSR)
- G. Brink, A. Glassman and R. Gupta, "Lifetime Measurement of the $(5d6p)^3D_3$ State of Barium by Dye-Laser Spectroscopy," *Opt. Comm.* 33, 17 (1980). (JSEP-work unit 1)
- L. K. Lam, R. Gupta, and W. Happer, "Hyperfine-Structure Measurements in the First Excited D Levels of Potassium, Rubidium, and Cesium by Cascade-Fluorescence Spectroscopy," *Phys. Rev. A* 21, 1225 (1980). (JSEP)
- C. A. Langhoff, K. Gnädig and K. B. Eisenthal, "Picosecond Laser Studies of I_2 Aromatic Complexes and the Formation of I Atom-Aromatic Complexes in Solution," *Chem. Phys.* 46, 1,2, 117 (1980). (NIH, NSF and AFOSR)
- Y. Wang, M. K. Crawford, M. J. McAuliffe and K. B. Eisenthal, "Picosecond Laser Studies of Electron Solvation in Alcohols," *Chem. Phys. Lett.* 74, 160 (1980). (NIH, NSF, AFOSR and JSEP-work unit 8).
- K. B. Eisenthal, N. J. Turro, M. Aikawa, J. A. Butcher, Jr., C. Dupuy, G. Hefferon, W. Hetherington, G. M. Korenowski and M. J. McAuliffe, "Dynamics and Energetics of the Singlet-Triple Interconversion of Diphenylcarbene," *J. Chem. Soc.* 102, 6563 (1980). (NSF, AFOSR and JSEP-work unit 9)
- Y. Wang, M. K. Crawford and K. B. Eisenthal, "Intramolecular Excited-State Charge-Transfer Interactions and the Role of Ground-State Conformations," *J. Phys. Chem.* 84, 2696 (1980). (NIH, NSF and AFOSR)
- K. B. Eisenthal, M. K. Crawford, C. Dupuy, W. Hetherington, G. Korenowski, M. H. McAuliffe and Y. Wang, "Photodissociation, Short-Lived Intermediates, and Charge Transfer Phenomena in Liquids," in *Picosecond Phenomena II*, R. Hochstrasser, W. Kaiser and C. V. Shank, editors, Springer-Verlag, New York, New York: 1980. (NSF, AFOSR and JSEP-work unit 9)
- R. Kachru, T. W. Mossberg and S. R. Hartmann, "Noble-Gas Broadening of the Sodium D Lines Measured by Photon Echoes," *J. Phys. B: Atom. Molec. Phys.* 13, L363 (1980). (ONR and JSEP-work unit 10)
- T. W. Mossberg, E. Whittaker, R. Kachru, and S. R. Hartmann, "Noble-Gas-Induced Collisional Broadening of the $3P_{1/2}$ - $3P_{3/2}$ Transition of Sodium Measured by the Trilevel-Echo Technique," *Phys. Rev. A* 22, 1962 (1980). (ONR and JSEP-work unit 10)
- R. Kachru, T. W. Mossberg, and S. R. Hartmann, " N_2 -CO-Induced Collisional Broadening of Forbidden Ground-to-Rydberg-State Transitions in Sodium as Measured by Trilevel Echoes," *Phys. Rev. A* 22, 1953 (1980). (ONR and JSEP-work unit 10)

- K. K. Ng and H. C. Card, "Asymmetry in the SiO_2 Tunneling Barriers to Electrons and Holes," J. Appl. Phys. 51, 2153 (1980). (DOE and JSEP-work unit 15)
- T. C. Poon and H. C. Card, "Energy and Electric Field Dependence of Si- SiO_2 Interface State Parameters by Optically Activated Admittance Experiments," J. Appl. Phys. 51, 6273 (1980). (JSEP-work units 15-17)
- E. Y. Chan and H. C. Card, "Near IR Interband Transitions and Optical Parameters of Metal-Germanium Contacts," Appl. Opt. 19, 1309 (1980). (JSEP-work unit 15)
- T. C. Poon and H. C. Card, "Admittance Measurements of Si- SiO_2 Interface States Under Optical Illumination," J. Appl. Phys. 51, 5880 (1980). (JSEP-work units 15-17).
- H. C. Card and W. Hwang, "On the Transport Theory of Schottky Barriers to Polycrystalline Silicon Thin Films," IEEE Transactions on Electron Devices, ED-27, 700 (1980). (DOE)
- W. Hwang, E. S. Yang, H. C. Card, and C. M. Wu, "Current Transport Mechanisms of Metal-Polycrystalline Silicon Schottky Barrier Solar Cells," Proceed. 14th IEEE Photovoltaic Specialists Conf., 404 (1980). (DOE)
- H. C. Card and W. Hwang, "Minority Carrier Injection in (Dark) Metal-Polycrystalline Silicon Contacts," IEEE Proceed. 1: Solid State and Electron Devices, 127, 161 (1980). (DOE)
- P. R. Prucnal, W. Hwang, and H. C. Card, "Statistical Fluctuations of Dopant Impurities in Ion-Implanted Bipolar Transistor Structures and the Minimum Device Dimensions for VLSI System Reliability," Microelectronics and Reliability, 20, 633 (1980). (JSEP-work units 13, 15)
- E. S. Yang and C. M. Wu, "Schottky Barrier Formation by Laser Irradiation Processing," Appl. Phys. Lett. 37, 462 (1980). (NSF and JSEP-work unit 15).
- C. M. Wu, E. S. Yang, W. Hwang and H. C. Card, "Grain Boundary Effects on the Electrical Behavior of Al-Poly-Si Schottky Barrier Solar Cells," IEEE Trans. Electron Devices, ED-27, 687 (1980). (NSF and DOE)
- C. M. Wu and E. S. Yang, "Current Suppression Induced by Conduction-Band Discontinuity in $\text{Al}_{0.35}\text{Ga}_{0.65}\text{As-GaAs}$ N-p Heterojunction Diodes," J. Appl. Phys. 51, 2261 (1980). (NSF and JSEP-work unit 15)
- E. S. Yang, C. M. Wu, H. J. Vollmer, T. O. Sedgewick and R. T. Hodgson, "Schottky Barrier Formation by Laser Irradiation Processing," Appl. Phys. Lett. 462 (1980). (NSF and JSEP-work unit 15)
- C. M. Wu and E. S. Yang, "Recrystallized Al-nSi Schottky Barriers with a Barriers Height of 0.98 eV," J. Appl. Phys. 51, 5889 (1980). (NSF and DOE)

- C. M. Wu and E. S. Yang, "Modification of Schottky Barrier Height by Surface Grain Boundaries of Polycrystalline Silicon," *Appl. Phys. Lett.* 37, 945 (1980). (DOE)
- E. S. Yang, E. Poon, C. M. Wu, H. C. Card and W. Hwang, "Impediment of the Majority-Carrier Current by Grain Boundary Potential in Al-Poly-Si Schottky Barrier Solar Cells," *Int. Electron Device Meeting Tech. Digest*, Washington, D.C., December 1980. (NSF and DOE)
- Eric Weitz and George Flynn, "Vibrational Energy Flow in the Ground Electronic States of Polyatomic Molecules," *Photoselective Chemistry, Part 2*, Joshua Jortner, Ed. John Wiley and Sons, pp. 185-235 (1981). (NSF and JSEP-work units 4,5,6)
- Irwin Shamah and George Flynn, "Vibrational Relaxation Induced Population Inversions in Laser Pumped Molecules, *Chem. Phys.* 55, 103 (1981). (NSF and JSEP-work units 4,5)
- M. I. Lester, R. Coulter, L. M. Casson, G. W. Flynn and R. B. Bernstein, "Laser Excitation of SF₆ in a Transparent Nozzle Beam: Collision Assisted Absorption and Up-Pumping," *J. Phys. Chem.* 85, 751 (1981). (NSF, DOE and JSEP-work units 4,5,6)
- G. Vannucci, M. C. Teich, "Dead-Time-Modified Photocount Mean and Variance for Chaotic Radiation," *J. Opt. Soc. Am.* 71, 164 (1981). (JSEP-work unit 14)
- M. C. Teich, "Role of the Doubly Stochastic Neyman Type-A and Thomas Counting Distributions in Photon Detection," *Appl. Opt.* 20, xxx (1981). (JSEP-work unit 13)
- C. Dupuy, G. M. Korenowski, M. McAuliffe, W. M. Hetherington III and K. B. Eisenthal, "Photodissociation of Diphenyldiazomethane and Energy Relaxation in the Diphenylcarbene Fragment," *Chem. Phys. Lett.* 77, 272 (1981). (NSF, AFOSR and JSEP-work unit 9)
- W. M. Hetherington II, G. M. Korenowski and K. B. Eisenthal, "Picosecond CARS as a Probe of the Multiphoton Photofragmentation of Benzene," *Chem. Phys. Lett.* 77, 275 (1981). (NSF, AFOSR and JSEP-work unit 8)
- T. W. Mossberg and S. R. Hartmann, "Diagrammatic Representation of Photon Echoes and Other Laser-Induced Ordering Processes in Gases," *Phys. Rev. A* 23, 1271 (1981). (ONR and JSEP-work unit 10)
- J. H. Eberly, S. R. Hartmann, and A. Szabo, "Propagation Narrowing in the Transmission of a Light Pulse Through a Spectral Hole," *Phys. Rev. A* 23, 2502 (1981).
- K. C. Kao and W. Hwang, Electrical Transport in Solids - With Particular Reference to Organic Semiconductors, International Series in the Science of the Solid State, Volume 14, Pergamon Press, Oxford, England (1981).

- C. M. Wu and E. S. Yang, "A Low-Temperature Fabrication Process of Poly-Silicon-Silicon P^+-n Junction Diode," Appl. Phys. Lett. scheduled to appear May, 1981. (NSF, DOE and JSEP-work unit 15)
- N. D. Bhaskar, J. Camparo, J. Ligare and W. Happer, "Particulate Production and Optical Bleaching of Cesium Deuterium Gas Cells Excited With a Tunable, CW Dye Laser," to be published in Phys. Rev. Lett. (NSF and JSEP)
- N. D. Bhaskar, J. Camparo, W. Happer, and A. Sharma, "Light Narrowing of Magnetic Resonance Lines in Dense Alkali Vapors," to be published in Phys. Rev. (AFOSR)
- M. K. Crawford, Y. Wang and K. B. Eisenthal, "Effects of Conformation and Solvent Polarity on Intramolecular Charge-Transfer: A Picosecond Laser Study," Chem. Phys. Lett (1981) submitted for publication. (NSF, AFOSR and JSEP-work unit 8)
- K. Chiang, E. A. Whittaker, and S. R. Hartmann, "Photon Echo Nuclear Double Resonance in $LaF_3:Pr^{3+}$," accepted for publication in Phys. Rev. (NSF and JSEP-work unit 11)
- T. W. Mossberg and S. R. Hartmann, "Coherent Transients Theorem: A Comment," submitted for publication. (ONR and JSEP-work unit 10)
- W. Hwang, P. Panayotatos, E. Poon and H. C. Card, "Carrier Transport and Recombination Processes at Grain Boundaries in Polycrystalline Silicon under Optical Illumination," Proceed. 15th IEEE Photovoltaic Specialists Conf., accepted for publication. (DOE)
- E. S. Yang, E. Poon, C. M. Wu, H. C. Card and W. Hwang, "Majority Carrier Current Characteristics in Large-Grain Polycrystalline Silicon Schottky Barrier Solar Cells," accepted for publication, IEEE Trans. Electron. Devices. (DOE)
- I. F. Chang, J. J. Cuomo and E. S. Yang, "Fabrication of Thin-Film Zinc Silicate Phosphors," IBM Technical Disclosure Bulletin, to be published.
- C. A. Chang and E. S. Yang, "Multi-Layered Integrated Structures," IBM Technical Disclosure Bulletin, to be published.
- E. S. Yang and J. M. Brownlow, "Thermal Release of Trapped Electrons and Phosphorescent Decay in Zinc Silicon Phosphors," J. Appl. Phys., accepted for publication. (JSEP-work unit 15)
- E. S. Yang, "Oscillators," in McGraw-Hill Encyclopedia of Science and Technology, 5th edition (to appear)
- C. M. Wu and E. S. Yang, "Dependence of Rectification Properties of Al-nSi: Contacts on Thermal Annealing and Quenching," J. Appl. Phys. (to appear. (DOE and JSEP-work unit 15)

Papers by CRL Staff Members Presented at Scientific Meetings

- K. Eisenthal, "Ultrafast Phenomena in Chemistry," UCLA Chemistry Department Golden Anniversary Symposium, University of California, Los Angeles, California, June 2, 1980.
- K. Eisenthal, "Picosecond Laser Studies of Electron and Proton Transfer in Liquids," Second Conference on Picosecond Phenomena, Massachusetts, June 18, 1980.
- K. Eisenthal, "Picosecond Laser Studies in Liquids," Gordon Research Conference on Radiation Chemistry, Brewster Academy, June 25, 1980.
- K. Eisenthal, "Picosecond Laser Studies of Ultrafast Processes in Liquids," ACS and APS Symposium on Laser Photochemistry in Large Molecules and Solids, San Jose, California, August 20, 1980.
- G. W. Flynn, "Vibrational Relaxation in Small Molecules," Gordon Conference on Vibrational Spectroscopy, Wolfboro, New Hampshire, August 19, 1980.
- S. R. Hartmann, "Overview of Physics via Coherent Transients," Invited Talk, 11th Winter Colloquium on Quantum Electronics, Snowbird, Utah, January 14-16, 1981.
- K. P. Leung, T. W. Mossberg, and S. R. Hartmann, "A Novel Method for Observing Coherent Emission," American Physical Society Meeting, Phoenix, Arizona, March 16-20, 1981.
- K. P. Leung, T. W. Mossberg, and S. R. Hartmann, "Raman Echo in Atomic Tl Vapor," American Physical Society Meeting, Phoenix, Arizona, March 16-20, 1981.
- T. W. Mossberg, R. Kachru, and S. R. Hartmann, "Observation of Quantum Mechanical Collisional Velocity Changes via Photon Echo Spectroscopy," Eleventh International Quantum Electronics Conference, Boston, Massachusetts, June 23-26, 1980.
- T. W. Mossberg, R. Kachru, E. Whittaker, and S. R. Hartmann, "Temporally Recurrent Population Gratings in Gases," Eleventh International Quantum Electronics Conference, Boston, Massachusetts, June 23-26, 1980.
- T. W. Mossberg, R. Kachru, and S. R. Hartmann, "Forward, Backward, and Long-Lived Stimulated Photon Echoes in Gases," Invited Paper, Eleventh International Quantum Electronics Conference, Boston, Massachusetts, June 23-26, 1980.
- T. W. Mossberg, "Optical Echo Measurements of Noble-Gas-Induced Broadening in Atomic Sodium and Thallium Vapor," 5th International Conference on Spectral Line Shapes, West Berlin, West Germany, July 7-11, 1980.

- T. W. Mossberg, "Collisional Broadening of Two-Photon Ground-to-Rydberg Transitions in Sodium," 5th International Conference on Spectral Line Shapes, West Berlin, West Germany, July 7-11, 1980.
- T. W. Mossberg and S. R. Hartmann, "Photon Echoes for Everyone," Invited Paper, Lasers '80 Conference, New Orleans, Louisiana, December 15-19, 1980.
- P. Prucnal, "Receiver Performance Evaluation Using Photocounting Cumulants," Annual Meeting of the Optical Society of America, Chicago, Illinois, October, 1980.
- M. Teich, "Infrared Heterodyne Detection Theory and Application Survey," Invited Plenary Session Lecture, NASA International Conference on Heterodyne Systems and Technology, Williamsburg, Virginia, April, 1980.
- E. S. Yang, W. Hwang, and C. M. Wu, "Influence of Grain Boundaries on Polycrystalline-Silicon Properties and its Implication on Schottky Solar Cells," DOE/SERI Poly-Silicon Solar Cell Review Meeting, Washington, D.C., June, 1980.
- E. S. Yang, E. Poon, C. M. Wu, H. C. Card, and W. Hwang, "Impediment of Majority Carrier Current by Grain Boundary Potential in Al-PolySi Schottky Barrier Solar Cells," International Electronic Devices Meeting, Washington, D.C., December, 1980.

Lectures

- T. Allik, "Infrared Laser Induced Fluorescence in Oxalyl Fluoride,"
Chemical Physics Seminar, Columbia University, New York, New York,
January 22, 1981.
- P. Beeken, "Photophysical Investigation of Br₂ Trapped in Rare Gas Matrices,"
Chemical Physics Seminar, Columbia University, New York, New York,
January 22, 1981.
- N. Bhaskar, "Alkali Vapors-Optical Pumping Photochemistry," Seminar,
Department of Applied Physics and Engineering, Princeton University,
Princeton, New Jersey, September 19, 1980; Exxon Research Center,
Linden, New Jersey, January 6, 1981.
- K. Eiseenthal, "Picosecond Laser Studies of Ultrafast Molecular Processes,"
Seminar, Stanford University, Stanford, California, June 10, 1980.
- K. Eiseenthal, "Modern Optics and Spectroscopy," Seminar, Massachusetts
Institute of Technology, Cambridge, Massachusetts, November 25, 1980.
- K. Eiseenthal, "Studies of Chemical Reactions and Energy Relaxation with
Picosecond Lasers," Seminar, University of Chicago, Chicago,
Illinois, December 1, 1980.
- K. Eiseenthal, "Ultrafast Energy Relaxation Processes in Molecular Systems,"
Seminar, University of California at San Diego, La Jolla, California,
February 13, 1981; Seminar, California Institute of Technology,
Pasadena, California, February 17, 1981; Seminar, University of
California at Santa Barbara, Santa Barbara, California, February 19,
1981.
- G. W. Flynn, "Vibrational Relaxation in Small Molecules," Massachusetts
Institute of Technology, Cambridge, Massachusetts, April 1, 1980;
University of Delaware, Newark, Delaware, April 9, 1980; Brookhaven
National Laboratory, Upton, New York, June 3, 1980.
- G. W. Flynn, "Laser Excitation of Molecules in Beams and Bulbs," Syracuse
University, Syracuse, New York, September 5, 1980; Oregon State
University, Corvallis, Oregon, September 26, 1980; University of
Florida, Gainesville, Florida, October 10, 1980; College of the
City of New York, New York, New York, October 22, 1980; Bell
Telephone Laboratories, New Jersey, November 5, 1980.
- W. Happer, "Dense Alkali Vapors," Seminar, Massachusetts Institute of
Technology, Cambridge, Massachusetts, April 16, 1980; Colloquium,
State University of New York, Binghamton, New York, April 25, 1980;
Colloquium, College of William and Mary, Williamsburg, Virginia,
January 23, 1981.
- W. Happer, "Optical Pumping for Combustion Diagnostics," Sandia Laboratories,
Livermore, California, February 12, 1981.

- S. R. Hartmann, "Photon Echoes for Everyone," Colloquia: Physics Department, University of Kyoto, Japan, May 13, 1980; Institute of Molecular Science in Okazaki, Japan, May 15, 1980; Institute of Solid State Physics in Tokyo, Japan, May 19, 1980; Physics Department, Yamaguchi University, Japan, June 4, 1980; Physics Department and Engineering Science Department, Osaka University, Japan, June 10, 1980.
- M. Lester, "Collision-Assisted Laser Excitation of SF₆ in a Supersonic Nozzle," Seminar: Northwestern University, Evanston, Illinois, October 15, 1980; Indiana University, Bloomington, Indiana, October 21, 1980; Los Alamos Scientific Laboratory, Los Alamos, New Mexico, October 28, 1980; National Bureau of Standards, Washington, D.C., November 14, 1980; University of Pennsylvania, Philadelphia, Pennsylvania, January 20, 1981; University of Illinois, Urbana, Illinois, February 9, 1981; Bell Laboratories, Murray Hill, New Jersey, February 22, 1981; IBM Watson Research, Yorktown Heights, New York, April 13, 1981.
- M. Mandich, "Vibrational Energy Transfer of OCS in the Gas Phase and Trapped in Rare Gas Matrices," Chemistry Department, California Institute of Technology, Pasadena, California, August 17, 1980; Chemistry Department, University of California, Los Angeles, California, August 18, 1980; Chemistry Department, University of California, Berkeley, California, August 29, 1980; Chemistry Department, Oregon State University, Corvallis, Oregon, September 4, 1980.

Resonance Seminars

Meetings are held periodically at Columbia University, New York, New York during the academic year and are open to all members of the New York Scientific community. Guest speakers are invited to discuss work in the general area of the research in the Columbia Radiation Laboratory.

Rodney T. Hodgson, I.B.M. Research Center, "Laser Heating--Laser Cooling," April 11, 1980.

B. E. A. Saleh, University of Wisconsin at Madison, "Image Processing and the Bilinear Model," April 25, 1980.

John Farley, University of Arizona, "The Effects of Thermal Radiation on Atoms," May 14, 1980.

S. Kimel, The Technion Israel Institute of Technology, Haifa, Israel, "IR Multiphoton Decomposition of CrO_2Cl_2 --Spectro Dynamics of the Visible Luminescence," May 16, 1980.

Curt Wittig, University of Southern California, "Uses of Infrared Multiphoton Excitation," September 22, 1980

Richard Osgood, M.I.T. Lincoln Laboratory, "Laser Microchemistry for Solid State Electronics," September 30, 1980.

James T. Yardley, Allied Chemical Company, "Laser Photofragmentation of Metal Carbonyl Compounds: Dynamics and Catalysis," October 2, 1980.

William Reinhardt, University of Colorado, Boulder, "Semiclassical Quantization of Non-Separable Systems," October 13, 1980.

David Pritchard, Massachusetts Institute of Technology, "Rotational Energy Transfer: 'Theory' and Experiment," October 16, 1980.

C. Harris, University of California, Berkeley, "Structural and Dynamical Properties of Liquids on a Picosecond Time Scale," October 17, 1980.

Leonard Mandel, "University of Rochester, "Are Optical Photons and Atomic Quantum Jumps for Real?" October 31, 1980.

Michael Feld, M.I.T., "Intersections of Laser Spectroscopy and Nuclear Spectroscopy," April 9, 1981.

Mark Levenson, I.B.M. Research Labs., "Laser Spectroscopy and Non Linear Optics in the More or Less Real World," April 22, 1981.

E. P. Ippen, M.I.T., "Recent Advances in Picosecond Devices and Techniques," April 29, 1981.

S. R. Hartmann, Columbia University, "Measurement of Collisional Broadening Parameters in Atomic Vapors Using Optical Coherent Transients," April 30, 1981.

I. QUANTUM DETECTION AND SENSING OF RADIATION

A. COHERENT DETECTION AND SENSING IN THE INFRARED

(M. C. Teich, L. Edelshteyn)

(Principal Investigator: M. C. Teich (212) 280-3117)

Heterodyne detection has a long and august history in the annals of electrical engineering, reaching back to the earliest years of the century. The term has its roots in the Greek words "heteros" (other) and "dynamics" (force).

In 1902, Reginald Fessenden was awarded a patent⁽¹⁾ "relating to certain improvements ... in systems where the signal is transmitted by [radio] waves differing in period, and to the generation of beats by the waves and the employment of suitable receiving apparatus responsive only to the combined action of waves corresponding in period to those generated . . ." The subsequent realization that one of these waves could be locally generated (the development of the local oscillator) provided a substantial improvement in system performance. Practical demonstrations of the usefulness of the technique were carried out between the "Fessenden stations" of the U. S. Navy at Arlington (Virginia) and the Scout Cruiser Salem, between the Salem and the Birmingham (1910), and at the National Electric Signaling Company. In 1913, John Hogan provided a thoroughly enjoyable account of the development, use, and performance of the Fessenden heterodyne signaling system in the first volume of the Proceedings of the IRE.⁽²⁾

It was not long thereafter, in 1917, that Edwin H. Armstrong of the Department of Electrical Engineering at Columbia University carried out a thorough investigation of the heterodyne phenomenon occurring in the oscillation state of the "regenerative electron relay".⁽³⁾ A major breakthrough in the field, the development of the superheterodyne receiver, was achieved by

Armstrong in 1921,⁽⁴⁾ and this famous invention is now used in systems as diverse as household AM radio receivers and microwave Doppler radars. The prefix "super" refers to "the super-audible frequency that could be readily amplified."

In the succeeding years, the application of heterodyne and superheterodyne principles followed the incessant march toward higher frequencies that culminated in the remarkable developments in microwave electronics about the time of World War II.

The marriage of heterodyning and the optical region took place in 1955. In a now classic experiment, Forrester, Gudmundsen, and Johnson⁽⁵⁾ observed the mixing of two Zeeman components of a visible (incoherent) spectral line in a specially constructed photomultiplier tube. With the development of the laser, optical heterodyning became considerably easier to observe and was studied in 1962 by Javan, Ballik, and Bond⁽⁶⁾ at $1.15\text{ }\mu\text{m}$ using a He-Ne laser, and by McMurtry and Siegman⁽⁷⁾ at $6943\text{ }\text{\AA}$ using a ruby laser.

The development of new transmitting and receiving components in the middle infrared region of the electromagnetic spectrum led Teich, Keyes, and Kingston⁽⁸⁾ in 1966 to perform a heterodyne experiment using a CO_2 laser at $10.6\text{ }\mu\text{m}$ in conjunction with a copper-doped germanium photoconductive detector operated at 4°K . Subsequent experiments with lead-tin selenide photovoltaic detectors confirmed the optimal nature of the detection process.⁽⁹⁾⁻⁽¹¹⁾ The state of the art in applying these results to coherent infrared radar was reviewed by Kingston in 1977.⁽¹²⁾ Elbaum and Teich⁽¹³⁾ have recently shown the importance of properly choosing the performance measure for a heterodyne system. This can sometimes be critical to avoid faulty estimates of signal and noise levels leading to inconsistent or incorrect results, as pointed out by a number of authors.^{(8),(14)} The foregoing introduction has dealt

with more-or-less idealized systems; it must be kept in mind that there are a variety of effects that can alter heterodyne performance in important ways.

We point out also that a number of system configurations employing different forms of nonlinear heterodyne detection have been proposed for various applications.^{(15),(16)} These make use of multiple frequencies, nonlinear detectors, and/or correlation schemes. All are aimed at increasing the signal-to-noise ratio in situations for which usual operating conditions are relaxed in particular ways. One of these schemes,^{(17),(15)} using a two-frequency transmitter, is currently under consideration for possible application in over-water pilot rescue missions where the use of a light-chopping mechanism is interdicted because of its interruptive nature (private communication with W. Tanaka, Naval Weapons Center).

We have carried out a study⁽¹⁸⁾ in which we relaxed the assumption that heterodyne detection takes place by means of photon absorption, as it does in the middle infrared and optical regions,⁽¹⁹⁾ or by means of electric-field detection, as it does in the radiowave and microwave regions. This has enabled us to examine the heterodyne detection process in the submillimeter/far-infrared region of the spectrum in a simple way. Caution must be exercised, however, in that the treatment we provide is intended to provide only a qualitative description of the underlying detection process.

The increasing importance of heterodyning and electric-field detection in the submillimeter, infrared, and optical^{(20),(21)} has encouraged us to examine the operation of such systems in relation to the more conventional photon-absorption detector.⁽²²⁾⁻⁽²⁴⁾

For heterodyne mixing with coherent signals in a two-level detector, a simple argument indicates that double- and sum-frequency terms in the detected power are multiplied by the factor $\text{sech}(\hbar\nu/2kT_e)$, which varies smoothly from

unity in the electric-field detection regime to zero in the photon-absorption detection regime. This factor depends on both the incident photon energy $h\nu$ and on the effective excitation energy of the (two-level) detector, kT_e . It is observed that these terms only appear when it cannot be determined whether photon absorption or photon emission has taken place. Difference-frequency signals, on the other hand, arise from our inability to determine from which beam a photon is absorbed in a heterodyne experiment. (19)

We consider a simple hypothetical two-level system with an effective temperature T_e . It is assumed that the system responds linearly to the incident radiation intensity, and that its interaction with the field is sufficiently weak such that the state of the field is not perturbed by the presence of the detector.

We label the initial and final states of the system as $|\alpha\rangle$ and $|\Omega\rangle$ and of the radiation field as $|i\rangle$ and $|f\rangle$, respectively. For an electric-dipole transition, the transition probability W_{fi} (which is related to the detected power) is given approximately by

$$W_{fi} = |\langle f | e q (E^+ + E^-) | \alpha i \rangle|^2, \quad (1)$$

where e is the electronic charge, q is the detector coordinate, and E^+ and E^- are the positive- and negative-portions of the electric-field operator, respectively. Since E^+ corresponds to photon absorption or annihilation, and E^- corresponds to photon emission or creation, the transition probability may be written as

$$W_{fi} = |\langle f u | e q a E^+ | l i \rangle + \langle f l | e q a_u E^- | u i \rangle|^2, \quad (2)$$

where $|l\rangle$ and $|u\rangle$ represent the lower and upper states of the two-level system, respectively. This equation assumes that the atomic system is, in general, in

a superposition state. Using microscopic reversibility, the quantity $|\langle u | e_q | l \rangle|^2$, which represents the quantum efficiency κ , may be factored out of Eq. (2). We then sum over the final states of the field,⁽²³⁾ which are not observed, to obtain

$$W \propto \langle i | a_l^* a_l E^- E^+ | i \rangle + \langle i | a_u^* a_u E^+ E^- | i \rangle \\ + \langle i | a_l^* a_u E^- E^- + a_l a_u^* E^+ E^+ | i \rangle. \quad (3)$$

The normally ordered first term corresponds to stimulated absorption, the antinormally ordered second term corresponds to photon emission,⁽²⁵⁾ and the third is an interference term.

We now assume that before the interaction, the probability amplitudes of the two possible states, a_l and a_u , were related by the Boltzmann factor, with lower and upper level energies represented by E_l and E_u , respectively, and with excitation energy kT_e defining the effective temperature of the detector. Thus,

$$|a_u|^2 / |a_l|^2 = \exp[-(E_u - E_l) / kT_e], \quad (4)$$

yielding

$$a_l = (1 + e^{-x})^{-1/2} e^{i\phi} \quad (5)$$

and

$$a_u = e^{-x/2} (1 + e^{-x})^{-1/2} e^{i\theta}, \quad (6)$$

with $x \equiv h\nu / kT_e$ and $e^{i\theta}$, $e^{i\phi}$ representing phase factors. Then, generalizing to an arbitrary radiation field represented by the density operator ρ , we obtain the expression

$$W \propto \left([e^{x/2} \operatorname{sech}(x/2)] \operatorname{tr} \{ \rho E^- E^+ \} + [e^{-x/2} \operatorname{sech}(x/2)] \operatorname{tr} \{ \rho E^+ E^- \} \right. \\ \left. + [\operatorname{sech}(x/2)] \operatorname{tr} \{ \rho (e^{-i\gamma} E^- E^- + e^{i\gamma} E^+ E^+) \} \right), \quad (7)$$

with $\gamma \equiv \phi - \theta$.

Considering ideal heterodyne detection, i.e., two parallel, monochromatic, and coherent waves of frequencies ν_1 and ν_2 impinging normally on the detector, and neglecting spontaneous emission so that the antinormally ordered and the normally ordered terms are equal in magnitude,⁽²⁵⁾ the first two terms above generate dc and difference-frequency signals, while the third term contributes double- and sum-frequency signals. This may be clearly seen by explicitly rewriting Eq. (7) as

$$W \propto |\epsilon_1^0|^2 + |\epsilon_2^0|^2 + 2|\epsilon_1^0||\epsilon_2^0| \cos[2\pi(\nu_1 - \nu_2)t + (\beta - \alpha)] \\ + [\operatorname{sech}(h\nu/2kT_e)] \{ |\epsilon_1^0|^2 \cos(4\pi\nu_1 t - 2\alpha - \gamma) + |\epsilon_2^0|^2 \cos(4\pi\nu_2 t - 2\beta - \gamma) \\ + 2|\epsilon_1^0||\epsilon_2^0| \cos[2\pi(\nu_1 + \nu_2)t - (\alpha + \beta) - \gamma] \} \quad (8)$$

where $\epsilon_1^0 = |\epsilon_1^0| e^{i\alpha}$ represents the complex electric-field amplitude of the constituent field with frequency ν_1 and phase α . Double- and sum-frequency terms in the heterodyne signal are therefore multiplied by the factor $\operatorname{sech}(h\nu/2kT_e)$.

For $h\nu/kT_e \rightarrow 0$, this factor approaches 1 and the classical electric-field heterodyne signal obtains

$$W_{\text{elec}} \propto [|\epsilon_1^0| \cos(2\pi\nu_1 t - \alpha - \frac{\gamma}{2}) + |\epsilon_2^0| \cos(2\pi\nu_2 t - \beta - \frac{\gamma}{2})]^2. \quad (9)$$

For $h\nu/kT_e \rightarrow \infty$, $\operatorname{sech}(h\nu/2kT_e) \rightarrow 0$ and the photon-absorption (optical)

heterodyne signal obtains,⁽¹⁹⁾

$$W_{\text{abs}} \propto \{ |\varepsilon_1^o|^2 + |\varepsilon_2^o|^2 + 2|\varepsilon_1^o||\varepsilon_2^o|\cos[2\pi(\nu_1 - \nu_2)t + (\beta - \alpha)] \}. \quad (10)$$

A graphical presentation of the function $\text{sech}(h\nu/2kT_e)$ vs. $(h\nu/kT_e)$ is provided in Fig. 1.

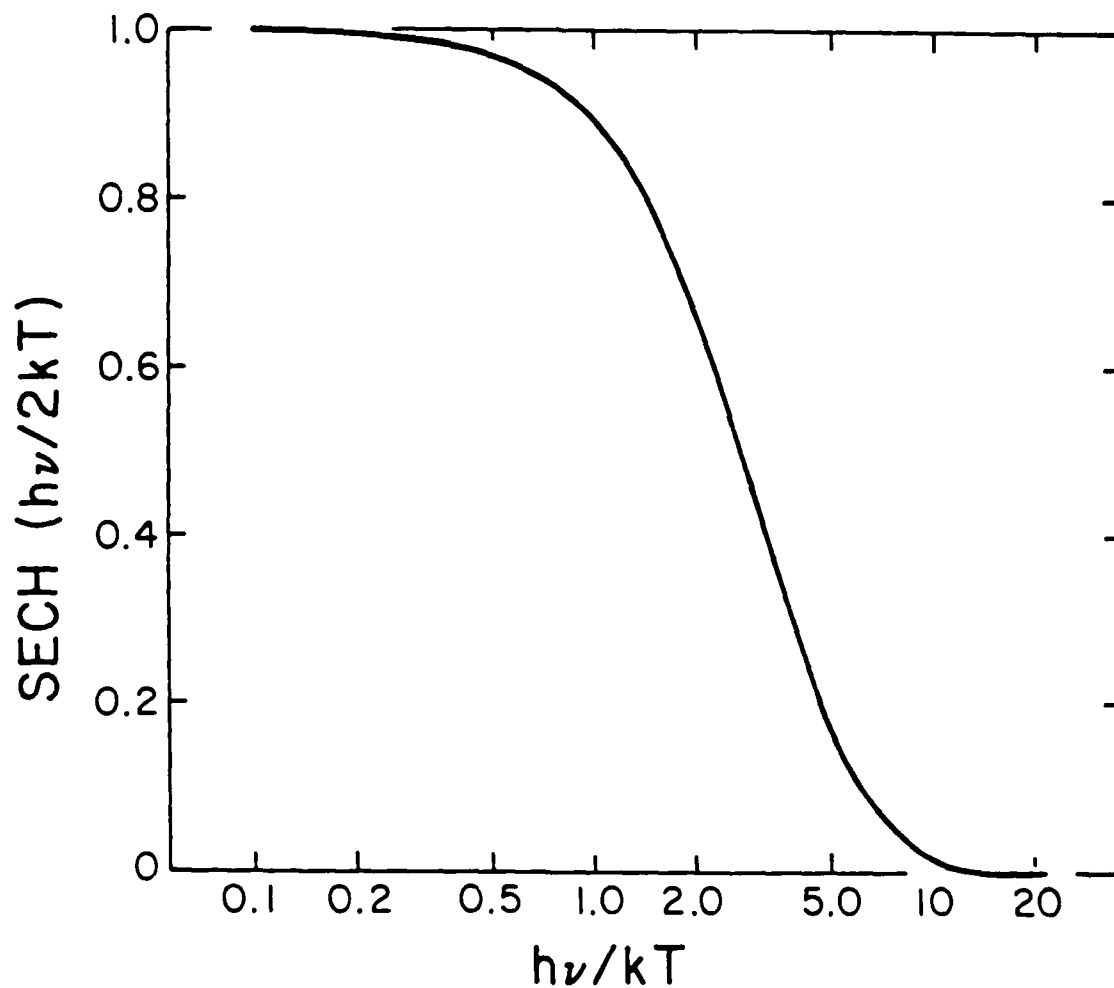


Figure 1. Factor $\text{sech}(h\nu/2kT)$ vs. $h\nu/kT$. This quantity appears as a coefficient in the absorption/emission interference term.

The result for the heterodyne case is easily reduced to the direct detection (video) case for a coherent signal by setting $|\epsilon_2^0| = 0$, which yields

$$W_{\text{dir}} \propto |\epsilon_1^0|^2 \{1 + [\text{sech}(h\nu/2kT_e)] [\cos(4\pi\nu_1 t - 2\alpha - \gamma)]\}. \quad (11)$$

Thus, double-frequency intensity fluctuations are discerned for electric-field direct detectors, while they are suppressed for photon-absorption direct detectors which respond simply as $|\epsilon_1^0|^2$.

The photon-absorption detector is, by definition, initially in its ground state and functions by the annihilation of a single (in general nonmonochromatic) photon. The presence of the difference-frequency signal is understood to arise from our inability to determine from which of the two constituent beams the single photon is absorbed.⁽¹⁹⁾ The two-level electric-field detector, on the other hand, has equal probability of being in the lower and in the upper state, so that the pure processes of photon annihilation and photon absorption occur with equal likelihood, and we must add the effects of both. When we are unable to determine which of these processes is occurring, we must add amplitudes rather than squares of amplitudes, thereby allowing interference to occur. Any attempt, in this case, to determine whether photon emission or photon absorption takes place would randomize the phase γ , and thereby wash out the sum- and double-frequency components. In general, then, a photon incident on a video detector induces upward and downward transitions with different probabilities. This, in turn, creates a quantum-mechanical probability density (and charge distribution) that varies in time, producing a current at the incident radiation frequency. The power absorbed then contains a double-frequency signal. For heterodyne detection, in the general case, sum-frequency signals are observed as well.

The foregoing heuristic model yields a simple result for an idealized

two-level system. Replacing the operator eq by the non-relativistic Hamiltonian $(\hat{p} - e\hat{A})^2/2m$, where \hat{p} and \hat{A} represent the momentum and vector-potential operators, respectively, would allow transitions more general than electric-dipole, and absorptions of more than one quantum to occur. A rigorous treatment should consider a collection of such systems (as a model for a bulk photodetector or metal antenna), in the presence of a surrounding reservoir, and should be carried out using the density matrix formalism. It is expected that the effects described here are important in a broad range of systems, including the Josephson detector.^{(26),(27)}

Tucker⁽²⁸⁾ has recently carried out a rigorous analysis of quantum-limited detection in tunnel junction mixers. He demonstrates that nonlinear tunneling devices are predicted to undergo a transition from energy detectors to photon counters at frequencies where the photon energy becomes comparable to the voltage scale of the dc nonlinearity. It is apparent that the character of this result is closely related to the discussion presented here.

- (1) R. A. Fessenden, Wireless Signaling, U. S. Patent No. 706, 740, August 12, 1902.
- (2) J. L. Hogan, Proc. IRE, 1, 75 (1913).
- (3) E. H. Armstrong, Proc. IRE, 5, 145 (1917).
- (4) E. H. Armstrong, Proc. IRE, 9, 3 (1921).
- (5) A. T. Forrester, R. A. Gudmundsen, and P. O. Johnson, Phys. Rev. 99, 1691 (1955).
- (6) A. Javan, E. A. Ballik, and W. L. Bond, J. Opt. Soc. Amer. 52, 96 (1962).
- (7) B. J. McMurtry and A. E. Siegman, Appl. Opt. 1, 51 (1962).
- (8) M. C. Teich, R. J. Keyes, and R. H. Kingston, Appl. Phys. Lett. 9, 357 (1966).
- (9) M. C. Teich, Proc. IEEE 56, 37 (1968). [reprinted in Infrared Detectors, R. D. Hudson, Jr. and J. W. Hudson, Eds. (Dowden, Hutchinson, and Ross, Stroudsburg, 1975)].

- (10) M. C. Teich, Proc. IEEE 57, 786 (1969).
- (11) R. H. Kingston, Optics News 3, 27 (1977).
- (13) M. Elbaum and M. C. Teich, Opt. Commun. 27, 257 (1978).
- (14) P. Brockman, R. V. Hess, L. D. Staton, and C. H. Bair, "DIAL with Heterodyne Detection Including Speckle Noise: Aircraft/Shuttle Measurements of O₃, H₂O, NH₃ with Pulsed Tunable CO₂ Lasers", Heterodyne Systems and Technology, NASA CP-2138, 1980.
- (15) M. C. Teich, "Nonlinear Heterodyne Detection", In Topics in Applied Physics, R. J. Keyes, Ed. (Springer-Verlag, Berlin/Heidelberg, 1977), vol. 19, Optical and Infrared Detectors, ch. 7, pp. 229-300.
- (16) M. C. Teich, Opt. Engineering 17, 170 (1978).
- (17) M. C. Teich, Appl. Phys. Lett. 15, 420 (1969).
- (18) M. C. Teich, "The Physics of Heterodyne Detection in the Far Infrared: Transition from Electric-Field to Photon-Absorption Detection in a Simple System", in Proc. International Conference on Heterodyne Systems and Technology, edited by S. Katzburg and J. M. Hoell (NASA Conf. Publ. No. 2138, 1980), pp. 1-10.
- (19) M. C. Teich, "Quantum Theory of Heterodyne Detection", In Proc. Third Photoconductivity Conf., E. M. Pell, Ed. (Pergamon, New York, 1971), pp. 1-5.
- (20) L. O. Hocker, D. R. Sokoloff, V. Daneu, A. Szöke, and A. Javan, Appl. Phys. Lett. 12, 401 (1968).
- (21) R. L. Abrams and W. B. Gandrud, Appl. Phys. Lett. 17, 150 (1970).
- (22) L. Mandel, Proc. Phys. Soc. (London), 74, 233 (1959).
- (23) R. J. Glauber, Phys. Rev. 131, 2766 (1963).
- (24) P. L. Kelley and W. H. Kleiner, Phys. Rev. 136, A316 (1964).
- (25) L. Mandel, Phys. Rev. 152, 438 (1966).
- (26) D. G. McDonald, A. S. Risley, J. D. Cupp, K. M. Evenson, and J. R. Ashley, Appl. Phys. Lett. 20, 296 (1972).
- (27) J. E. Zimmerman, J. Appl. Phys. 41, 1589 (1970).
- (28) J. R. Tucker, IEEE J. Quantum Electron. QE-15, 1234 (1979).

B. THE EFFECTS OF WAVE NOISE ON THE ABSORPTION AND DETECTION OF INFRARED AND OPTICAL RADIATION*

(M. C. Teich, P. R. Prucnal, B. E. A. Saleh)

(Principal Investigator: M. C. Teich (212) 280-3117)

It is just over 40 years since Neyman introduced a family of straightforward but intriguing generalizations of the binomial and Poisson distributions.⁽¹⁾ He called the simplest and perhaps most useful of these "the contagious distribution of Type-A with two parameters" (see Fig. 1). Neyman's work was motivated by a variety of experimental observations in entomology and bacteriology with which calculations based on the ordinary Poisson failed to agree. He reasoned that the effects of contagion were important in these studies, and he succeeded in introducing this property in a remarkably elegant yet simple way. The description "contagious" implies that each favorable event increases (or decreases) the probability of succeeding favorable events. Feller⁽²⁾ and others have argued that there are essentially two kinds of contagion: "true contagion" as described above, and "apparent contagion", where there is an inhomogeneity of the population. It has long been known that certain distributions, such as the negative binomial and the Neyman Type-A, could be derived in terms of both types of contagion.⁽²⁾ Indeed, the negative binomial distribution was obtained by Greenwood and Yule⁽³⁾ in terms of apparent contagion and subsequently by Eggenberger and Polya in an independent study in terms of true contagion.⁽⁴⁾⁻⁽⁶⁾

A closely related counting distribution has also proved useful in our study. In 1949, Marjorie Thomas⁽⁷⁾ introduced a two-parameter counting distribution distinct from the Neyman Type-A only in that primary pulses appeared in the final process along with secondary pulses. Though she originally

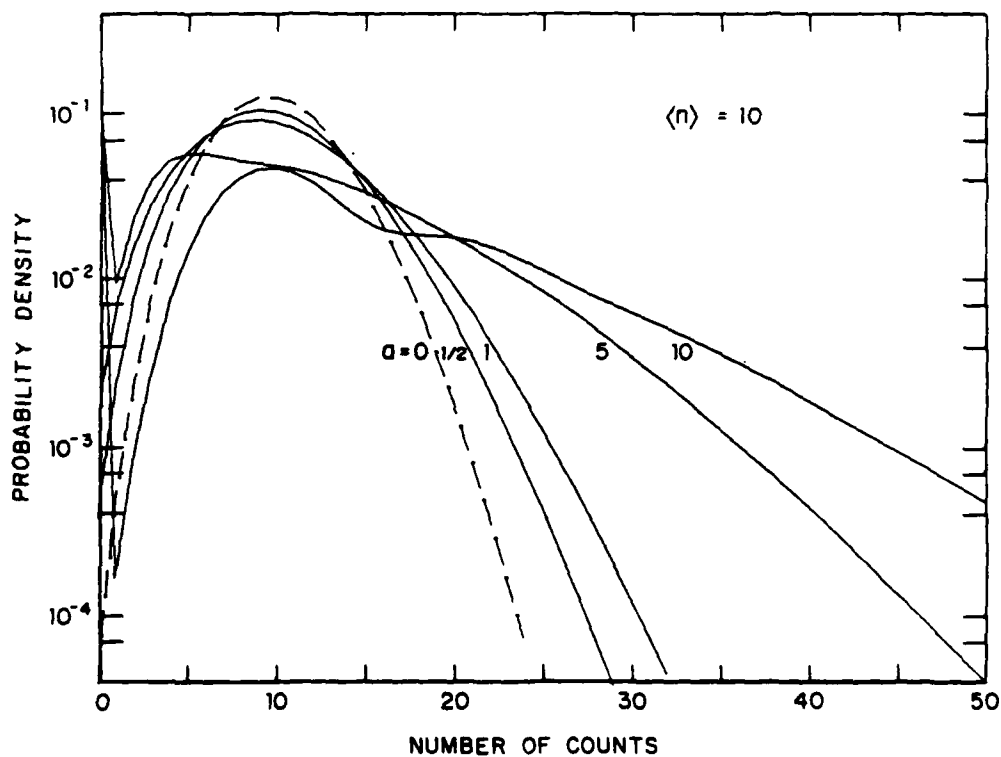


Figure 1: Semilogarithmic plot of the Neyman Type-A counting distribution $p(n|W)$ vs the count number n . The overall mean $\langle n \rangle = 10$. Curves are labeled according to the value of the parameter a . In the limit as $a \rightarrow 0$, the Neyman Type-A approaches the Poisson (dashed curve). The multimodal character of the distribution is evident.

referred to this as the double-Poisson distribution, it has since come to be called the Thomas distribution. Like the Neyman Type-A, it is obtainable from a Neyman-Scott cluster process.

We have developed various properties and limits of the simple and doubly stochastic versions of the two-parameter Neyman Type-A, Thomas, and fixed multiplicative Poisson distribution.⁽⁸⁾ We have discovered many applications to photon, particle, and pulse counting in optics and have begun to investigate the performance of systems containing such counting detectors. Finally, we have looked into a number of related contagious distributions pertinent to photon counting and optical communications.

The Neyman Type-A and Thomas counting distributions turn out to provide a good description for the counting of photons generated by multiplied Poisson processes, as long as the time course of the multiplication is short in comparison with the counting time.⁽⁹⁾ We have obtained⁽⁹⁾ analytic expressions for the probability distributions, moment generating functions, moments, and variance-to-mean ratios. Sums of Neyman Type-A and Thomas random variables have been shown to retain their form under the constraint of constant multiplication parameter. Conditions under which the Neyman Type-A and Thomas converge in distribution to the fixed multiplicative Poisson and to the Gaussian have been determined. This latter result is most important for it provides a ready solution to likelihood-ratio detection, estimation, and discrimination problems in the presence of many kinds of signal and noise. The doubly stochastic Neyman Type-A, Thomas, and fixed multiplicative Poisson distributions have also been considered.

A number of explicit applications are important. These include⁽⁹⁾ (1) the photon-counting scintillation detection of nuclear particles, when the particle flux is low, (2) the photon-counting detection of weak optical signals in the presence of ionizing radiation, and (3) the design of a star-

scanner spacecraft guidance system for the hostile environment of space. A number of more complex "contagious" distributions arising from multiplicative processes have also been investigated with particular emphasis on photon counting and direct-detection optical communications.

In the nuclear counting domain we often detect ionizing radiation optically through a radiation-matter interaction in which a single high-energy particle produces a shower of lower energy particles. A case in point is the scintillation detector which is a combination of a scintillation crystal (e.g., NaI:Tl, plastic) with a photomultiplier tube.⁽¹⁰⁾ When the incident high-energy particles (e.g., β , p , γ) are Poisson distributed, and when each particle produces a Poisson distribution of luminescence photons with a specified efficiency, such as occurs in fluorescence and phosphorescence, the resulting photon-counting distribution representing the signal is the Neyman Type-A. If Čerenkov radiation is also present, primary pulses will be registered and the outcome is the Thomas, assuming again that we are performing photon counting. It is usually assumed in the literature, generally tacitly, that the fixed multiplicative Poisson distribution describes the luminescence photon statistics and indeed, when the counting time is long and a is large, this is a good approximation. But if photon counting is used, and the luminescence is weak, it will be necessary to use the more accurate forms described above. Similar statistics will apply to the detection of cathodoluminescence and photoluminescence.

In certain applications where we wish to count the photons in an optical signal (e.g., in space), it sometimes happens that the distributions discussed in the previous paragraph are characteristics of the noise rather than of the signal. Viehmann and Eubanks^{(11),(12)} have discussed sources of noise in photomultiplier tubes in the radiation environment of space. Such noise may

arise from several mechanisms such as luminescence and Čerenkov radiation in the photomultiplier window; secondary electron emission from the window, photocathode, and dynodes; Bremsstrahlung in turn causing such secondary electron emission; cosmic-ray bursts; and, of course, thermionic emission dark current. These effects clearly degrade both the dynamic range and the photometric accuracy of low-light-level measurements, and therefore must be clearly understood. Photon counting can be particularly advantageous in such situations: Even if a large number of photoelectrons are produced by the Čerenkov radiation arising from a single charged particle (which constitutes noise in this case), they will be counted as only a single pulse since the Čerenkov radiation emission time is much shorter than the transit time in the photomultiplier.

The mathematical properties of the Neyman Type-A, Thomas, and fixed multiplicative Poisson distributions are very useful for the study of the performance of systems. The permanence under convolution of distributions with identical parameters a , α , or A facilitates their use in statistical detection and estimation problems for signal and noise distributions of arbitrary means.⁽¹³⁾ But it is the convergence in distribution of the Neyman Type-A and Thomas to the Gaussian that can simplify calculations quite a bit in many neural-, nuclear-, and photon-counting applications. In that limit (a, α finite, $W \rightarrow \infty$), the Neyman Type-A (Thomas) random variable with arbitrary $a(\alpha)$ may be added together with any number of arbitrary random variables that converge in distribution to the Gaussian (e.g., Poisson, binomial, Neyman Type-A, Thomas) to yield an overall Gaussian random variable with mean $\langle n \rangle = \sum_i \langle n_i \rangle$ and variance $\langle (\Delta n)^2 \rangle = \sum_i \langle (\Delta n_i)^2 \rangle$.

This is an important result because it means that the statistical decision theory and estimation theory literature relating to Gaussian random variables⁽¹⁴⁾ can be brought to bear on the problem. Some results that follow

are single-threshold detection,⁽¹⁵⁾ well-known solutions for estimation problems,⁽¹³⁾ and a simple form for the just-noticeable difference or detection law.⁽¹⁶⁾

The conveyance in distribution to the Gaussian is a very helpful tool, but a far more potent characterization is needed to properly deal with performance specifications (e.g., error rate) for a system incorporating a signal or noise specified by the Neyman Type-A or Thomas distribution.

We have recently developed a generalized performance parameter for single-threshold detection systems⁽¹⁷⁾ and this should prove very useful in just such a specification.

The performance of single-threshold communication systems can be characterized in a number of ways, including the probabilities of error, detection, and false alarm, the sensitivity (detectability), and the traditional signal-to-noise ratio (SNR). The SNR, which is a ratio of signal power to noise power, has a variety of specific definitions,⁽¹⁸⁾⁻⁽²⁴⁾ depending upon the particular application, is easy to measure experimentally in terms of peak or root mean-square values, and provides an accurate measure of performance for constant signals in Gaussian noise. In the Gaussian case, the SNR varies monotonically with the probability of error ϵ , and is therefore sufficient to describe system performance. In general, however, the SNR might not vary monotonically with ϵ , and is not necessarily sufficient as the sole measure of system performance.⁽²²⁾⁽²⁵⁾⁽²⁶⁾ The inadequacy of the SNR is evident where the noise is non-Gaussian or signal fluctuations are important, such as wave noise (photon bunching) in photocounting optical communication systems, and has been observed in both optical homodyne⁽²²⁾ and heterodyne⁽²⁵⁾ systems.

From the preceding discussion it is evident that it would be useful to obtain a generalized parameter which varies monotonically with system per-

formance. We have developed⁽¹⁷⁾ such a new generalized performance parameter that provides a more consistent measure of system performance than the conventional SNR. The analysis relies on a transformation of random variables which converts the Bayes risk for arbitrary statistics into an expression involving error functions only. A class of parameters p which vary monotonically with the Bayes risk was derived. It was shown explicitly that this parameter decreases monotonically as the Bayes risk and probability of error increase, and that it reduces to the SNR under appropriate conditions.

For example, for Neyman Type-A noise of mean $\langle n \rangle$ and Neyman Type-A signal-plus-noise of mean $\langle s \rangle + \langle n \rangle$, the traditional SNR has the form

$$\text{SNR} = \frac{\langle s \rangle}{[(\alpha+1)\langle n \rangle]^{1/2}} \quad (1)$$

where α is assumed to be the multiplication parameter of the signal and noise and the denominator corresponds to the noise energy. The generalized performance parameter for this case is

$$p = \frac{2}{\alpha+1} \left[\frac{\sqrt{t} - \langle (s+n) \rangle^{1/2}}{(\langle s \rangle + \langle n \rangle)^{1/2}} - \frac{\sqrt{t} - \langle \sqrt{n} \rangle}{\langle n \rangle^{1/2}} \right] \quad (2)$$

which is substantially different from the conventional SNR. In particular, a situation was investigated in which p was monotonic with system performance, but the SNR was not. The result is shown in Fig. 2, in which p indeed varies monotonically with system performance, whereas the SNR does not.

The above analysis, which utilizes normalizing transformations, is also useful in the direct calculation of the Bayes risk, probability of error, and sensitivity. It has led to a new technique⁽²⁷⁾ for evaluating optical communication system performance. This technique is most useful in situations where

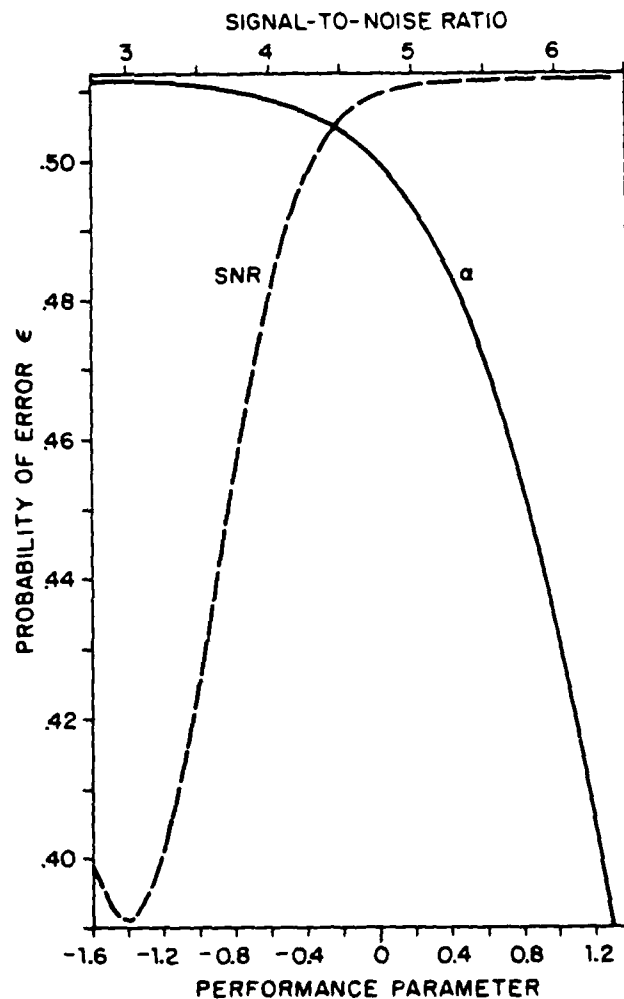


Figure 2: Linear plot of probability of error ϵ vs the SNR (dashed curve) and the generalized performance parameter (solid curve) for the case of a single observation of a Gaussian signal in additive, independent, standard Gaussian noise.

exact, explicit, closed form solutions exist for the photocounting cumulants, but do not exist for the photocounting distribution, such as in the generalized case of communication through lognormal atmospheric turbulence. Using this technique, theoretical probability of error curves were generated for communication through lognormal atmospheric turbulence, for a superposed coherent-in-chaotic signal, embedded in additive, independent Poisson noise, with arbitrary ratio of sampling time to source coherence time, arbitrary ratio of coherent to chaotic component, arbitrary mean frequencies of the coherent and chaotic components, and where the chaotic component need not be stationary and may have arbitrary spectral distribution. Since no solution exists for the photocounting distribution itself in this generalized case, the corresponding performance calculation has not previously been possible. As an example, Fig. 3 illustrates the probability of error versus SNR for a lognormally modulated superposed coherent-in-chaotic signal embedded in additive independent Poisson noise. Here β is the ratio of the detector counting interval to twice the coherence time of the source, and γ is the ratio of coherent to chaotic component. The case described applies to the detection of radiation originating from a multimode laser or scattered from a rough target, and passing through atmospheric turbulence.

*This research was also supported by the National Science Foundation under Grant NSF-ENG78-26498 and by the Jet Propulsion Laboratory, California Institute of Technology, under Contract Nos. 955335 and 955336.

- (1) J. Neyman, Ann. Math. Stat. 10, 35 (1939).
- (2) W. Feller, Ann. Math. Stat. 14, 389 (1943).
- (3) M. Greenwood and G. U. Yule, J. Royal Stat. Soc. Ser. A. 83, 255 (1920).
- (4) F. Eggenberger, Mitteilungen der Vereinigung Schweizerischer Versicherungs-Mathematiker, 31 (1924).
- (5) F. Eggenberger and G. Polya, Zeitschrift für Angewandte Mathematik und Mechanik, 1, 279 (1923).

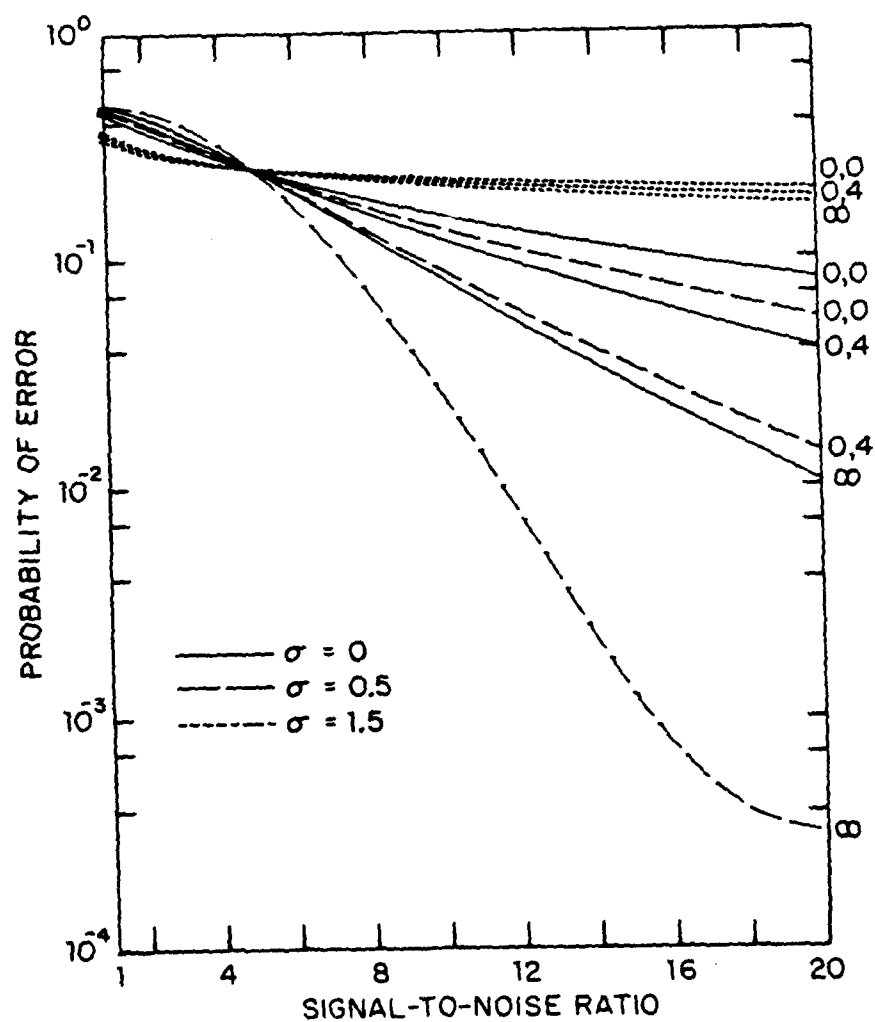


Figure 3: Probability of error $\Pr(\epsilon)$ vs SNR γ for single-detector Neyman-Pearson photocounting receiver. A lognormally modulated superposed coherent-in-chaotic signal (of Lorentzian spectrum with $\omega_c = \omega_r$) is embedded in additive independent noninterfering Poisson noise. Curves labelled ∞ correspond to $\beta \gg 1$, curves labelled 0.4 corresponded to $\beta \ll 1$ and $y = 4$, and curves labelled 0.0 correspond to $\beta \ll 1$ and $y = 0$. Here $\langle n \rangle = 1$, $t = 6$, and $P_F = 5.94 \times 10^{-4}$.

- (6) The negative binomial often masquerades under other identities, e.g., the Pascal, Greenwood-Yule, Polya-Eggenberger, and Polya. One simple example of the dual interpretation ascribable to the negative binomial arises in the photocounting detection of light. The Bose-Einstein distribution, which is a limiting case of the negative binomial, is observed when a photocathode is irradiated by chaotic (thermal) light and certain coherence and sampling conditions are obeyed. It may be considered as arising from the bunching of photons in the particle view of light (true contagion), or as reflecting the inhomogeneity of the radiation intensity in the semiclassical wave view of light (apparent contagion).
- (7) M. Thomas, *Biometrika*, 36, 18 (1949).
- (8) The reader is cautioned that terminology has changed over the years; what Feller (see Ref. 2) called a generalized Poisson distribution is now usually called a compound Poisson distribution, and we use this latter designation. And what Feller called a compound Poisson distribution (when the rate is a random variable) is now often referred to as a mixed Poisson distribution. When the rate is a random process, current terminology dictates using the modifier "doubly stochastic," though this designation is often used in place of mixed as well.
- (9) M. C. Teich, Role of the doubly stochastic Neyman Type-A and Thomas counting distributions in photon detection, *Appl. Opt.* (1981), to be published.
- (10) J. B. Birks, *The Theory and Practice of Scintillation Counting*, (Pergamon, New York, 1964).
- (11) W. Viehmann and A. G. Eubanks, "Noise limitations of multiplier phototubes in the radiation environment of space," (NASA Technical Note D-8147, Goddard Space Flight Center, Greenbelt, Maryland, March 1976).
- (12) W. Viehmann, A. G. Eubanks, G. F. Pieper and J. H. Bredekamp, *Appl. Optics*, 14, 2104 (1975).
- (13) J. F. Walkup and R. B. Asher, *Optics News*, 5 - No. 4, 8 (1979).
- (14) H. L. Van Trees, *Detection, Estimation, and Modulation Theory, Part 1*, (Wiley, New York, 1968).
- (15) P. R. Prucnal and M. C. Teich, *IEEE Trans. Inform. Theory*, IT-25, 213 (1979).
- (16) P. R. Prucnal and M. C. Teich, *J. Math. Psychol.* 21, 168 (1980).
- (17) P. R. Prucnal, *Appl. Opt.* 19, 3606 (1980).
- (18) C. W. Helstrom, *Statistical Theory of Signal Detection* (Pergamon Press, New York, 1960).

- (19) R. S. Kennedy, Fading Dispersive Communication Channels (Wiley, New York, 1969).
- (20) R. M. Gagliardi, Introduction to Communication Engineering (Wiley, New York, 1978).
- (21) L. E. Franks, Signal Theory (Prentice-Hall, New Jersey, 1969).
- (22) E. Jakeman, C. J. Oliver, and E. R. Pike, "Optical Homodyne Detection," Advances in Physics, vol. 24, pp. 349-404, May, 1975.
- (23) S. D. Personick, Proc. IEEE, 65, 1670 (1977).
- (24) A. Papoulis, Probability, Random Variables, and Stochastic Processes (McGraw-Hill, New York, 1965).
- (25) M. Elbaum and M. C. Teich, Opt. Comm. 27, 257 (1978).
- (26) M. Elbaum and P. Diamant, Appl. Opt. 15, 2268 (1976).
- (27) P. R. Prucnal, Appl. Opt. 19, 3611 (1980).

C. PHOTON COUNT ANTIBUNCHING FOR OPTICAL COMMUNICATIONS, RADAR,
IMAGING, AND SPECTROSCOPIC APPLICATIONS *

(M. C. Teich, G. Vannucci, N. Pierce, R. O'Connor)

(Principal Investigator: M. C. Teich (212) 280-3117)

The probability distribution for a dead-time-modified pulse counter^{(1),(2)} has been studied by a number of researchers in a broad variety of disciplines, such as photon counting,⁽³⁾⁻⁽⁹⁾ nuclear counting,⁽⁸⁾⁻⁽¹²⁾ and neural counting.^{(5),(8),(13),(14)} Many cases have been studied in detail, including paralyzable and nonparalyzable counting under blocked, unblocked, and equilibrium conditions. Attention has also been given to the gradual recovery (sick-time) system and to the variable dead-time case.^{(2),(14)} Müller has summarized the results of a number of authors^{(11),(12)} and has compiled a comprehensive bibliography on dead-time effects.⁽¹⁵⁾

Although most of the work cited above is applicable only when the input to the counter is a Poisson point process with constant rate, a few results are also available for the case in which the rate is not constant. Cantor and Teich,⁽⁴⁾ Teich and McGill,⁽⁵⁾ and Bédard⁽³⁾ present expressions for the photocounting distribution when the intensity of the light is a random process, with the sampling time much smaller than the coherence time of the light.

In a prior work,⁽¹⁶⁾ we obtained expressions for the mean and the variance of the number of events in a fixed sampling time for a nonparalyzable dead-time counter when the input process is Poisson with a rate that is a known function of time. We have now extended those results to the case in which the rate of the input process is an arbitrary stochastic process, under the constraint that it vary slowly with respect to the duration of the dead time.⁽¹⁷⁾ No constraints on the sampling time are imposed. We have shown

how the dead-time-modified mean and variance depend on the first- and second-order statistics of the rate. In the context of the detection of light, we have obtained explicit expressions for the photocount mean and variance for chaotic radiation of arbitrary spectral properties. Although the magnitude of the variance depends explicitly on the power spectrum of the radiation in the absence of dead time, it has been shown that the decrease in variance with increasing dead time is basically spectrum independent. Analytical and graphical results for the dead-time-modified mean and variance are therefore now available for chaotic light of Lorentzian and Gaussian spectra.

The principal results of this effect comprise analytic expressions, complemented by computer results, for the mean and variance of a dead-time-modified Poisson counting process driven by a continuous rate process representative of chaotic radiation. (It has been assumed that the nonparalyzable dead time is small in comparison with the coherence time (inverse bandwidth) of the light.) In this limit, as well as in the absence of dead time, the photocount mean is explicitly shown to depend only on the first-order statistics of the radiation (see Fig. 1). As was expected, the counting efficiency lies below that for a constant intensity source for all values of the dead-time parameter $\bar{\lambda}\tau_d$, where $\bar{\lambda}$ is the mean driving rate and τ_d is the dead time.

The photocount variance, on the other hand, exhibits a strong dependence on the spectral properties of the radiation even in the absence of dead time (see Fig. 2). The forms of the dead-time-modified analytic expressions for the cases of Lorentzian and Gaussian spectra are therefore substantially different. Nevertheless, numerical computer evaluation of these expressions (variance as a function of $\bar{\lambda}\tau_d$) demonstrates that the effect of dead time on the variance is essentially independent of the spectral shape of the light, (see Fig. 3) although a dependence can be discerned to develop at higher

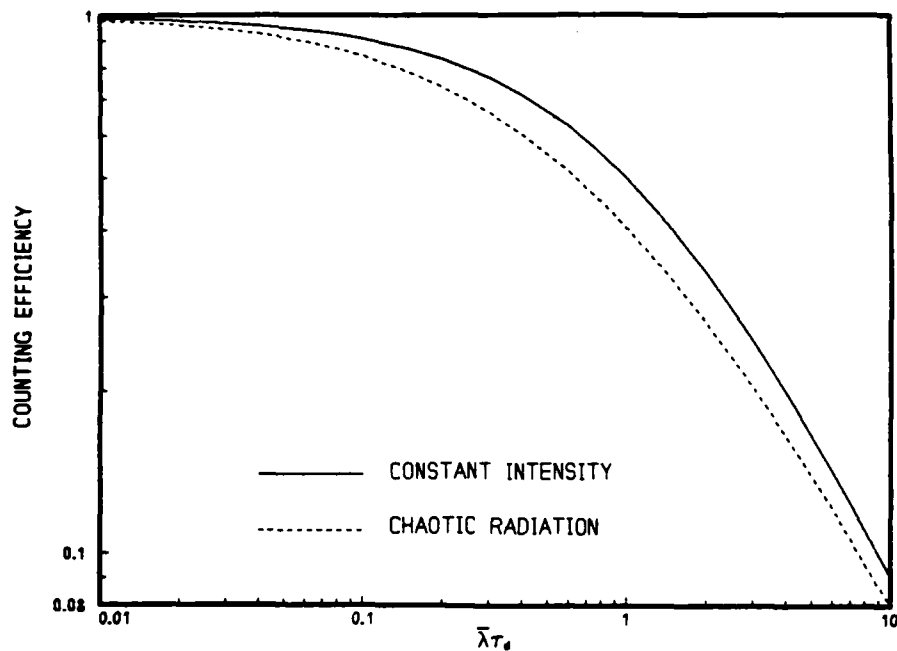


Figure 1: Counting efficiency ($E[n]/\bar{\lambda}T$) versus $\bar{\lambda}\tau_d$, where $\bar{\lambda}$ is the driving rate and τ_d is the dead time. Curves are for a Poisson process in which the rate is constant (solid curve) and for chaotic radiation of arbitrary spectrum (dashed curve). It is clear that the efficiency is significantly reduced (up to 24%) when the rate is not constant. The results are analogous to those presented in Fig. 1 of Ref. 16 for a rate that is a known function of time.

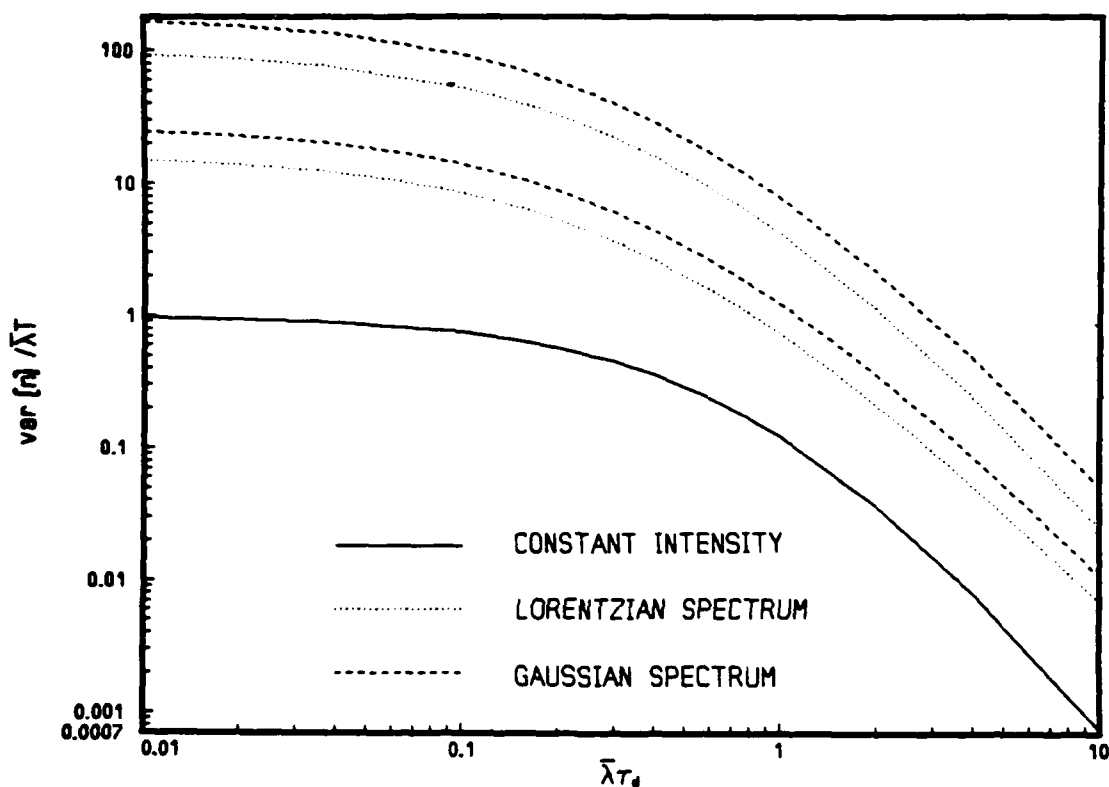


Figure 2: Ratio of dead-time-modified variance to unmodified mean ($\text{var}[n]/\lambda T$) versus $\lambda \tau_d$ for a Poisson process with constant rate (solid curve), for chaotic radiation with Gaussian spectrum (dashed curves), and for chaotic radiation with Lorentzian spectrum (dotted curves). The values of the parameters for the chaotic radiation curves are $\Gamma T = 100$, $\lambda T = 10,000$ (upper curves) and $\Gamma T = 2$, $\lambda T = 40$ (lower curves). The vertical separation between any of the curves for chaotic radiation is essentially independent of $\lambda \tau_d$, an indication that the different curves are scaled versions of one another. Thus the normalized variance will be essentially the same for all four curves, as is demonstrated in Fig. 3.

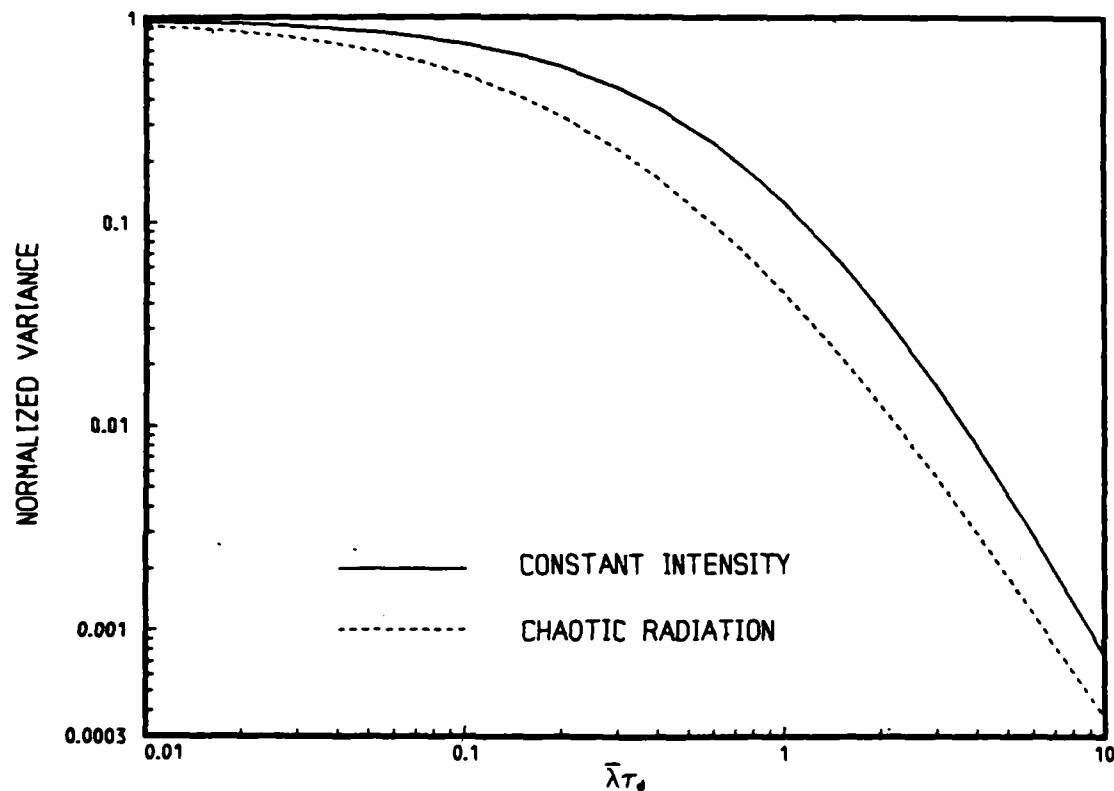


Figure 3: Normalized variance (ratio of dead-time-modified variance to unmodified variance) versus $\bar{\lambda}\tau_d$. Curves are for a Poisson process with constant rate (solid curve) and for chaotic radiation (dashed curve). All results were obtained under the assumption that the dead time is much shorter than the coherence time ($\tau_d \ll 1/\Gamma$), in which case the effect of dead time turns out to be virtually independent of spectral shape (see text). The normalized variance is therefore the same function of $\bar{\lambda}\tau_d$ for all types of chaotic radiation. The results are similar in character to those presented in Fig. 2 of Ref. 16 for a rate that is a known function of time.

values of $\bar{\lambda}\tau_d$. This can be understood by noting that our results are applicable only when the dead time is much shorter than the coherence time ($\tau_d \ll 1/\Gamma$). For sufficiently small τ_d , the rate of the Poisson process can be locally approximated as being constant so that the dead-time-modified point process has a rate that is locally a function of the unmodified rate only and as such is not influenced by the second-order statistical properties of the radiation.

In light of our results, we may expect that the dead-time-modified count variance will exhibit an increasing dependence on the spectrum as τ_d becomes larger; indeed, this dependence should become substantial as τ_d approaches $1/\Gamma$. An analysis in that regime, although difficult to carry out, might therefore lead to the intriguing possibility of using a dead-time counter to extract spectroscopic information about a radiation source. The notion of dead-time spectroscopy is not unlike photocounting spectroscopy,⁽⁶⁾ but the upper limit of bandwidths that could be measured by the technique would be ~ 10 GHz. This value is higher than the upper limit for photocounting spectroscopy, ~ 100 MHz, because the dead time can in principle be made about a factor of 100 smaller than the 10-nsec minimum counting time in which variations can be detected with commercially available fast electronic circuits. The region of usefulness of dead-time spectroscopy would probably be similar to that of the Fabry-Perot étalon.

Finally, we point out that the dead-time-modified count mean may also depend on the spectral properties of the light for $\tau_d \sim 1/\Gamma$, in which case dead-time spectroscopy could be implemented quite easily. Kikkawa et al.⁽¹⁸⁾⁽¹⁹⁾ have calculated the efficiency (normalized mean) of a dead-time-modified photon counter for Lorentzian light and have discussed the dependence of

this quantity on spectral parameters. Their results are valid only in the limit where the coherence time is much smaller than the mean time interval between pulses, however, and this is not a useful region [see remarks following Eq. (10) in Ref. 18].

*This research was also supported by the National Science Foundation under Grant NSF-ENG78-26498.

- (1) W. Feller, "On probability problems in the theory of counters," in Studies and Essays: A Volume for the Anniversary of Courant (Wiley, New York, 1948), p. 105.
- (2) E. Parzen, Stochastic Processes (Holden-Day, San Francisco, 1962), pp. 117-186.
- (3) G. Bédard, Proc. Phys. Soc. 90, 131 (1967).
- (4) B. I. Cantor and M. C. Teich, J. Opt. Soc. Am. 65, 786 (1975).
- (5) M. C. Teich and W. J. McGill, Phys. Rev. Lett. 36, 754 (1976).
- (6) B. Saleh, Photoelectron Statistics (Springer-Verlag, Berlin/Heidelberg/New York, 1978), pp. 101-102, 116, 175, 272-279.
- (7) M. C. Teich and G. Vannucci, J. Opt. Soc. Am. 68, 1338 (1978).
- (8) M. C. Teich and B. I. Cantor, IEEE J. Quantum Electron. QE-14, 993 (1978).
- (9) G. Vannucci and M. C. Teich, Appl. Opt. 18, 3886 (1979).
- (10) I. DeLotto, P. F. Manfredi, and P. Principi, Energ. Nucl. (Milan) 11, 557 (1964).
- (11) J. W. Müller, Nucl. Instrum. Methods 112, 47 (1973).
- (12) J. W. Müller, Nucl. Instrum. Methods 117, 401 (1974).
- (13) L. M. Ricciardi and F. Esposito, Kybernetik 3, 148 (1966).
- (14) M. C. Teich, L. Marin, and B. I. Cantor, J. Opt. Soc. Am. 68, 386 (1978).
- (15) J. W. Müller, ed., "Bibliography on dead time effects," Bureau International des Poids et Mesures, Sèvres, France, Report No. BIPM-75/6, 1975 (unpublished); update (1981).
- (16) G. Vannucci and M. C. Teich, Opt. Commun. 25, 267 (1978).

- (17) G. Vannucci and M. C. Teich, J. Opt. Soc. Am. 71, 164 (1981).
- (18) A. Kikkawa, K. Ohkubo, H. Sato, and N. Suzuki, Opt. Commun. 12, 227 (1974).
- (19) A. Kikkawa, K. Ohkubo, T. Yoshimura, and N. Suzuki, Jpn. J. Appl. Phys. 13, 1226 (1974).

II. PHYSICAL PROPERTIES AND EFFECTS IN ELECTRONIC MATERIALS

A. CARRIER TRANSPORT ACROSS HETEROJUNCTION INTERFACE *

(C. M. Wu, E. S. Yang)

(Principal Investigator: E. S. Yang (212) 280-3120)

In our previous study, we have calculated the quantum transmission coefficient⁽¹⁾ by solving Schrodinger's equation across the heterojunction potential barrier in which the perpendicular momentum is conserved.⁽²⁾ Application of our model to an N-p heterojunction shows that its forward current may be dominated by either thermionic emission or tunneling current if the effective masses of both sides of the junction are much smaller than the free electron mass.⁽³⁾ In most cases, however, the thermionic emission current is large compared with the diffusion current so that the forward current is controlled by minority carrier diffusion. As for a p-P heterojunction, rectifying characteristics are obtained. However, the reverse current appears to be non-saturated, but the forward current remains constant at large forward voltage. These results are in agreement with our experiment data and have been confirmed by others.⁽⁴⁾

An important consideration not included in the previous calculation is the charge in the heterojunction interface. Kroemer et al⁽⁵⁾ showed that the charge of the interface state should be taken into account for the band diagram calculation. Since the potential notch formed at the narrow band-gap side can trap injected carriers under forward bias, we find it necessary to include the electron accumulation there. In our work, an $\text{Al}_{.35}\text{-Ga}_{.65}\text{-As}$ GaAs N-p heterojunction is fabricated by the LPE technique. The N-type epitaxial layer is grown on the p-type substrate at 789°C with a cooling rate of $0.2^{\circ}\text{C}/\text{min}$. Multilayer ohmic contacts, Sn-Au-Ni and Zn-Au-Ni , are deposited on the n-side and p-side

respectively. The experimental devices's current-voltage characteristics deviate significantly from the exponential form, particularly at high bias voltage as if a large series resistance were in the structure. The series resistance thus obtained is, however, too large for the given bulk doping and does not agree with that of the control sample. By taking into account the carrier accumulation in the potential notch, we are able to explain the nature of current suppression through the modulation of the effective barrier height. The result explains the discrepancy between the theoretical prediction and experimental data reported by Kroemer et al.⁽⁵⁾ In addition, the activation energy from the temperature data as a function of bias is found to be a convenient way of measuring the conduction band discontinuity at the heterojunction interface (Fig. 1).

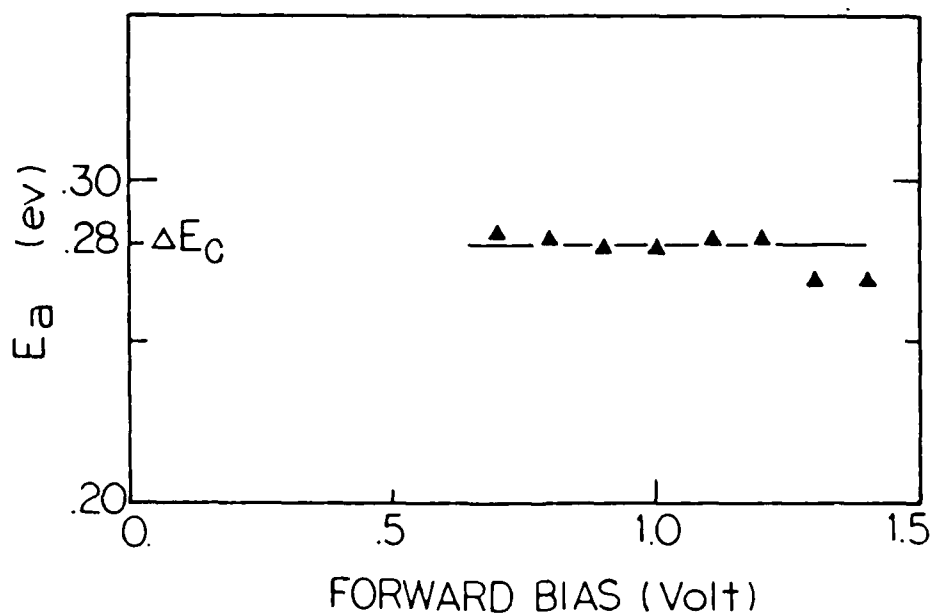


Figure 1

* This research was also supported by the National Science Foundation under Grant NSF-ENG78-19426.

- (1) C. R. Crowell and S M. Sze, J. Appl. Phys. 37, 2683 (1966).
- (2) E. O. Kane, J. Appl. Phys. 32, 83 (1961).
- (3) C. M. Wu and E. S. Yang, Solid-State Electronics 22, 241 (1979).
- (4) A. Chandra and L. F. Eastman, Solid-State Electronics 23, 599 (1980).
- (5) H. Kroemer, W. Y. Chien, H. C. Casey Jr., and A. Y. Cho, Appl. Phys. Lett. 33, 749 (1978).

B. ELECTRONIC PROPERTIES OF POLY Si-Si DIODES*

(C. M. Wu, E. S. Yang)

(Principal Investigator: E. S. Yang (212) 280-3120)

Low temperature processes for forming a rectifying junction are attractive in the production of low-cost solar cells⁽¹⁾⁻⁽³⁾ and in possible applications in low-performance active structures.⁽⁴⁾⁽⁵⁾ In this letter, we report a new low-temperature method of preparing an aluminum-diffused p^+-n junction by making use of the high diffusivity of Al in poly-silicon.⁽⁶⁾ Experimental I-V and C-V curves are shown along with a simple model to explain the data.

The fabrication procedure of the aluminum-diffused polysilicon p^+-n junction starts with E-beam evaporated multi-layers (100 \AA Si-2000 Al-1000 \AA Si) on an n-type (111) silicon substrate ($1 \sim 2 \text{ cm}$) as shown in the insert of Fig. 1. It is followed by heat-treatment (HT) at 600°C in flowing hydrogen for one hour. Thus, an Al-riched p-type polycrystalline layer is formed, which may be used as an Al-diffusion source if a subsequent drive-in process is employed.⁽⁷⁾ It is important to note that the cap silicon layer and the hydrogen gas are employed to prevent the aluminum film from reacting with the environment at the HT.⁽⁸⁾ The HT temperature should not be higher than the Al melting point (660°C). Here, the p^+-n junction under investigation is a device without the drive-in step and the p^+ -layer is a polycrystalline silicon layer. After making ohmic contact on the back side, we measure the I-V and C-V characteristics at different temperatures. We also find that a diode fabricated with a thin Al film (100 \AA) gives similar electric properties with good transparency, but with a large series resistance.

The room temperature I-V curves are shown in Fig. 1. The forward current magnitude is much higher than that obtained in the single crystal p^+-n junction ($J_0 \sim 10^{-10} \text{ amp/cm}^2$). A plausible interpretation is that the p-type polycrystalline layer is full of localized states caused by grain boundaries

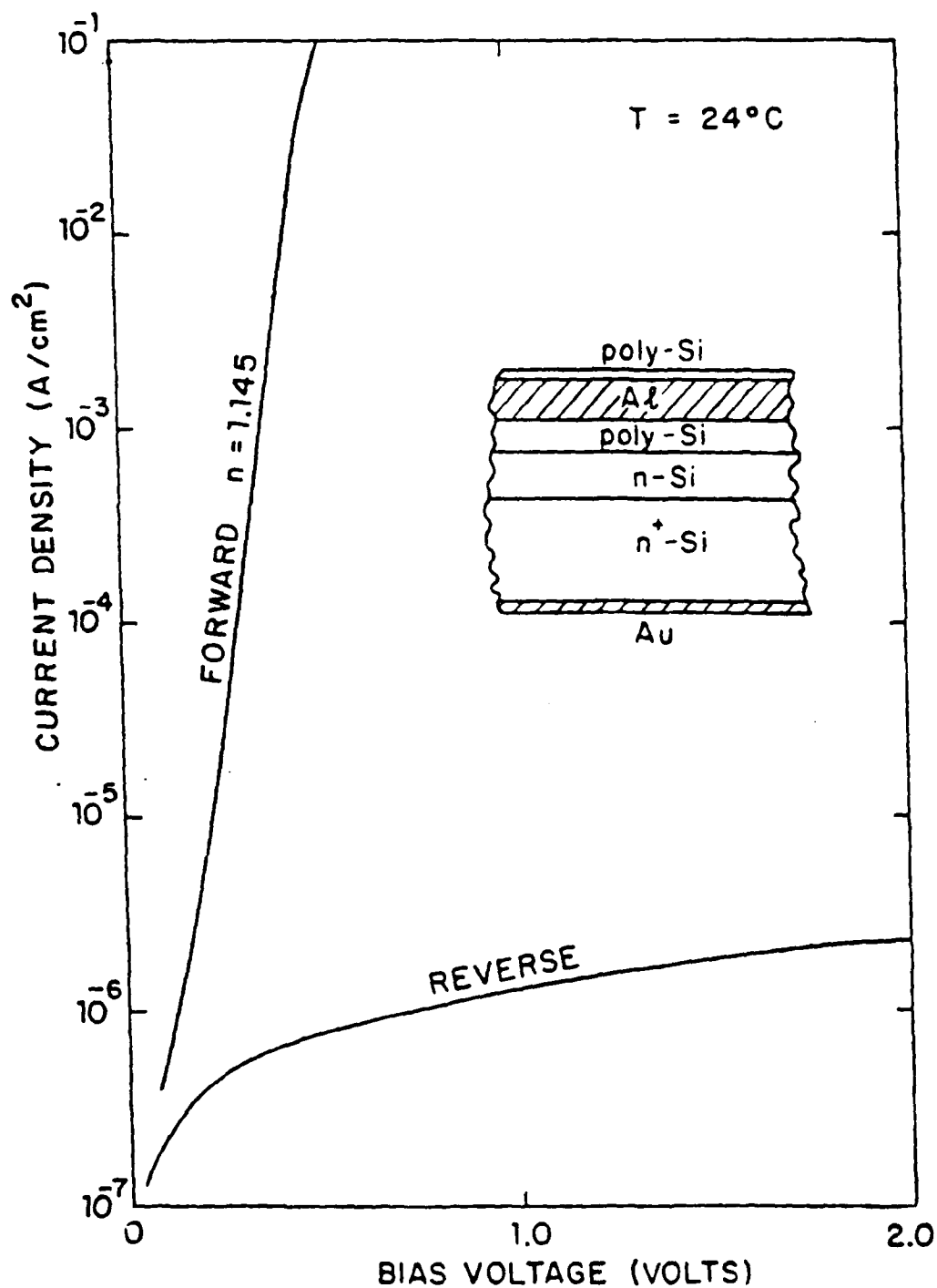


Figure 1: The I-V characteristics of the p^+n junction at room temperature. The insert is a structure of the diode before the heat-treatment.

and dislocation networks where electrons recombine after injection from the single-crystal n-type region.

Since the silicon film is evaporated without substrate heating, the grain size is very small, and the mobility is low. As a result, the diffusion length of electrons in Al-doped polysilicon layer is short, and carrier recombination mostly occurs at the interface between the polysilicon and the single crystal substrate. If we assume a constant recombination velocity S , the total forward current is equal to the electron current, which is given by

$$J = qSN_d \exp\left(-\frac{q\phi_D}{kT}\right) \quad (1)$$

where N_d is the donor density, and ϕ_D is the built-in potential only in the n-side. However, ϕ_D is a function of the bias voltage and is given by

$$\phi_D = \frac{V_{bi} - V}{1 + N_d/N_a} \quad (2)$$

where V_{bi} is the zero-bias built-in potential across the whole junction, V is the bias voltage, and N_a is the doping in the polysilicon layer.

Therefore, the forward current can be rewritten as

$$J = J_o \exp\left(\frac{qV}{nkT}\right) \quad (3)$$

and

$$J_o = qSN_d \exp\left[-\frac{qV_{bi}}{nkT}\right] \quad (4)$$

where n is equal to $1 + N_d/N_a$. The C-V and I-V characteristics are measured at different temperatures from -60°C to 60°C . The slope of the $1/C^2$ curve versus the bias voltage does not vary with temperature and gives the impurity density of the lightly-doping side,⁽⁹⁾ which is $6.7 \times 10^{15} \text{ cm}^{-3}$ and is consistent with the impurity of the n-side. The extrapolation of the $1/C^2$ curve

intersects the voltage axis at ϕ_{int} and yields the built-in potential $V_{\text{bi}} = \phi_{\text{int}} + 2 kT/q$ ⁽⁹⁾ at zero bias. The zero-bias current J_0 can be obtained by the extrapolation of the I-V curve to the current axis. Table I lists the experimental values of J_0 and n from the I-V data and ϕ_{int} from the C-V data. It is noted that the ideality factor (n -value) decreases as the temperature increases. According to the relation of the doping density to the n -value, the impurity density of the p-type region can be deduced and is listed in Table I. It is observed that the active impurity density in the polysilicon increases with the temperature. This is probably due to the high ionization energy of aluminum in silicon (0.057 eV). As a result, some of the aluminum atoms are not electrically active in the polysilicon.

By considering the variation of the Fermi potentials with the temperature on both sides, we obtain the sum of the built-in potential V_{bi} and the Fermi potentials which is equal to the energy gap with an error of 2%. Therefore, the zero-bias current density J_0 has a temperature-dependent activation energy which is predicted by Eq. (4). Using a recombination velocity of 5×10^4 cm/sec at 0°C and assuming S to be proportional to the thermal velocity, we obtain the theoretical values of J_0 by Eq. (4), as shown by the solid line in Fig. 2. We find that our simple model is in agreement with the experimental data obtained from I-V data when the temperature is higher than -40°C. In Eq. (1), we consider the electron current as the dominant component and this might not be true below -40°C. For example, the recombination in the depletion region may be higher than the electron current. However, the conduction mechanism does not conform to the simple model at temperatures below -40°C.

According to the above discussion, the injected electrons from the n-side are recombined at the interface between the p^+ -polysilicon layer and the crystalline substrate and the recombination velocity S here should be in the order

Table I. Experimental data from I-V and C-V curves
and the Fermi-potential V_n at the n-side.

T(°C)	I-V		C-V	$N_a (x 10^{16} \text{ cm}^{-3})$
	n-value	J_o (Amp)	ϕ_{int} (volt)	
-60	1.349	1.17×10^{-13}	0.817	1.9
-40	1.233	7.18×10^{-13}	0.793	2.9
-20	1.215	1.60×10^{-11}	0.763	3.1
0	1.200	3.10×10^{-10}	0.735	3.4
20	1.170	2.85×10^{-9}	0.709	3.9
40	1.166	3.33×10^{-8}	0.677	4.0
60	1.165	2.51×10^{-9}	0.650	4.1

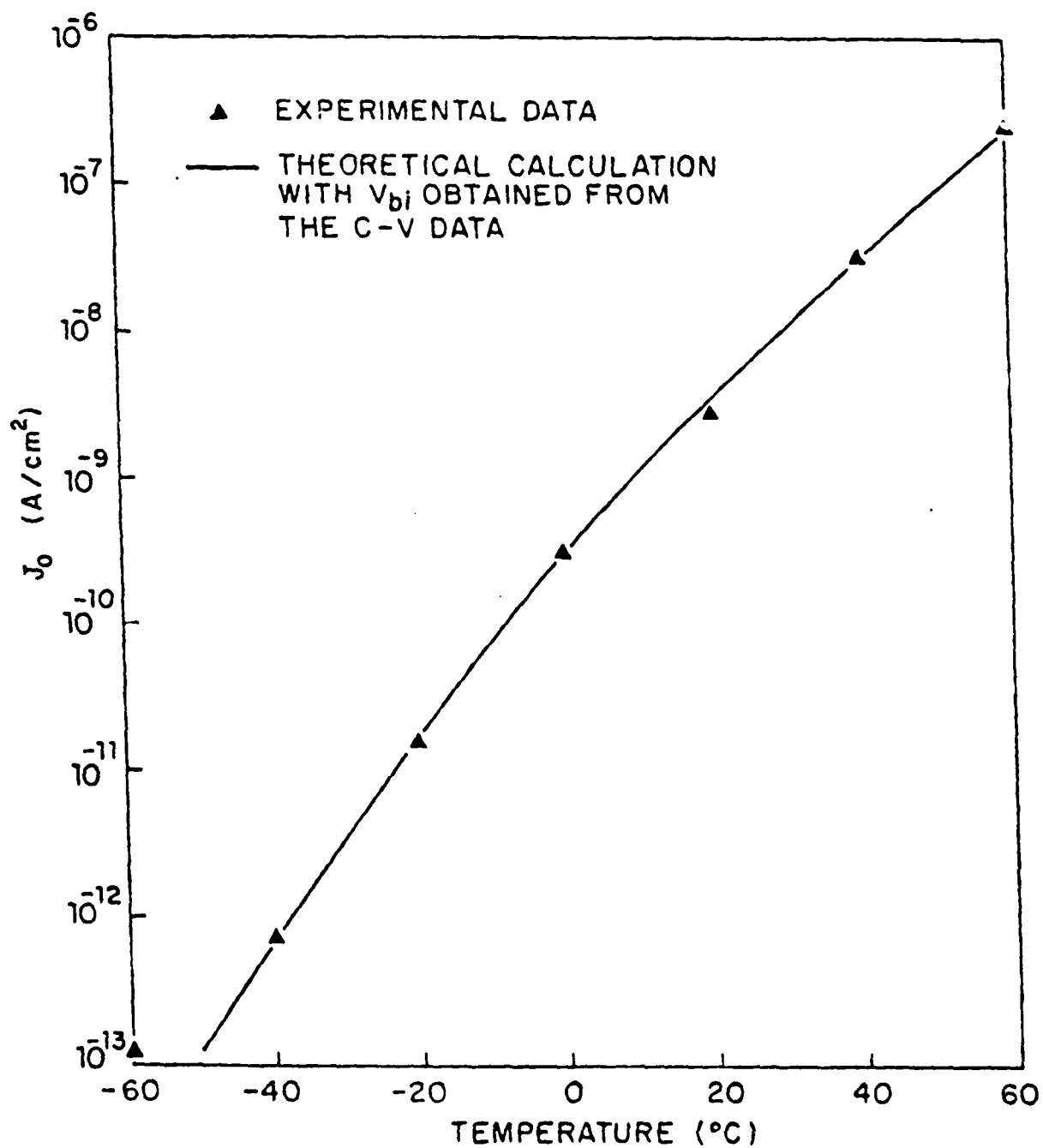


Figure 2: Theoretical calculation of J_0 using V_{bi} (from C-V data) and experimental data of J_0 (from I-V data).

of that found at the grain boundaries of polysilicon. Our empirical value of S is consistent with Ghosh's result (3×10^4 cm/sec).⁽¹⁰⁾

In summary, we have developed a method using aluminum as the p-type impurity to form a polysilicon-silicon p^+-n junction at low temperatures. Because of the simplicity in the fabrication process, this rectifying junction may provide a low-cost method of producing solar cells. However, thinner aluminum ($< 50 \text{ \AA}$) and polysilicon ($< 100 \text{ \AA}$) layers will be necessary to improve the transparency and to lower the series resistance. Further studies are required to obtain the optimum structure.

*This research was also supported by the Department of Energy under Contract DOE/SERI xz-φ-9226.

- (1) A. P. Genis, P. A. Smith, K. Emery, R. Singh, and J. B. DuBow, Appl. Phys. Lett. 37, 77 (1980).
- (2) W. A. Anderson, G. Rajeswaran, K. Rajkanan, and G. Hoeft, IEEE Electron Device Lett. 1, 128 (1980).
- (3) C. M. Wu, E. S. Yang, W. Hwang, and H. C. Card, IEEE Trans. Electron Devices, ED-27, 687 (1980).
- (4) T. I. Kamins and P. J. Marcous, IEEE Electron Device Lett. 1, 159 (1980).
- (5) J. F. Gibbons and K. F. Lee, IEEE Electron Device Lett. 1, 117 (1980).
- (6) J. C. M. Hwang, P. S. Ho, J. E. Lewis, and D. R. Campbell, J. Applied Phys. 51, 1576 (1980).
- (7) C. M. Wu and E. S. Yang, unpublished.
- (8) C. M. Wu and E. S. Yang, J. Appl. Phys. 51, 5889 (1980).
- (9) S. M. Sze, "Physics of Semiconductor Devices", (J. Wiley, New York, 1969), Chapter 3, pp. 77-90.
- (10) A. K. Ghosh, C. Fishman, T. Feng, J. Appl. Phys. 51, 446 (1980).

C. LASER PROCESSED SCHOTTKY BARRIERS*

(E. S. Yang, C. M. Wu, H. J. Vollmer,[†] T. O. Sedgwick,[†] R. T. Hodgson[†])

(Principal Investigator: E. S. Yang (212) 280-3120)

We report a novel technique for fabricating Schottky barrier junctions by laser-irradiation process (LIP). Both pulsed and cw irradiation have been employed. The electrical characteristics of the LIP diodes are presented.

The devices were prepared by depositing 2000-Å-thick aluminum dots on n/n^+ (100) silicon wafers. The resistivity of the n -epilayer was measured to be $0.4 \Omega\text{cm}$. Half of the Al dots were covered by a 100-Å-thick e-beam-evaporated silicon film. Gold was evaporated on the back side of the wafer to provide a good ohmic contact to the n^+ substrate. The current-voltage characteristics of these devices were tested before LIP and were found to be ohmic with a low resistance. The devices were then subjected to either the pulsed or cw laser irradiation. In the pulsed LIP, we used a Q-switched Nd:YAG laser ($\lambda = 1.06 \mu\text{m}$) with a pulse width of 60 ns and energy density of approximately 1 J/cm^2 . The substrate is not heated. The aluminum dots without the silicon top layer did not show any change in their electrical characteristics although damage in aluminum was seen. However, dots with a silicon cover layer showed striking transformation. In the cw LIP, we used an argon laser (4880 and 5145 Å) operated between 10 and 13 W and focused to a spot size of $50 \mu\text{m}$. The spacing between adjacent scanning lines is $20 \mu\text{m}$ so that complete coverage of the surface by the laser beam is ensured. The substrate temperature was set at 350°C (the minimum temperature in the experimental setup) and the stepping motor movement (with a speed of 2 cm/sec) gives rise to overlapping spots of laser irradiation. Again, the dots without the silicon cover layer appeared to be unaffected by the laser beam. In contrast, rectifying characteristics are plotted in Fig. 1 for diodes obtained by both

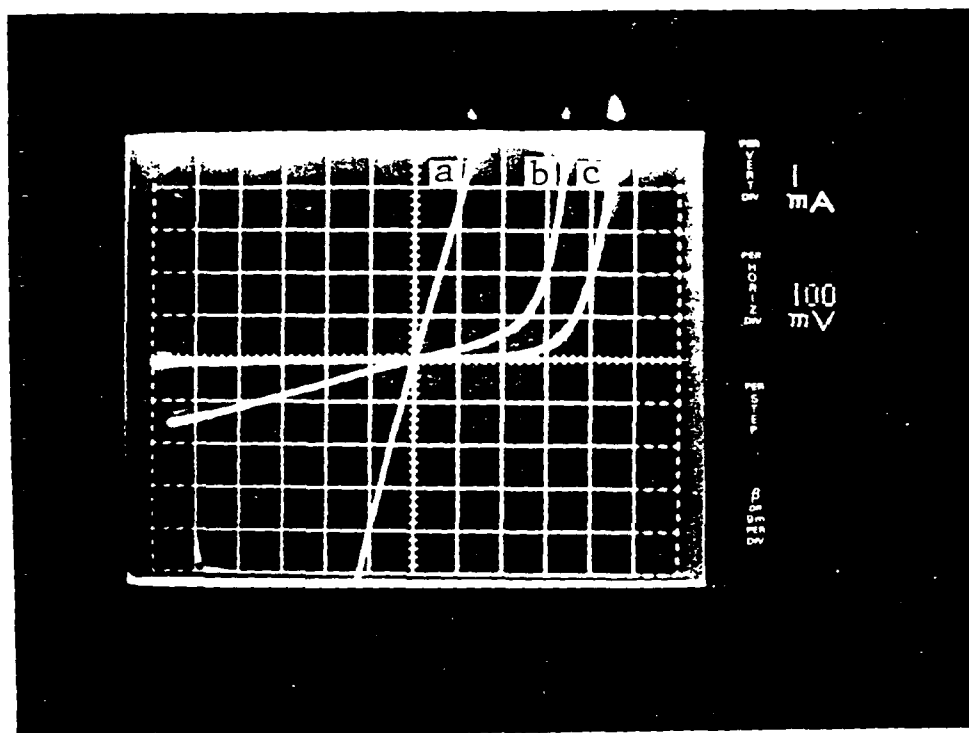


Figure 1: Current-voltage characteristics of Schottky diodes: (a) before laser irradiation, (b) after pulse Nd:YAG laser LIP, and (c) after cw argon laser LIP.

cw and pulsed LIP. The calculated barrier height from capacitance-voltage data is 1 eV, which is very close to the band-gap energy. The cw LIP produces diodes with a lower current at the same bias voltage. The higher current in the pulsed LIP diodes is caused by incomplete treatment of the dots since manual scanning was employed. The aluminum layer appears to have melted, and the surface damage is severe and not uniform.

For aluminum dots without a silicon cover, it appears that the laser light is not absorbed because of the reflection of the aluminum surface. The silicon cover facilitates strong absorption so that heating of the Al-Si

interface is effected. It is reasonable to assume that the surface temperature is higher than the Al-Si eutectic so that the aluminum-silicon interface melts and recrystallizes. Furthermore, part of the aluminum may have diffused into silicon to form a p^+ region. The resulting structure is an Al- P^+ -n Si Schottky barrier with a thin p^+ layer located within the junction space-charge region underneath the surface. The barrier height of the untreated Al-n Si contact is very low because of the low work function of aluminum; therefore the contact is ohmic, as shown in curve (a) of Fig. 1. The introduction of aluminum forms a thin p^+ layer and gives rise to p-n junction-like characteristics Figs. 1(b) and 1(c). However, the new rectifier differs from the p-n junction in that the p^+ region is completely depleted. This leads to the features of high barrier height and an ideality factor substantially larger than unity. These results are similar to those for thermally annealed Schottky diodes⁽¹⁾ and are in agreement with the simple model proposed recently by Van der Ziel.⁽²⁾ The large current in the low-bias regime with $n=3$ is likely to be the result of surface recombination.

In conclusion, we have found that a rectifying junction can be formed by laser irradiation. The ohmic contact of Al on n-Si has been converted to a Schottky barrier with a large barrier height. The characteristics of these diodes are comparable to those of thermally annealed Al-n-Si Schottky barriers. Because of its inherent advantage of low temperature (except in the junction region), LIP technology may be important in device applications.⁽³⁾

*This research was also supported by the National Science Foundation under Grant NSF-ENG-78-19426.

†IBM T. J. Watson Research Center, Yorktown Heights, N. Y. 10598

- (1) C. M. Wu and E. S. Yang, J. Appl. Phys. 51, 5889 (1980).
- (2) A. Van der Ziel, Solid State Electron 20, 269 (1977).
- (3) H. C. Card, E. S. Yang, and P. Panayotatos, Appl. Phys. Lett. 30, 643 (1977).

D. ELECTRON TRAPS IN ZINC SILICATE PHOSPHORS

(E. S. Yang, J. M. Brownlos⁺)

(Principal Investigator: E. S. Yang (212) 280-3120)

In the study of Zn_2SiO_4 : Mn (willemite) Phosphors, it has been observed that the phosphorescent decay can be described by three or more time constants, the shortest of which is typically between 10 and 20 ms. This short time constant is believed to be limited by the intrinsic Mn^{++} radiative transition rate. The long decay time constants are, however, related to the release of electrons from deep traps. Although deep traps have been determined by thermoluminescence experiments, there has been little published work attempting to correlate these trap distributions to the phosphorescent decay data. The difficulty is that the phosphorescent decay time in willemite crystals is found to be weakly dependent on temperature.⁽¹⁾ This is contrary to the strong temperature dependence of decay time expected from thermally activated traps. Here, we present measurements on the thermal dependence of decay curves of willemite phosphors for correlation with trap distribution measurements made on the same samples.

In our experiments, we have used different types of willemite samples including commercial P1 and P39 as well as specially prepared phosphores prepared. The powder phosphor is placed in a sample holder within an evacuated chamber and its temperature can be varied between 100 K and 670 K. The excitation source is a dc mercury lamp whose light passes through an input monochromator set at 2536 Å. Details of the experimental setup have been given in a previous paper.⁽²⁾ With the same experimental arrangement we obtain the thermoluminescent (glow curve) and phosphorescent decay data. A typical glow curve of a zinc silicate phosphor has four glow peaks, and the corresponding trap depths are calculated to be 0.13, 0.24, 0.53, and 0.87 eV. We then measure the phosphorescent decay at the temperatures corresponding

to the minima in the glow curve so as to determine the decay time constant for the trap next to the minimum on the high temperature side. The results are shown in Fig. 1. It is noted that the decay time cannot be described by a single exponential term and the initial decay rate does not change by more than a factor of 2 for a wide range of temperatures. In addition, the decay time increases between -170°C and -48°C , then drops at 0°C and eventually goes back up at 46°C . This fluctuating behavior is observed in all samples showing multiple peaks in the thermoluminescent experiment.

The B725 sample has very different characteristics. This phosphor is prepared by using a mixture of ZnO , SiO_2 , and MnO fired at 1150°C for 15 minutes. It is subsequently ground to powder and refired. The glow curve of B725 has a single peak which is unique among willemite crystals, and it has an activation energy of 0.433 eV. The decay curves depicted in Fig. 2 show a monotonic decrease of the first time constant with increasing temperature. In other words, when there is only one trap, the decay time constant does not increase at any temperature in contrast with the multiple-trap behavior of P1 shown in Fig. 1.

When arsenic is introduced in small dosages ($\sim 0.1\%$), the willemite is known as P39 and the characteristics are substantially modified. The glow curve of P39 is found to have one main peak near 0°C and two other widely separated peaks. The trap energies are calculated to be 0.334, 0.63, and 1.78 eV, and the temperature dependence of the decay curves is similar to that shown in Fig. 1.

By examining the change of intensity and of half-width of the glow curves, we find that the data of P1 follow closely the pattern described by Cher⁽³⁾ and Kivits.⁽⁴⁾ If the thermal release of electrons from the trap is monomolecular, then the decay should have a single time constant.

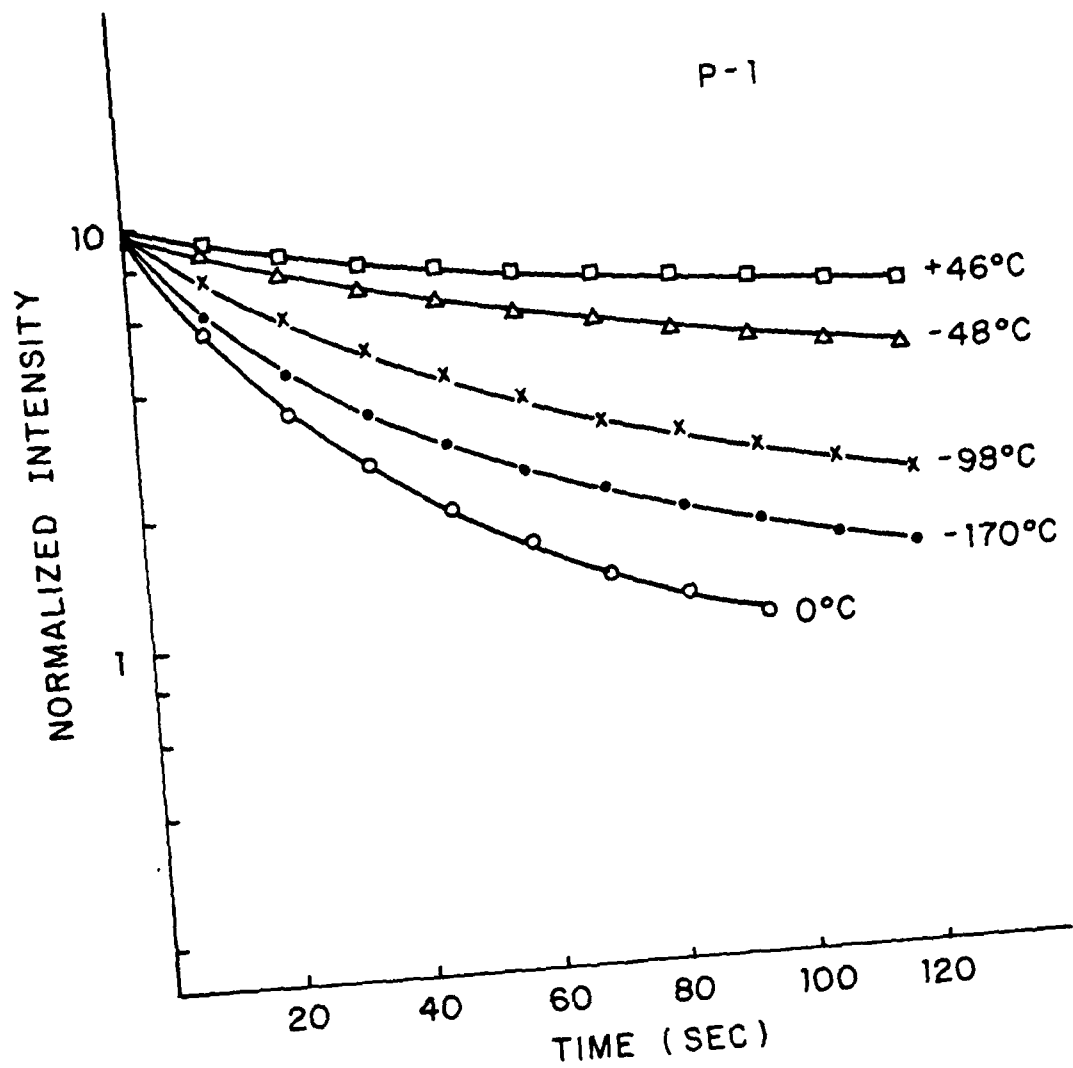


Figure 1: Phosphorescent decay curves of P1 as a function of temperature. Note that this is a semi-log plot.

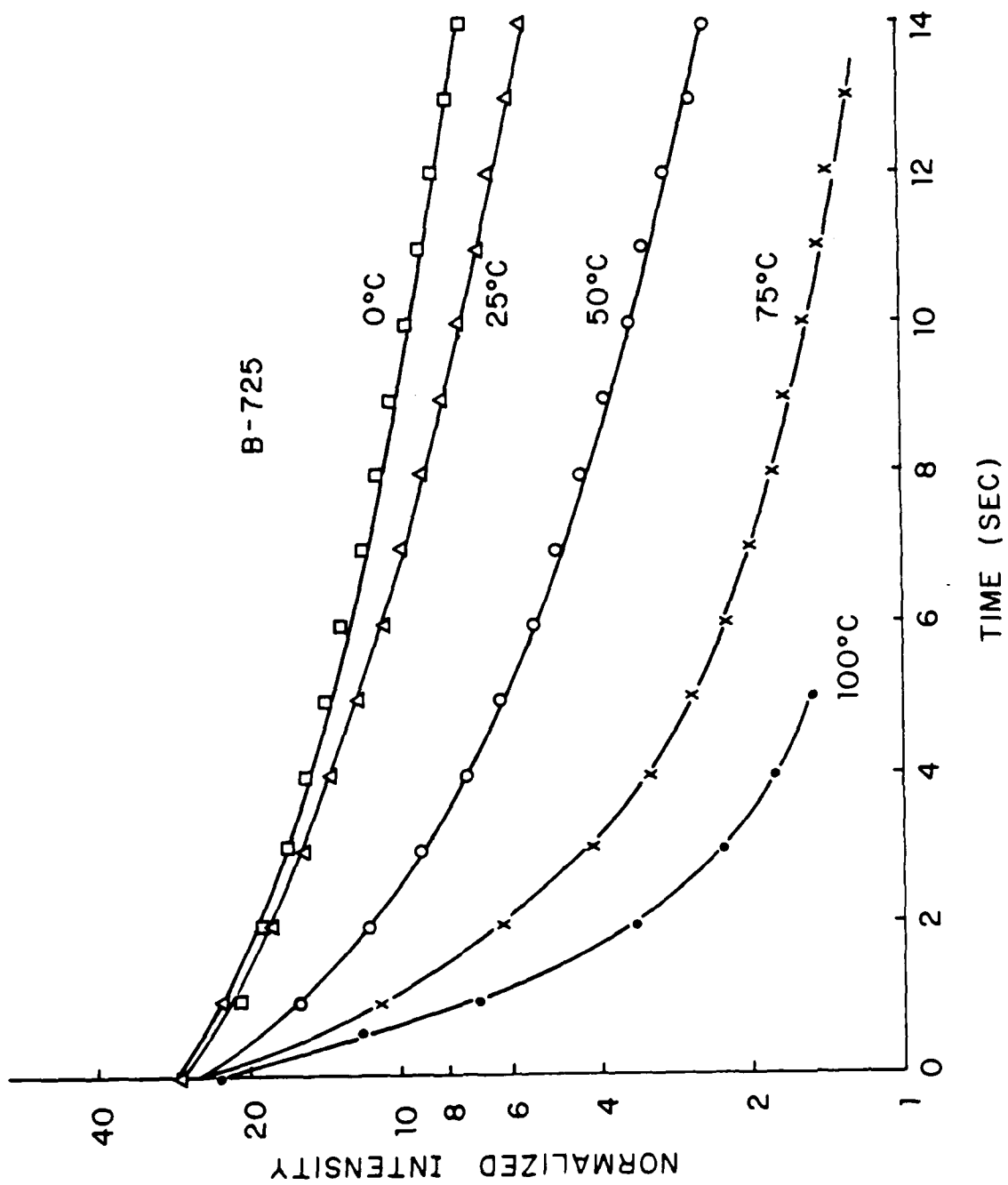


Figure 2: Phosphorescent decay curves of B625 showing monotonic decrease of the decay time.

However, the data shown in Fig. 1 clearly indicate non-exponential decay. Let us consider a model where the thermally released electrons are contributed by more than one trap at any time such that the decay curve is the result of composite luminescence. Then we can argue that the fluctuating nature of the decay time constant has the appearance of temperature independent characteristic and is caused by the overlapping of thermal release of electrons from energetically adjacent traps. As the temperature is increased, the most shallow trap is the first to give up its electrons, and its decay time decreases with increasing temperature. However, if the next deeper trap starts to contribute before the first trap is completely empty, the overall decay time will increase rather than decrease since the deeper trap has a longer decay time constant. If the traps are energetically close, the decay time is related to the integrated luminescence from the traps involved such that the contribution of each trap is difficult to isolate. This is the case for the P1 phosphor. The rate limiting process can be identified unambiguously if there is only one trap such as in B725 or if the traps are widely separated such as in P39.

For the two low temperature traps in P39, the trap depths may be obtained by representing the decay curve as a summation of exponential terms and plotting the time constants as functions of temperature. Using only two exponential terms at each temperature, we obtain the time constants and plot the result in Fig. 3. The agreement between the thermal glow curve and decay time experiments is quite good, since the trap depths and the frequency factors agree within one order of magnitude. This agreement is remarkable in view of the fact that the frequency factor is exponentially related to the temperature.⁽⁵⁾ However, other powders show less favorable correlation as a result of the non-exponential decay due to tunneling or

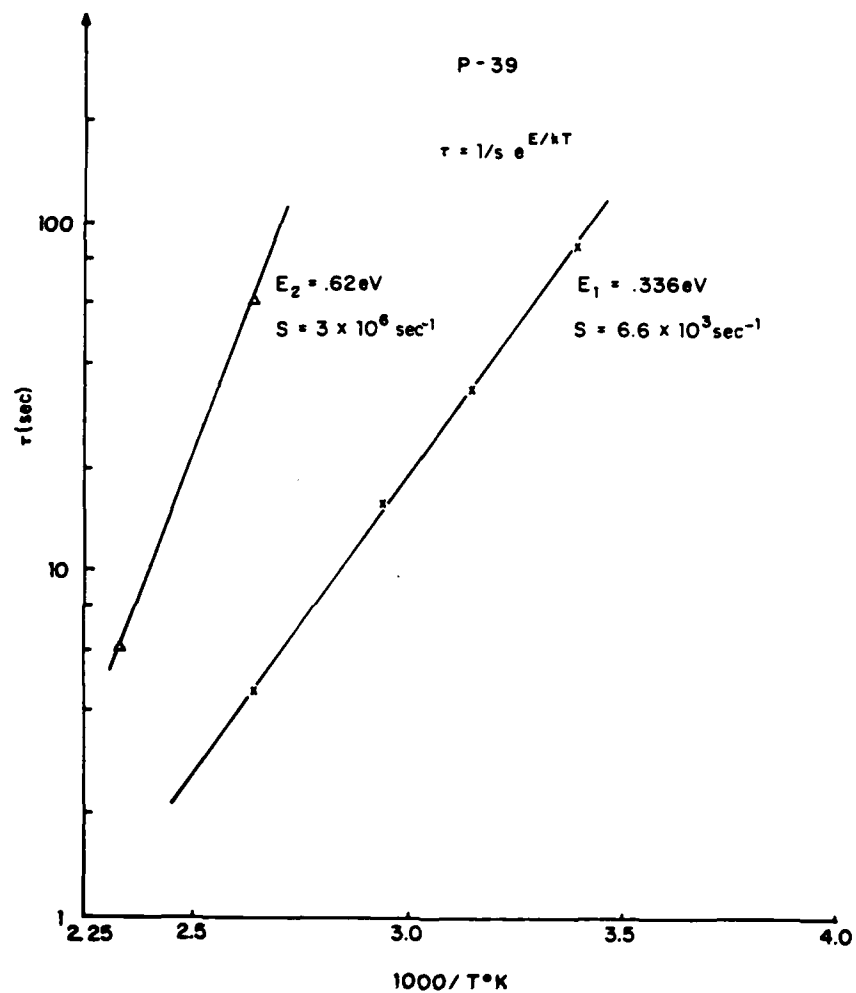


Figure 3: Plot of the first and second decay time constants vs inverse temperature. The energy and S-factor obtained from the glow curve method are $E_1=0.334$ eV, $S_1=2.4 \times 10^4$ 1/sec and $E_2=0.63$ eV and $S_2=9 \times 10^6$ 1/sec.

bimolecular mechanisms.

- (1) D. Curie, "Luminescence in Crystals," p. 149, Methuen & Wiley, N.Y. (1963).
- (2) E. S. Yang, D. B. Dove, M. Shafer, and I. F. Chang, J. Electronic Materials, to appear.
- (3) R. Chen, J. Appl. Phys. 40, 570 (1969).
- (4) P. Kivits and H. J. L. Hagebeuk, J. Luminescence 15, 1 (1977).
- (5) Please see Fig. 6 of reference 2.

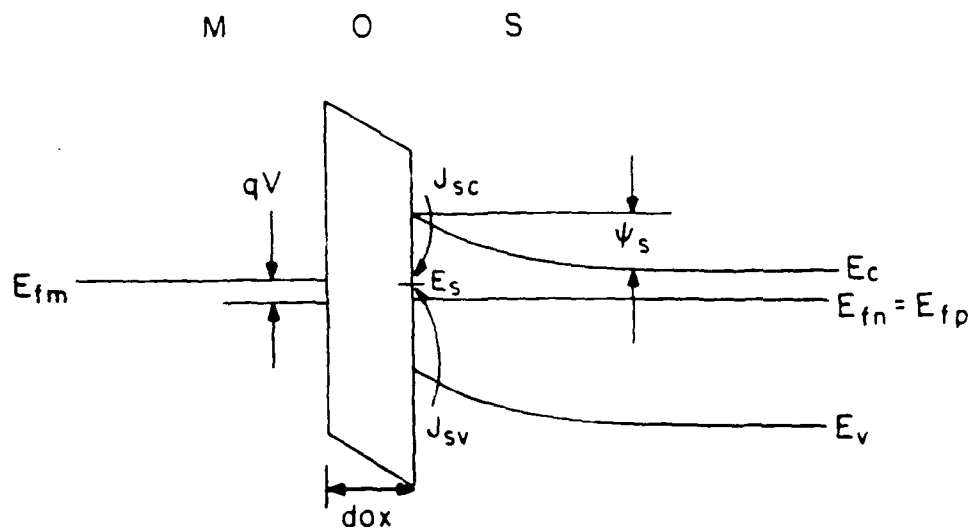
E. ENERGY AND ELECTRIC FIELD DEPENDENCE OF Si-SiO₂ INTERFACE STATE PARAMETERS BY OPTICALLY ACTIVATED ADMITTANCE EXPERIMENTS

(T. C. Poon, H. C. Card, S. M. So, W. Hwang)

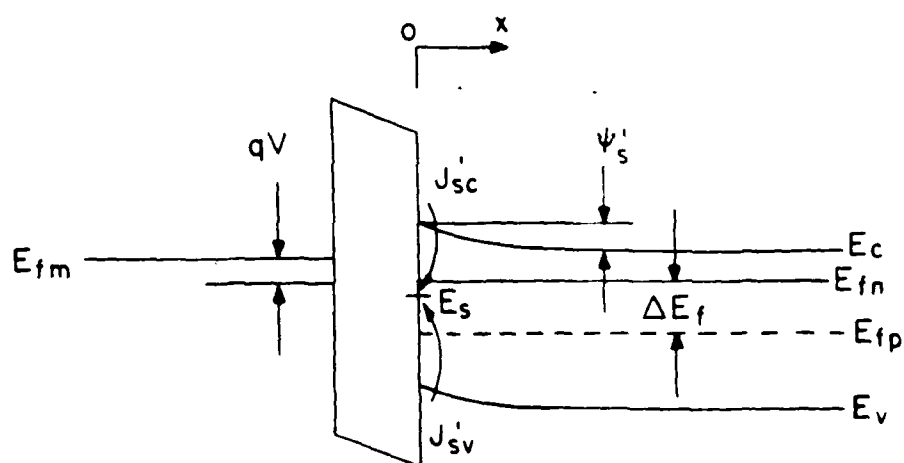
(Principal Investigator: W. Hwang (212) 280-3115)

Si-SiO₂ interface states have been the subject of considerable experimental⁽¹⁾⁻⁽⁵⁾ and theoretical⁽⁶⁾⁻⁽⁹⁾ study, and understanding of the origin of these states depends upon additional experimental information beyond that obtained by conventional admittance measurements. In a previous paper,⁽¹⁰⁾ we have described a new experimental method by which to obtain the interface state parameters in a metal oxide semiconductor (MOS) structure, which involves measurements of the ac admittance as a function of frequency under a background of optical illumination. This technique provides for an experimental determination of the capture cross sections of interface states for both electrons and holes, as well as for the energy dependence of the capture cross sections and interface state densities.

Consider an MOS structure as shown in Fig. 1 under a bias voltage V , and exposed to optical illumination of photon energy in excess of the silicon energy gap. Depending on the illumination level, minority carriers (holes) are generated optically in the region near the surface of the semiconductor ($x = 0$). Under the conditions where the surface concentration of holes exceeds that of electrons, i.e., $p(0) > n(0)$, the loss process described by Nicollian and Goetzberger⁽¹¹⁾ is dominated by the interaction between the minority carriers and interface states. Hence conductance measurements of the ac losses involved in the charge exchange give information regarding those interface states at the energy where the minority-carrier quasi-Fermi-level E_{fp} intersects the surface. Here we have assumed that the rate of photogeneration and supply of minority carriers to the surface is sufficient so as not to interfere with the rate of charge exchange with interface states. Since the basic



(a) IN DARKNESS



(b) OPTICALLY ACTIVATED

Figure 1: Energy-band diagram for a MOS structure on an n-type semiconductor under a given voltage bias V (a) in darkness, (b) under optical illumination with $h\nu > E_g$. E_{fn} and E_{fp} represent the electron and hole Fermi levels, E_s the energy of an interface state, and J_{sc} and J_{sv} are the currents associated with charge exchange of interface states with the conduction and valance bands (as described in Ref. 10).

phenomena of the conductance technique due to Nicollian and Goetzberger are therefore preserved, the time constant and capture cross section associated with the minority-carrier interaction can be determined as well as the interface state density.⁽¹⁰⁾

To better understand the admittance of the optically excited MOS structure, we now solve Poisson's equation for the case of low-level injection caused by the optical illumination. A horizontal quasi-Fermi-level E_{fp} is assumed here and this will be justified in a later section. Low-level injection implies that

$$n_{no}^* = n_i \exp[(E_{fn} - E_i)/kT] \approx N_d \quad (1)$$

and

$$p_{no}^* = n_i \exp[(E_i - E_{fp})/kT], \quad (2)$$

where n_{no}^* and p_{no}^* are the zero-field ($\psi_s = 0$) electron and hole concentrations, n_i is the intrinsic concentration corresponding to an intrinsic level E_i , and N_d is the doping density. Poisson's equation states that

$$\frac{\partial^2 \psi}{\partial x^2} = - \frac{\zeta(x)}{\epsilon_s}, \quad (3)$$

where ψ is the potential in the semiconductor at a distance x from the surface, ϵ_s is the dielectric constant of the semiconductor, and

$$\zeta(x) = q(n_{no}^* - p_{no}^* + p_n - n_n) \quad (4)$$

is the space-charge density. By substituting the basic equations

$$n_n = n_{no}^* \exp(q\psi/kT), \quad (5)$$

$$p_n = p_{no}^* \exp(-q\psi/kT), \quad (6)$$

and using Eq. (4) in Eq. (3), the second-order differential equation can be solved. The results for the surface electric field and charge density are

$$|\mathcal{E}_s| = (2kT/qL_D)G^*(\psi_s, P_{n0}/N_d, \Delta E_f), \quad (7)$$

$$|Q_{sc}| = (2\epsilon_s kT/qL_D)G^*(\psi_s, P_{n0}/N_d, \Delta E_f), \quad (8)$$

where

$$\begin{aligned} G^*(\psi_s, P_{n0}/N_d, \Delta E_f) &= \left\{ \left[\exp\left(\frac{q\psi_s}{kT}\right) - \frac{q\psi_s}{kT} - 1 \right] + \frac{P_{n0}}{N_d} \right. \\ &\quad \times \exp\left(\frac{\Delta E_f}{kT}\right) \left[\exp\left(\frac{-q\psi_s}{kT}\right) + \frac{q\psi_s}{kT} - 1 \right] \left. \right\}^{1/2}, \end{aligned} \quad (9)$$

$$L_D = (2\epsilon_s kT/q^2 N_d)^{1/2}, \quad (10)$$

where L_D is referred to as the extrinsic Debye length, P_{n0} is the zero-field minority-carrier concentration in darkness, ψ_s is the surface potential of the semiconductor, and

$$\Delta E_f = E_{fn} - E_{fp} \quad (11)$$

corresponds to the separation or "splitting" of the majority-and minority-carrier Fermi levels due to the optical illumination and the resultant enhancement of $p(0)$. If the surface potential under illumination is ψ_s^* , the change in surface potential due to illumination is

$$\Delta\psi_s = \psi_s - \psi_s^*; \quad (12)$$

the corresponding change in surface charge is

$$\Delta Q_s = C_{ox} \Delta \psi_s, \quad (13)$$

since $\Delta \psi_s = -\Delta V_{ox}$ for a given bias voltage V between metal and semiconductor, and $\Delta Q_s = -Q_{ox}$, where C_{ox} is the oxide capacitance obtained from the accumulation capacitance, and V_{ox} is the potential difference across the oxide layer. Hence the surface charge density under illumination is

$$Q_s^* = Q_s + \Delta Q_s. \quad (14)$$

The value of ΔE_f can be determined graphically from the new values of ψ_s^* and Q_s^* .⁽¹⁰⁾ Once this parameter is obtained, the surface concentration of minority carriers can readily be found from

$$P(0) = P_{n0} \exp[(\Delta E_f - q\psi_s^*)/kT]. \quad (15)$$

Notice that the effect on ΔQ_s of a change in charge density in interface states ΔQ_{is} is not included in our analysis. It turns out, as we shall discuss in more detail in a later section, the contribution of this charge can be neglected when the interface state density is sufficiently low, as it is in the present samples.

The silicon wafers used in these investigations were (111)-oriented, polished n-type epitaxial layers with film resistivity of 7.83 Ω cm grown on heavily doped n^+ substrates. These slices were cleaned in hot organic solvents, and in a solution of $H_2SO_4:H_2O_2$ in the ratio of 5:1. Deionized water of 10-M Ω purity was used to rinse the samples, before and after the surfaces were etched in dilute hydrofluoric acid (HF). The samples were dried in N_2 gas, and oxidized in dry O_2 at 1200°C in the presence of hydrogen chloride (HCl). High-temperature (1200°C) annealing for 10 min with high-purity N_2 gas was performed immediately after the oxidation process. The SiO_2 thicknesses were measured by

ellipsometry prior to metallization. Thin Al electrodes ($\sim 100 \text{ \AA}$ thick and 1 mm in diameter) were evaporated through an out-of-contact mask at a base pressure of 10^{-7} Torr. Postmetallization annealing with forming gas (35% H_2 + 65% N_2) at 450°C for a duration of 10 min was employed prior to the removal of oxide layers and evaporation of Ohmic contacts at the back surfaces of the samples.

The frequency dispersion of the ac admittance (capacitance and conductance vs dc bias voltage) was measured between 32 Hz and 200 KHz by phase-sensitive detection techniques, using a PAR Model 124 lock-in amplifier. Accuracy is checked by a Hewlett Packard HP 4274 A impedance meter. A slow ramp ($\lesssim 10 \text{ mV/s}$) was employed for the dc bias, and data was recorded on a X-Y recorder, while at the same time being digitized and stored in a DEC-PDP 11/03 minicomputer. This system has been described in previous studies.⁽¹⁰⁾⁽¹²⁾ The optical illumination is provided by a tungsten lamp through an optical conductor so as to maintain the measuring sample at room temperature. The received optical intensity is controlled by adjusting the distance d of the source above the sample in order to maintain a constant spectral content of the illumination. Resultant relative illumination levels (proportional to $1/d^2$) and the corresponding quasi-Fermi-level separations are given in Table I for the five illumination intensities used in this experiment.

The resultant experimental dependence of interface state density N_{is} on energy is shown in Fig. 2. The full circles correspond to dark conductance measurements, the open circles to conductance measurements under optical illumination. N_{is} vs E has also been determined from the low-frequency capacitance characteristic in darkness, and excellent agreement with Fig. 2 was obtained, in justification of the present measurements. The agreement between various measurements of N_{is} has also been described in our earlier papers.⁽¹⁰⁾

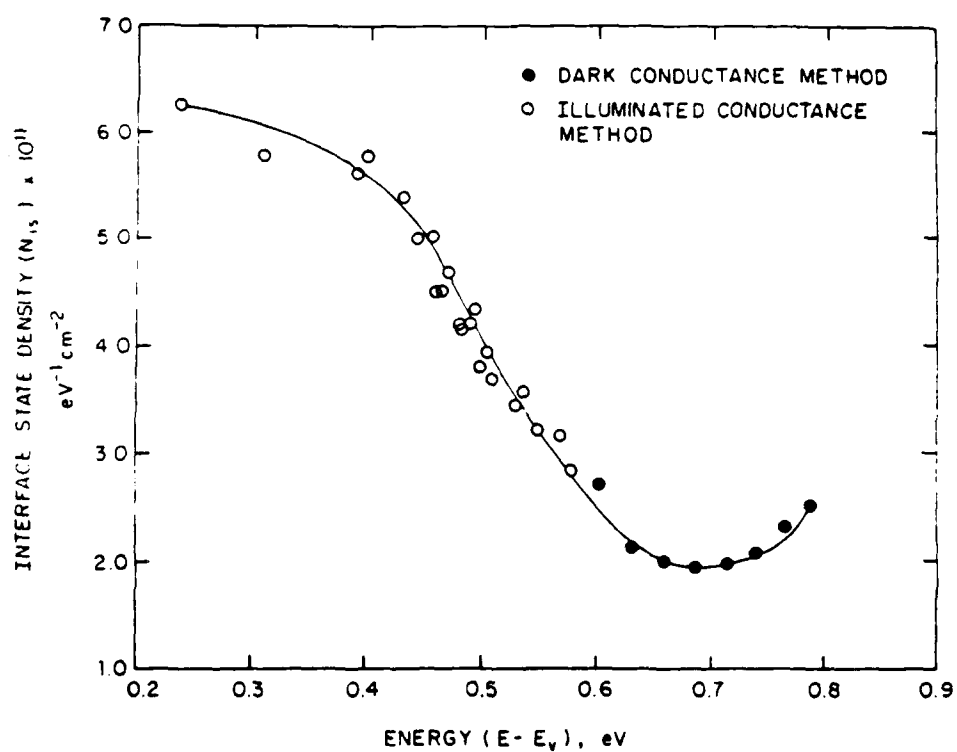


Figure 2: Energy distribution of interface state density obtained from dark and optically illuminated conductance measurements.

Table I
Data for the five illumination levels
used in the present experiments.

Illumination Levels	Relative Illumination Levels	E_f , eV
Dark	0	0.000
1	1	0.070
2	7.7	0.137
3	25.0	0.200
4	68.8	0.245
5	156.3	0.270

Figure 3 shows the observed dependence on energy of the capture cross sections for electrons and for holes, σ_n and σ_p , respectively, for the interface states of the devices. A strong dependence of σ_p on energy is obtained, and σ_p is found to be several orders of magnitude larger than σ_n . The three curves for σ_p correspond to illumination levels shown in Table I and we note that the same σ_p is not obtained, for a given energy with different illumination levels, for reasons discussed below. The results for σ_p and σ_n have been obtained from data such as that shown in Fig. 2 for various values of applied bias voltage V . Let us first consider the dependence of σ_p on energy. In the present technique, we can obtain σ_p as a function of energy by using several different combinations of illumination intensity and bias voltage, since both of these affect the position in

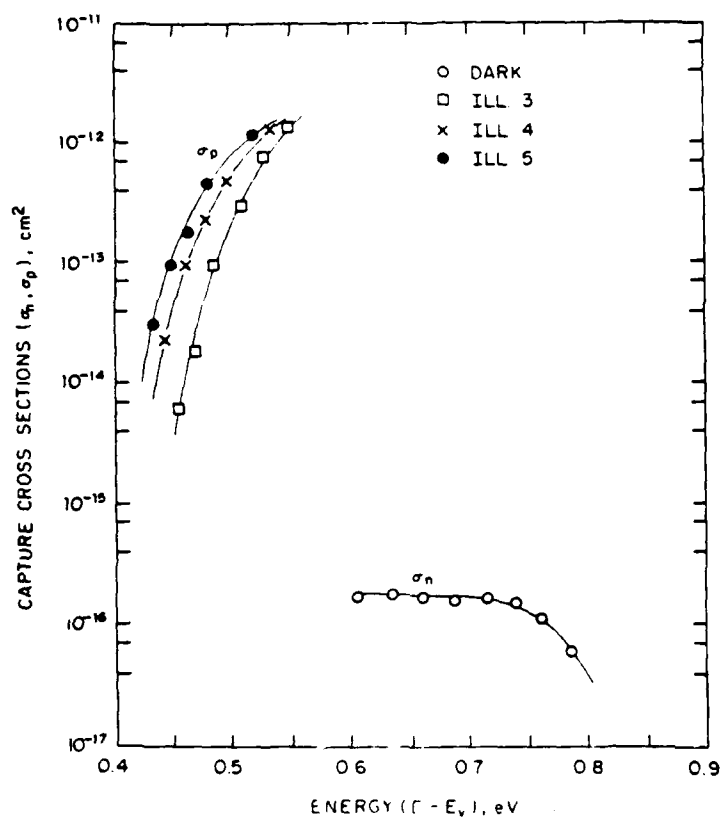


Figure 3: Capture cross sections of majority carriers σ_n and minority carriers σ_p as a function of energy. Illumination levels 3-5 correspond to the levels as in Table I.

the energy gap of the hole quasi-Fermi level E_{fp} .

The capture cross sections σ_p of interface states for minority carriers (holes) are shown to be orders of magnitude larger than those for electrons σ_n indicative of an acceptor-like coulomb capture process, and also to exhibit a strong dependence upon energy in the lower half of the silicon energy gap, for Al-SiO₂ (111) structures with oxide thickness of ≈ 800 Å. This apparent dependence on energy actually arises from a dependence on the electric field at the semiconductor surface and not from the energy of the state itself.⁽¹³⁾ Optically activated admittance measurements are an effective means of separating these dependences. The physical theory underlining the field dependence of the capture cross-section is being investigated.

- (1) A. Goetzberger, E. Klausmann, and M. J. Schulz, CRC Crit. Rev. Solid State Sci. 6, 1 (1976).
- (2) K. L. Wang, IEEE Trans. Electron. Dev. ED-26, 819 (1979).
- (3) R. J. Kriegler, T. F. Deneyi, K. D. Chik, and J. Shappir, J. Appl. Phys. 50, 398 (1979).
- (4) W. E. Dahlke and D. W. Greve, Solid State Electron. 22, 893 (1979).
- (5) Y. C. Cheng, Prog. Surf. Sci. 8, 181 (1977).
- (6) F. Stern and W. E. Howard, Phys. Rev. 163, 816 (1967).
- (7) A. J. Bennett and L. M. Roth, J. Chem. Solids 32, 1251 (1971).
- (8) R. B. Langhlin, J. D. Joannopoulos, and D. J. Chadi, in The Physics of SiO₂ and Its Interfaces, edited by S. T. Pantelides (Pergamon, New York 1978), p. 321.
- (9) B. G. Martin and R. F. Wallis, Phys. Rev. B 18, 5644 (1978).
- (10) T. C. Poon and H. C. Card, J. Appl. Phys. 51, 5880 (1980); J. Appl. Phys. 51, 6273 (1980).
- (11) E. H. Nicollian and A. Goetzberger, Bell Syst. Tech. J. 46, 1055 (1967).
- (12) T. C. Poon and H. C. Card, Electron. Lett. 15, 756 (1979).
- (13) K. C. Kao and W. Hwang, Electrical Transport in Solids, Pergamon Press, Oxford (1981).

F. STATISTICAL FLUCTUATIONS OF DOPANT IMPURITIES IN ION-IMPLANTED BIPOLAR TRANSISTOR STRUCTURES AND THE MINIMUM DEVICE DIMENSIONS FOR VLSI SYSTEM RELIABILITY

(P. R. Prucnal, W. Hwang, H. C. Card)

(Principal Investigator: W. Hwang (212) 280-3115)

With the trend towards increasing functional density of very large scale integrated circuits, there are a number of physical phenomena that will result in limitations to the successful operation of these circuits and systems. An excellent review of these phenomena has been presented by Keyes⁽¹⁾ and several authors have treated one or more of the limiting mechanisms with varying degrees of generality.⁽²⁾⁻⁽¹³⁾ Among the more serious limitations, i.e. those which are encountered first as the physical device and circuit dimensions are decreased, are maximum power dissipation, metal electromigration, edge leakage currents, and statistical fluctuations of dopant impurities. Other factors such as punch through of depletion regions, hot carrier injection into insulators, and carrier velocity saturation are the result of operating the smaller devices under different conditions of electric field and current density than their larger counterparts, and are not essential results of a truly scaled technology.⁽⁵⁾⁽¹³⁾

We consider only one of the above limitations to the continual reduction in device dimensions, the problems associated with the statistical nature of the positions of the dopant impurities. Furthermore, we restrict ourselves to the particular case of ion implanted impurities in a bipolar transistor structure, but we feel that the results obtained for this structure in terms of minimum allowable dimensions will be approximately correct for other devices.

As the size of any characteristic physical feature of the bipolar transistor (for example, the dimensions of the implanted emitter or base regions in the plane of the silicon surface, or the width of the base region in the

direction normal to the plane of the surface) is reduced, the statistical fluctuations among devices of the number of implanted impurities in the active volume becomes important for two reasons. First, the impurity concentrations in a device that has been scaled down in size by a factor k is increased by this same factor k .⁽⁵⁾⁽¹³⁾ Since all dimensions are scaled by k , the active volume of the device is $1/k^3$ of the larger device, so that the number of impurities within the device is reduced by $1/k^2$. If this number of impurities is treated as Poisson random variable, since the standard deviation is then the square root of the mean, the ratio of the standard deviation to the mean is increased by k . Second, there will be a corresponding increase of k^2 in the number of components (all of whose behavior influences that of the system) per chip, if the conservative estimate is made that the chip size itself does not increase. This second consideration is of consequence because one can tolerate a larger standard deviation with a smaller number of devices for a given yield of the chip. In order to calculate the yield, one must postulate a tolerable limit to the minimum or maximum number of impurities per device in order that the device (and hence the system on the chip of which it is a part) will function within the specifications. We are primarily interested in the minimum dimensions for adequate yield, and since both the statistical fluctuations are increasing and the fluctuations we can tolerate are decreasing with reducing size, the exact choice of allowed fluctuation of any electrical parameter for the device will not greatly affect the results.⁽¹⁴⁾

One final point should be made regarding the operation of all devices on the chip. With VLSI systems it will not be possible to test all devices or circuit functions, and "bad" devices are likely to escape unnoticed, until exhaustive use of the system detects the fault. Because of this, it will be necessary to be very conservative in determining the allowed probability of

a faulty device on the chip. One will have to aim for very high yields when considering any limitation such as this one where the origin of a failure arises from a random process. As an example, we describe the effects of the random fluctuations among devices in the number of dopant impurities on the behavior of ion-implanted bipolar transistor structures.⁽¹⁵⁾

Let us assume that we can tolerate a 100 $\lambda\%$ variation in the current gain β of the transistors assembled on a given chip. This means that the variations in the base Gummel number must be less than 100 $\lambda\%$ for any device on the chip, if no additional variations in β are introduced by fluctuations in the emitter Gummel number.⁽¹⁵⁾ Fluctuations in the base Gummel number are induced by variations in the total number of impurities n in the base region, which has mean value $G_b L^2 = N_b$, where L is the device dimension and N_b is the mean number of base impurities. The probability that a device fails is then equal to the probability that n deviates from N_b by more than 100 $\lambda\%$. Using the well-known Tschebechev inequality,⁽¹⁶⁾ the probability P_1 that a given device of dimension L fails is then

$$P_1 = P_r\{|n - N_b| \geq \lambda N_b\} \leq \frac{1}{\lambda^2 N_b} \quad (1)$$

The probability P_{chip} of one or more device failures on a chip containing N_{chip} devices is, from Eq. (1) and the binomial distribution,

$$P_{\text{chip}} \leq 1 - \left[1 - \frac{1}{\lambda^2 N_b}\right]^{N_{\text{chip}}} \quad (2)$$

Now as the device size L changes by a factor k , Eqs. (1) and (2) become

$$P_1 \leq \frac{1}{\lambda^2 N_b'} = \frac{1}{\lambda^2 k^2 N_b} \quad (3)$$

and

$$P_{\text{chip}} \leq 1 - \left[1 - \frac{1}{k^2 \lambda^2 N_b} \right]^{\frac{N_{\text{chip}}}{k^2}} \quad (4)$$

In Eq. (4) we see that by both decreasing the average number of impurities in any given device by k^2 , and increasing the number of devices by k^2 , the probability of failure P_{chip} of one or more devices on a chip increases dramatically with a reduction in dimensions. To remedy this problem, an N-bit parity check may be used. In this way, the probability of error in an N-bit word is approximately the binomial probability P_N that two devices in N fails:

$$P_N \approx \frac{N(N-1)}{2} P_1^2 (1-P_1)^{N-2} \quad (5)$$

Furthermore, the probability P_{chip}^N of one or more N-bit words failing on a chip is

$$P_{\text{chip}}^N \approx 1 - \left[1 - P_N \right]^{\frac{N_{\text{chip}}}{N k^2}} \quad (6)$$

In Fig. 1 we show the dependence of P_1 , P_{chip} and P_{chip}^N on the lateral dimension L of the implanted bipolar devices, for various word lengths N , where $\lambda = 0.20$. As the number of bits involved in a parity check N is reduced, the minimum dimension L for a given probability of chip failure decreases, or the probability of success for a given L increases. From results such as those of Fig. 1, we are able to plot the dependence of the minimum dimension L upon N , for various values of chip yield $Y = 1 - P_{\text{chip}}^N$ (Fig. 2). As we pointed out above, the design must be rather conservative (design for high yield) when considering against a random device fault which may not easily be discovered during testing or field operation. As N decreases, the fraction of bits

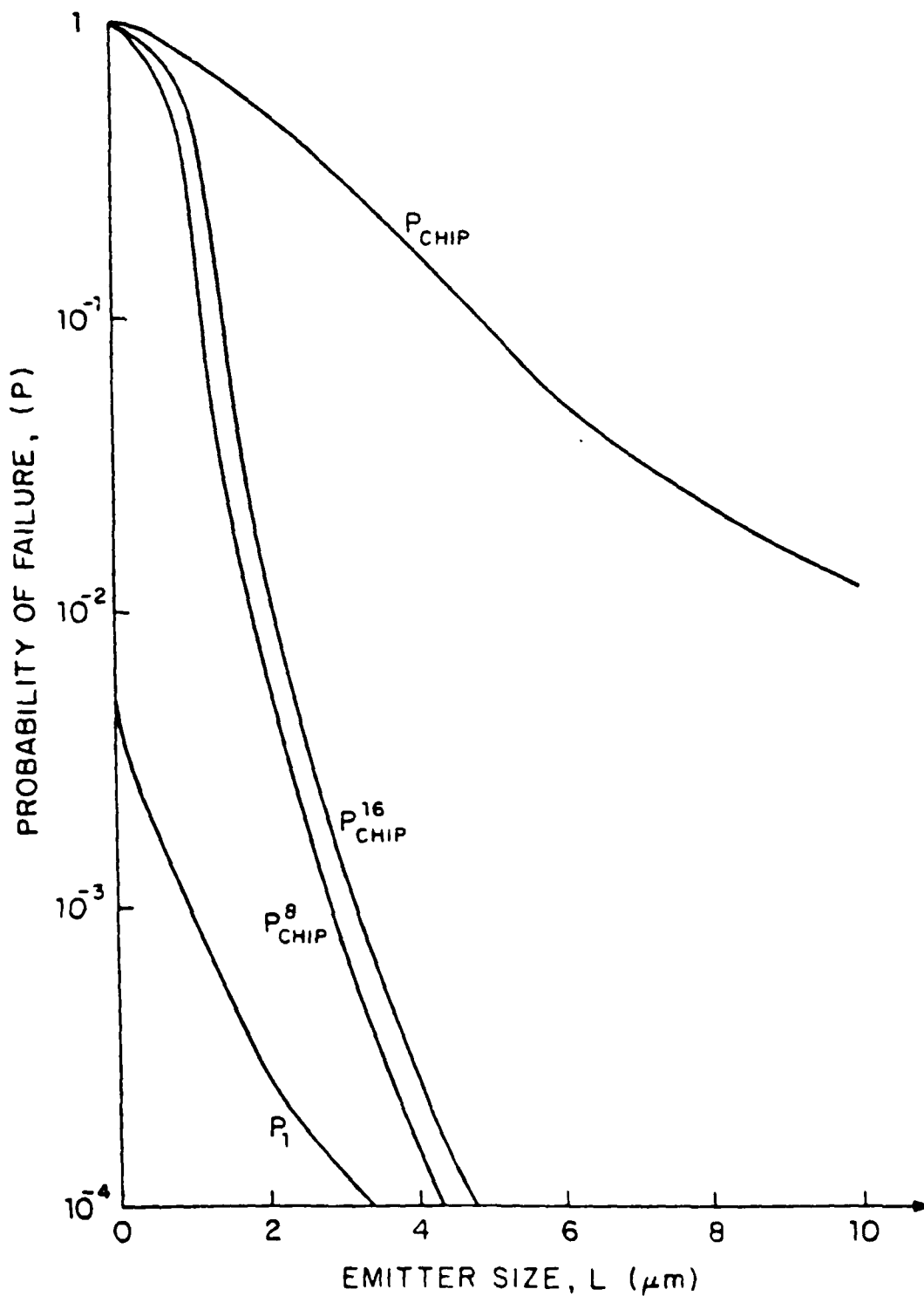


Figure 1: Probability of device failure P_1 , probability of chip failure P_{chip} , and probability of chip failure with N-bit parity check P_{chip}^N versus emitter dimension L.

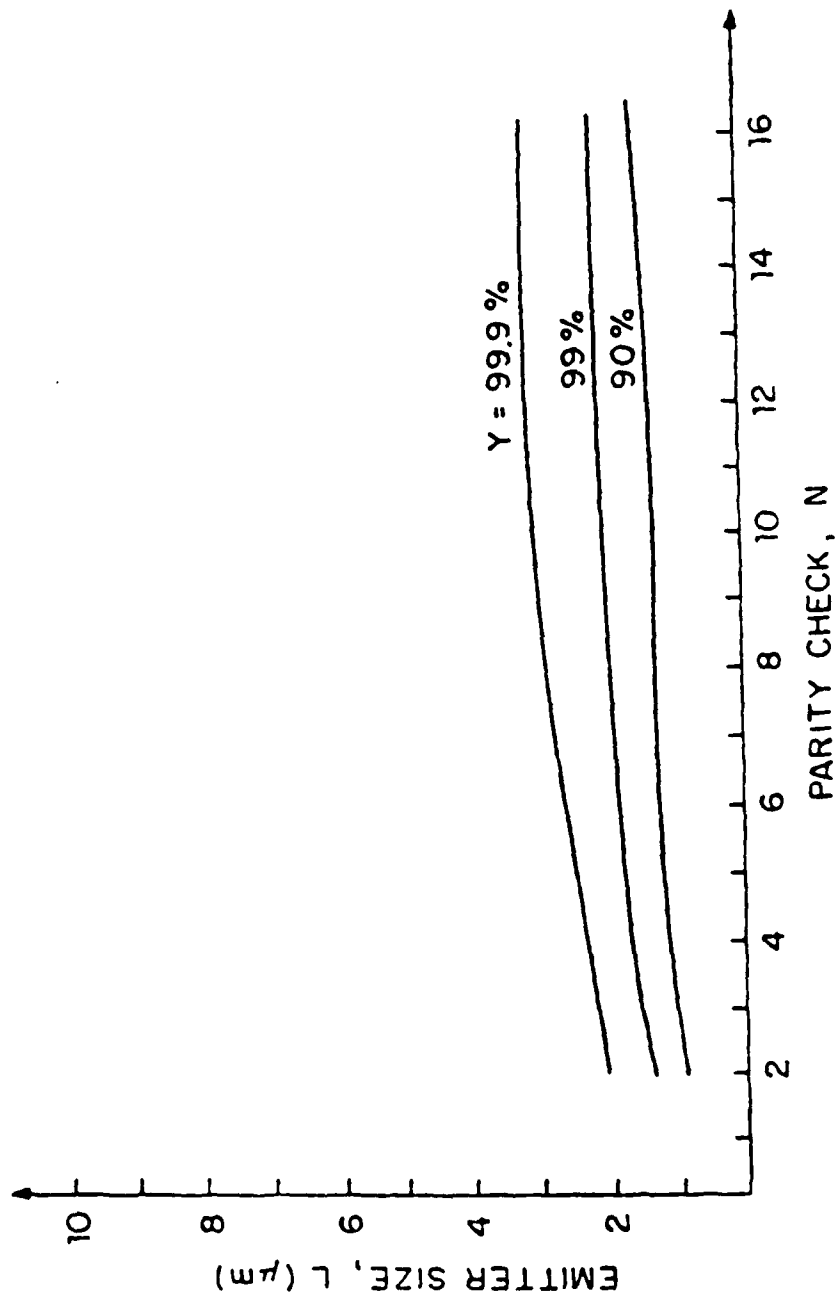


Figure 2: Minimum dimension L versus number of bits N in parity check, for various chip yields.

unavailable for information processing of course decreases. In the worst case $N = 2$ and only every second bit is used for storage of information, so that the useful chip area is effectively halved. For this case, the minimum L for a yield of 99% from Fig. 2 is $\approx 1.5 \mu\text{m}$.

The random fluctuations in the number of ion implanted impurities in the base region of bipolar transistor structures is a serious limitation to the continued reduction in device size demanded by very large scale integration of these devices. These fluctuations have a doubly stochastic nature by virtue of uncertainties in the implantation parameters such as the standard deviation of the implanted profiles, so that the simple Poisson statistics are not sufficient to determine the minimum device size for tolerable chip yields. These doubly-stochastic effects will be studied in the future. This minimum device size expressed as the minimum lateral dimension (emitter size) is expected to be on the order of $1 \lesssim L \lesssim 5 \mu\text{m}$ with a more exact value given above and dependent on the chip organization for parity checks.

- (1) R. W. Keys, IEEE Trans. ED-26, 271 (1979).
- (2) R. W. Keyes, Proceeding IEEE, 63, 740 (1975).
- (3) B. Hoeneisen and C. A. Mead, Solid-State Electronics, 15, 819 (1972).
- (4) B. Hoeneisen and C. A. Mead, Solid-State Electronics, 15, 891 (1972).
- (5) R. H. Dennard, F. H. Gaensslen, H. N. Yu, V. L. Rideout, E. Bassous, and A. R. Leblanc, IEEE J. Solid State Circuits, SC-9, 256 (1974).
- (6) D. W. Dutton, D. A. Divekar, A. G. Gonzalez, S. E. Hansen, and D. I. Antoniadis, IEEE J. Solid St. Circuits, SC-12, 349 (1977).
- (7) S. P. Gaur, IEEE Trans. ED-26, 415 (1979).
- (8) F. F. Fang and B. L. Crowder, "Ion-implanted microwave MOS FET's", presented at the IEEE Int. Electron Dev. Meeting, Washington, DC, Nov. 1970.
- (9) H. N. Yu, A. Reisman, C. M. Osburn, and D. L. Critchlow, IEEE Trans. on Electron Devices ED-26, 318 (1979).

- (10) R. H. Dennar, F. H. Gaensslen, E. J. Walker, and P. W. Cook, IEEE Trans. Electron Devices, ED-26, 325 (1979).
- (11) P. A. H. Hart, T. Van T. Hof, and F. M. Klassen, IEEE Trans. on Electron Devices, ED-26, 411 (1979).
- (12) J. R. Brews, W. Fichtner, E. H. Nicollian, and S. M. Sze, IEEE Electrons Devices Letters, EDL-1, 2 (1980).
- (13) P. M. Solomon and D. O. Tang, "Bipolar Circuit Scaling", presented at IEEE International Solid-State Circuits Conference, p. 86 (1979).
- (14) P. R. Prucnal and M. C. Teich, J. Opt. Soc. Am. 69, 539 (1979).
- (15) P. R. Prucnal, W. Hwang, and H. C. Card, Microelectron. Reliab. 20, 633 (1980).
- (16) A. Papoulis, Probability and Random Processes, McGraw-Hill, New York, (1965).

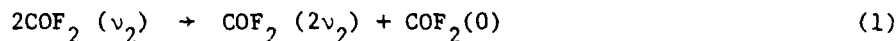
III. ENERGY TRANSFER AND RELAXATION IN SMALL POLYATOMIC MOLECULES

A. VIBRATIONAL ENERGY TRANSFER IN LASER EXCITED COF_2 : INFRARED FLUORESCENCE FROM THE INTERMEDIATE MODE ν_4^*

(R. K. Bohn, K. H. Casleton, Y. V. C. Rao, G. W. Flynn)

(Principal Investigator: G. W. Flynn (212) 280-4162)

In a previous study⁽¹⁾ COF_2 was shown to absorb CO_2 infrared laser radiation in the ν_2 mode (C-F symmetric stretch). The overtones of the ν_2 mode were found to be rapidly populated by the ladder climbing process (1).



Since the $2\nu_2$ level is Fermi mixed with the ν_1 carbonyl stretch state, strong IR emission is observed from $2\nu_2 \rightarrow 0$ at $\lambda \sim 5\mu$. For certain CO_2 lines, the population of the $2\nu_2$ state can be directly populated by hot band pumping of the $\nu_2 \rightarrow 2\nu_2$ transition.⁽¹⁾ Because of the rapid coupling of ν_2 and $2\nu_2$ via process (1), which requires an average of 30 gas kinetic collisions to reach steady state, fluorescence from $2\nu_2$ simply reflects the changes in population of the ν_2 state for processes slower than (1).

There are several features of vibrational energy transfer in COF_2 which distinguish it from other polyatomic molecules, mostly derivatives of CH_4 ,⁽²⁾ that have been investigated in detail. Since COF_2 is completely composed of heavy atoms, most of the fundamental vibration frequencies are relatively low frequency rather than clustered into regions of high and low frequencies. The large moments of inertia of COF_2 are expected to reduce the importance of rotational motions in the vibrational energy transfer processes⁽³⁾ and to allow for direct collisional energy transfer between the fundamentals ($v = 1$ levels) of most modes. Relatively strong

fluorescence may be observed from at least four different states ($2\nu_2$, ν_1) at 5μ , ν_4 at 8μ , ν_6 at 13μ , and ν_3 and/or ν_5 at $(16-17\mu)$. Thus, the populations of these states may be independently monitored as a function of time after pulsed laser pumping. COF_2 is a tetra-atomic molecule with relatively dense energy levels whose energy transfer properties should more closely approximate those of larger molecules. Stretch-stretch vibrational energy transfer occurs rapidly in CH_4 , 11+3 collisions, for the symmetric-asymmetric stretch transfer which is endothermic by about 100 cm^{-1} .⁽⁴⁾ Since COF_2 contains no hydrogen atom, determination of stretch-stretch energy transfer rates will indicate whether heavy atom molecules behave differently.

The 8μ fluorescence from the ν_4 state of COF_2 is particularly interesting because its growth after pulsed laser pumping is characterized by two exponential rises. This characteristic is rather unusual and has not been frequently observed in IR fluorescence studies of vibrational energy transfer. The consequences of this double rise for understanding energy transfer in COF_2 are the major subject of this study.

The experimental apparatus for laser-induced fluorescence was composed of a Q-switched CO_2 laser previously described in detail.⁽⁵⁾ In most of the experiments the P(22) or the R(14) lines of the 10.6μ band were used for excitation. Laser pulses were repeated at 200 Hz with $\sim 1 \text{ mJ pulse}^{-1}$ and a width of $\sim 1 \mu\text{s}$ (FWHM). Typically, >80% of the laser power was carried by the exciting line. The stainless steel fluorescence cell had an outgas rate of $<10 \text{ mtorr hr}^{-1}$. Pressure was measured with a corrosion-resistant capacitance manometer (MKS Baratron).

Carbonyl fluoride samples were obtained from both PCR Research Chemicals (Gainesville, FL) and Synthatron Corp. (Parsippany, NJ) which contained

~10% CO₂ impurity. Samples were purified gas chromatographically using a 1.5 ft x 1/4 in. stainless steel column filled with Carbosieve S (Supelco, Inc., Bellefonte, PA). Another column apparently identical to that used in an earlier purification⁽⁶⁾ did not separate CO₂ from COF₂.

Fluorescence perpendicular to the laser beam was observed at 8μ using a 7.5 - 8.5μ band pass filter and a Au:Ge (77K) detector. At 5μ fluorescence was monitored with a MgF₂ exit window, a 4.6μ long pass filter and either the Au:Ge detector or an InSb (77K) detector. The fluorescence signal was observed with a transient digitizer/digital signal averager combination and stored on floppy disks for subsequent analysis. Data were analyzed using a modification of a non-linear least squares program.⁽⁷⁾ Fluorescence data were fit to the function, $\sum_{i=1}^n A_i e^{-r_i t} + B$ where B is a background, A_i is the amplitude of the ith term, r_i is the corresponding rate, and n can be chosen as one or two. A_i, r_i and B can be varied but B was held fixed at the pre-laser pulse value in our analyses. Fluorescence curves composed of more than two exponential terms were analyzed by fitting the slowest exponential terms, subtracting the calculated fits, and fitting the difference curves to further sums of exponential terms.

An abbreviated vibrational energy level diagram for COF₂ is shown in Fig. 1.⁽⁸⁾ The CO₂ laser pumps ground state molecules into the ν₂ level. Emission from the ν₄ level occurs at 8μ. This fluorescence, shown in Fig. 2, is describable by two exponential rise terms and two exponential fall terms. One of these is a very slow but large amplitude decay which is due to the flow of heat from the center of the fluorescence cell to its walls at a rate controlled by the thermal conductivity of the gas.⁽⁹⁾ The rise terms are characterized by the rate constants $156 \pm 18 \text{ ms}^{-1} \text{ torr}^{-1}$ and $29 \pm 5 \text{ ms}^{-1} \text{ torr}^{-1}$. The reported uncertainties are two standard deviations. The

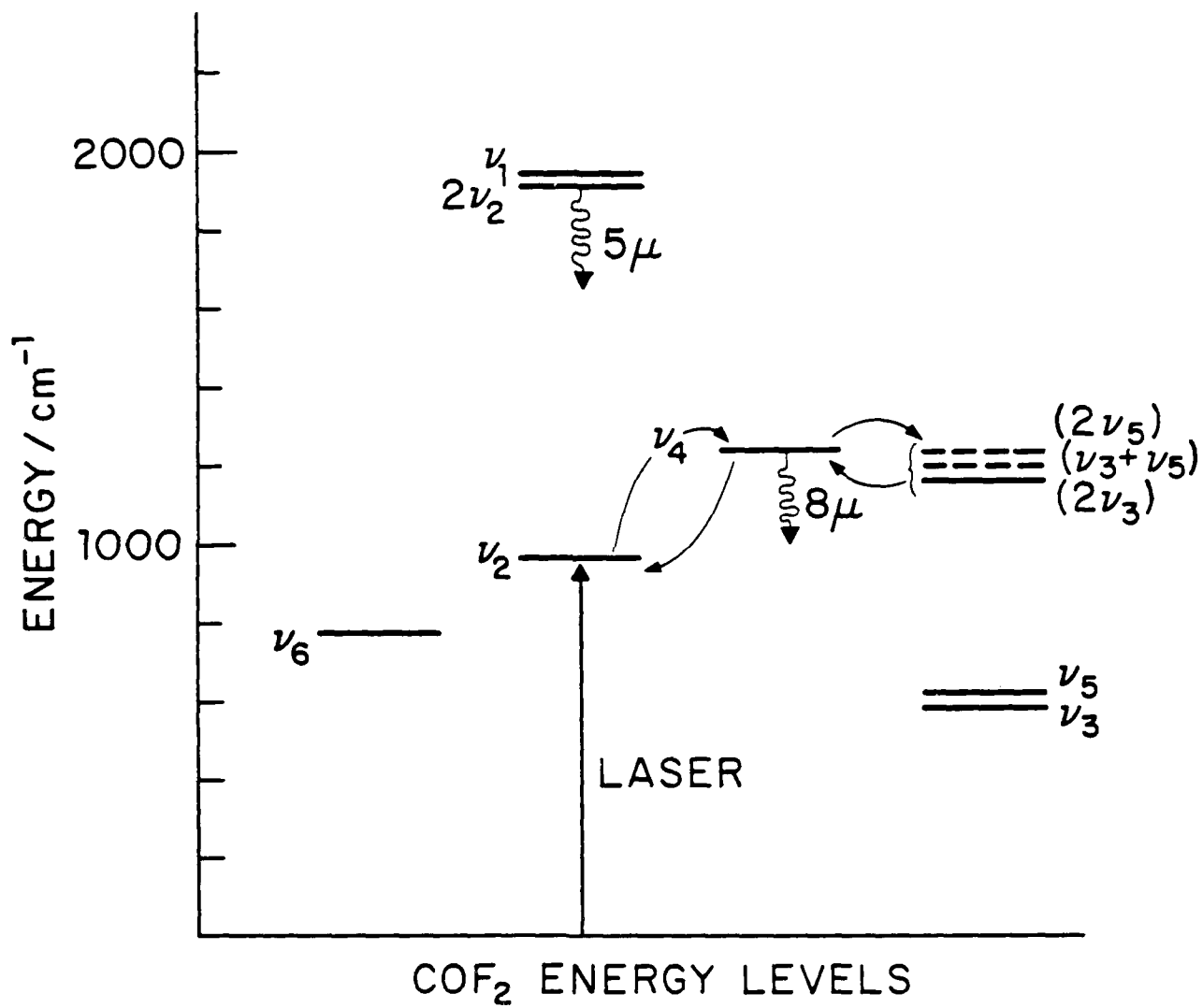


Figure 1

AD-A100 755

COLUMBIA RADIATION LAB NEW YORK

F/G 20/14

RESEARCH INVESTIGATION DIRECTED TOWARD EXTENDING THE USEFUL RAN--ETC(U)

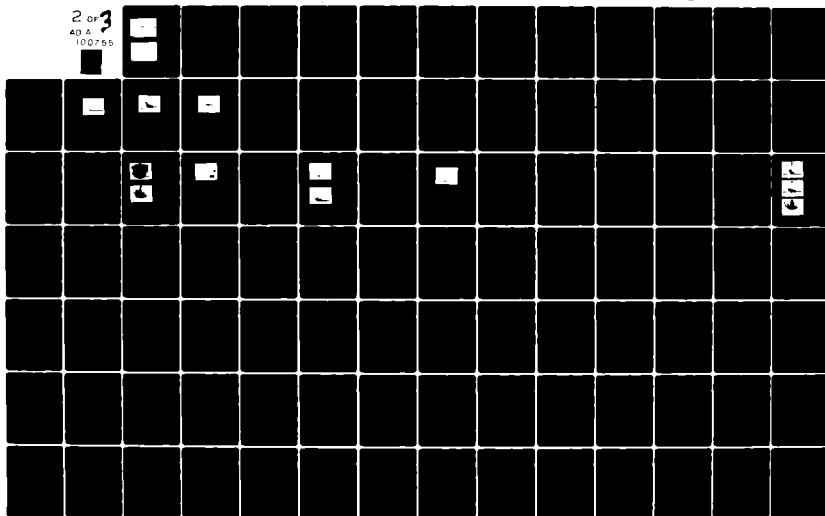
MAR 81 G W FLYNN

DAA629-79-C-0079

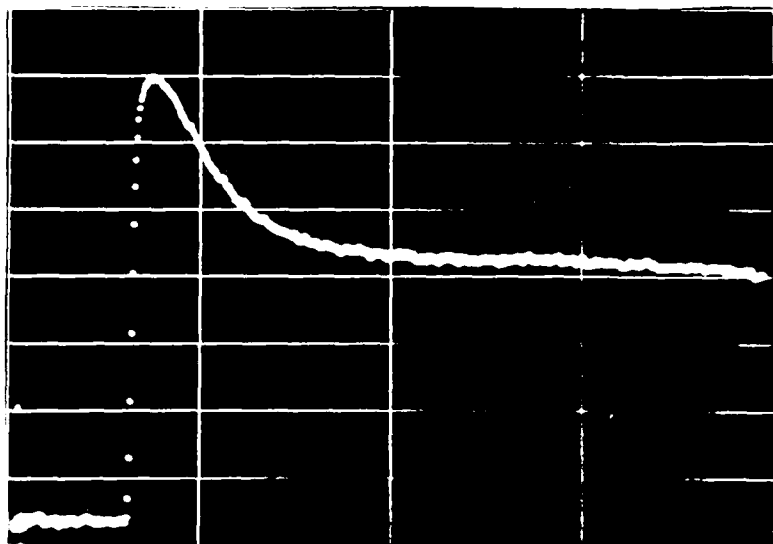
NL

UNCLASSIFIED

2 of 3
AD A
100755

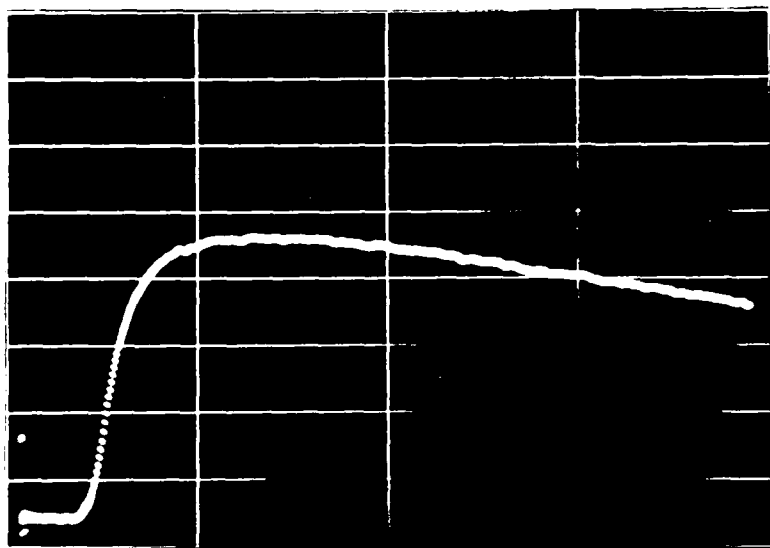


COF_2 8μ FLUORESCENCE



a. 7 Torr

$64 \mu\text{sec/div}$



b. 2 Torr

$26 \mu\text{sec/div}$

Figure 2

amplitude of the $29 \text{ ms}^{-1} \text{ torr}^{-1}$ process is about one-half that of the $156 \text{ ms}^{-1} \text{ torr}^{-1}$ process. The primary fall of the fluorescence is described by the rate constant $5.6 \pm 0.2 \text{ ms}^{-1} \text{ torr}^{-1}$. The thermal conductivity rate, which was not measured, was of the order of 100 sec^{-1} .

An earlier study⁽¹⁾ demonstrated that the overtone of the pumped state, $2\nu_2$, Fermi mixed with ν_1 , is populated rapidly by the ladder climbing process (1). Therefore, the 5μ fluorescence from this state reflects population changes in the ν_2 state since $2\nu_2$ and ν_2 are so rapidly coupled. The decay of the 5μ fluorescence is describable by three exponential terms, one of which is a very slow but small amplitude thermal decay. The rate constants for the two major decays are $34 \pm 2 \text{ ms}^{-1} \text{ torr}^{-1}$ and $7.4 \pm 1.2 \text{ ms}^{-1} \text{ torr}^{-1}$. The amplitude of the faster process, which was reported in the earlier study,⁽¹⁾ is about 7 times that of the slower process.

There seems little doubt that the measured rate constants of 5.6 ± 0.2 and $7.4 \pm 1.2 \text{ ms}^{-1} \text{ torr}^{-1}$ in the 8μ and 5μ fluorescence, respectively, simply reflect the same kinetic eigenvalue observed in two different states. Furthermore, this is the rate most closely associated with "vibration-translation/rotation" (V-T/R) relaxation of the vibrational manifold since it is the slowest rate and one that is immediately followed by thermal heating of the system (which is suggestive of overall equilibration of all degrees of freedom at a temperature above ambient). In COF_2 some caution must be exercised in ascribing this rate to V-T/R relaxation of just the very lowest levels (ν_3 , ν_5). Because of the relatively balanced coupling between different modes and the moderately slow intermode energy transfer for this molecule, the slowest or "V-T/R" eigenvalue is expected to contain substantial contributions from one or more intermode vibration-vibration (V-V) processes.⁽¹⁰⁾

The rates of 29 ± 5 and $34 \pm 2 \text{ ms}^{-1} \text{ torr}^{-1}$ observed in the 8μ and 5μ fluorescence, respectively, also appear to reflect the same kinetic eigenvalue appearing in two different states. The 8μ rate is particularly difficult to measure accurately because it is the third eigenvalue stripped off the fluorescence curve and has only about half the total signal amplitude. In addition the 8μ fluorescence signals, though good for the infrared, are noticeably more noisy than those at 5μ . Thus we assume that these two rates are the same kinetic eigenvalue appearing with different amplitudes in the two different fluorescences. There are other compelling reasons, as noted below, for believing that the major decay rate for ν_2 loss must appear in the rise of ν_4 .

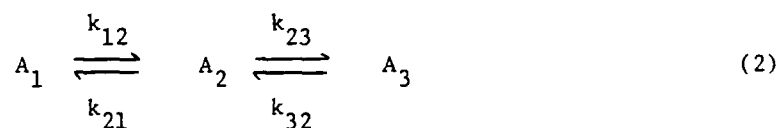
In proposing a mechanism to explain the observed data for these two fluorescing states, the following points are very important: (1) ν_4 must be filled from either the ν_2 pumped state or the $2\nu_2$ overtone, ν_1 Fermi mixed set. Given the energy gap between $2\nu_2$, ν_1 and ν_4 plus the relatively small populations in these high "overtone" states, filling from ν_2 is by far the most reasonable mechanism. (2) Except for the "V-T/R" eigenvalue, the $2\nu_2$, ν_1 states decay only at a single rate of approximately $34 \text{ ms}^{-1} \text{ torr}^{-1}$. As noted above, due to the rapid coupling of ν_2 to $2\nu_2$ (and ν_1) via (1), this decay surely represents flow of energy (population) out of the ν_2 level and into the other vibrational modes. The 5μ decays merely reflect the behavior of the lower level ν_2 . (3) Despite the solid conclusions of the above two comments, ν_4 appears initially to fill faster ($156 \text{ ms}^{-1} \text{ torr}^{-1}$) than ν_2 decays ($34 \text{ ms}^{-1} \text{ torr}^{-1}$). Since the ν_2 reservoir must be the source of energy for ν_4 , the fast filling of ν_4 is extremely anomalous.

The above features taken together suggest that the fast rise ($156 \text{ ms}^{-1} \text{ torr}^{-1}$) of ν_4 actually corresponds to the loss of population from ν_4 even

though the $156 \text{ ms}^{-1} \text{ torr}^{-1}$ rate appears in the fluorescence rise! In addition the slow decay of ν_2 ($34 \text{ ms}^{-1} \text{ torr}^{-1}$) also appears in the rise as would be expected if ν_4 filled from ν_2 . As will be shown below in the discussion of kinetics, a state being filled slowly (e.g. $34 \text{ ms}^{-1} \text{ torr}^{-1}$) but emptied rapidly (e.g. $156 \text{ ms}^{-1} \text{ torr}^{-1}$) can exhibit exactly this behavior. While such a situation is kinetically unusual, it is by no means unique. For example, when the stretching modes of SO_2 are laser pumped, they in turn fill the bending mode more slowly than it is emptied by V-T/R relaxation.⁽¹¹⁾

Two exponential rise terms in the population of a state, ν_4 in this instance, could also occur if the state is filled from two different reservoirs at two different rates. Since COF_2 is initially excited to only a single state, ν_2 , it is conceivable that energy is transferred in such a way that two population reservoirs develop which each fill the ν_4 state at different rates. However, the energy levels near the ν_2 state are sparse enough that this mechanism seems unlikely. Furthermore, one of the population reservoirs must ultimately have its source in the ν_2 state, which decays with a rate constant of $34 \text{ ms}^{-1} \text{ torr}^{-1}$. Thus there seems to be no way to generate another population reservoir so quickly that it fills the ν_4 state with a rate constant of $156 \text{ ms}^{-1} \text{ torr}^{-1}$.

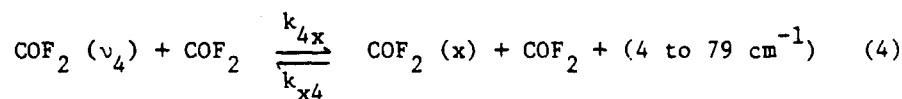
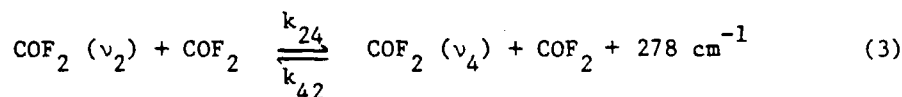
In 1910, Lowry and John⁽¹²⁾ discussed the kinetics of successive, reversible first-order reactions (2)



Lowry and John emphasized that if $k_{12} > k_{32}$, i.e. the rate constant for filling A_2 from the initial state A_1 is greater than the rate constant for filling A_2 from the final state A_3 , then the population of the intermediate species, A_2 , passes through a maximum. What they did not emphasize is that if $k_{32} > k_{12}$, then the population of A_2 rises asymptotically to an equilibrium value and that the rise is a sum of two exponential terms.

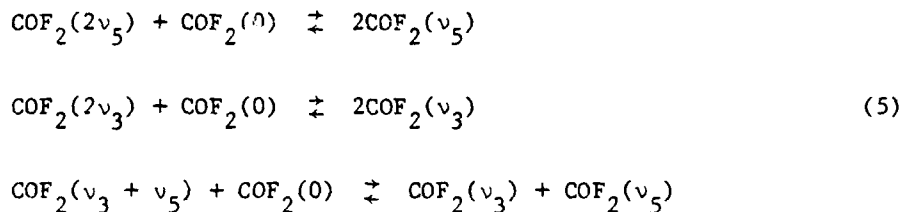
Thus, if one identifies the species A_1 with the initially pumped state, v_2 , the intermediate species A_2 with the fluorescing state, v_4 , and the final species A_3 with a state or states such as $v_3 + v_5$, $2v_3$, and/or $2v_5$ (see Fig. 1) then the rise of the v_4 state is expected to be described by two exponential terms if $k_{32} > k_{12}$. This mechanism is also completely compatible with the rate constant $34 \pm 2 \text{ ms}^{-1} \text{ torr}^{-1}$, equaling the slower rise of the intermediate state, $29 \pm 5 \text{ ms}^{-1} \text{ torr}^{-1}$. Thus, we conclude that the mechanism in which the v_4 state is an intermediate between the initially prepared v_2 state, and a final state is most compatible with the observation.

Reexpressing mechanism (2) for COF_2

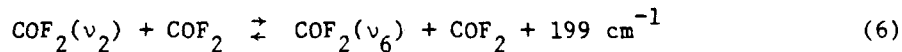


where state x probably refers to either $2v_3$ ($\Delta E = 4 \text{ cm}^{-1}$), $2v_5$ ($\Delta E = 79 \text{ cm}^{-1}$) or $v_3 + v_5$ ($\Delta E = 43 \text{ cm}^{-1}$). Although the Lowry-John model also predicts that the initially pumped state (v_2) will decay via two exponential terms, the amplitude of the faster decay would be so small in the present case as to be experimentally unobservable.

The relaxation mechanism (3,4) is incomplete since it does not account for the other fluorescences observed in COF_2 nor does it include V-T/R relaxation which allows all of the state populations to return to equilibrium values. It is this process which is largely involved in the $\sim 6 \text{ ms}^{-1} \text{ torr}^{-1}$ exponential decays observed in both the 8μ and 5μ fluorescence. If we choose for the elementary rate constants the values $k_{24} = 20 \text{ ms}^{-1} \text{ torr}^{-1}$ (800 collisions) and $k_{4x} = 50 \text{ ms}^{-1} \text{ torr}^{-1}$ (325 collisions), we obtain 160 and $36 \text{ ms}^{-1} \text{ torr}^{-1}$ as the fluorescence rise rates for the v_4 state with the amplitude of the faster term twice that of the slower term. The effects of other processes which must occur in the complete energy transfer pathway will modify the values of the elementary rate constants in order to maintain agreement with the observed rate parameters. For example, deactivation of $\text{COF}_2(x)$ states must occur at a near gas kinetic rate via processes such as



In addition there is some evidence in other fluorescence emissions⁽¹⁰⁾ that the relaxation of v_2 via



may be competitive with deactivation through v_4 (process b).

Conclusions

(1) The ν_4 asymmetric stretch mode of COF_2 fills from the ν_2 symmetric stretch level via a relatively inefficient collisional mechanism which is translationally endothermic.

(2) Efficient loss of population from ν_4 occurs rapidly through the overtone combination levels $2\nu_3$, $2\nu_5$, $\nu_3 + \nu_5$ which are nearly resonant with ν_4 .

(3) The slow filling of ν_4 coupled with its rapid emptying creates a kinetic anomaly in which the filling and emptying rates both appear in the rise of fluorescence from this state.

(4) The initially pumped mode ν_2 of COF_2 appears to decay via two competing mechanisms (the endothermic path through ν_4 and an exothermic path through ν_6).

(5) The rate of collision induced intermode energy transfer in COF_2 is quite slow (~ 500 collisions) for a four atom polyatomic. The features which seem to lead to this situation are the relatively wide spacing of vibrational mode frequencies and the presence of all heavy atoms in the molecule. Thus the amplitude of vibrational motions and the ability of rotations to take up energy are reduced compared to hydrogen or deuterium containing species.

(6) The overall vibration-translation/rotation relaxation process for pure COF_2 requires approximately 2500 collisions on the average.

*This research was also supported by the National Science Foundation under Grant NSF-CHE77-11384 and by the Department of Energy under Contract DE-AS02 - ER-78-S-02-4940.

(1) K. H. Casleton and G. W. Flynn, J. Chem. Phys. 67, 3133 (1977).

- (2) E. Weitz and G. Flynn, Adv. in Chem. Phys., to be published. A notable exception is the energy transfer pathway in OCS, M. Mandich and G. W. Flynn, J. Chem. Phys. 73, 1265 (1980).
- (3) C. B. Moore, J. Chem. Phys. 43, 1265 (1965).
- (4) P. Hess, A. H. Kung, and C. B. Moore, J. Chem. Phys. 72, 5525 (1980).
- (5) E. Weitz, G. W. Flynn, and A. M. Ronn, J. Chem. Phys. 56, 6060 (1972).
- (6) G. A. Drennon and R. A. Matula, J. Chromatog., 34, 77 (1968).
- (7) E. Würzburg and P. L. Houston, J. Chem. Phys. 72, 5915 (1980). We are indebted to Professor Houston for sending us a copy of his original program.
- (8) P. D. Mallinson, D. C. McKean, J. H. Holloway, and I. A. Oxton, Spectrochem. Acta. 31A, 143 (1975).
- (9) R. D. Bates, Jr., J. T. Knudtson, and G. W. Flynn, J. Chem. Phys. 57, 4174 (1972).
- (10) R. K. Bohn, K. H. Casleton, Y. V. C. Rao, and G. W. Flynn, manuscript in preparation.
- (11) D. Siebert and G. W. Flynn, J. Chem. Phys. 62, 1212 (1975).
- (12) T. M. Lowry and W. T. John, J. Chem. Soc. 97, 2634 (1910). Part of this work has been recast in A. Frost and R. Pearson, "Kinetics and Mechanism", 2nd ed., p. 175, John Wiley and Sons, New York (1961). We are using the nomenclature of Frost and Pearson.

B. TEMPERATURE DEPENDENCE OF SO_2 ENERGY TRANSFER RATES*

(J. L. Ahl, G. W. Flynn)

(Principal Investigator: G. W. Flynn (212) 280-4162)

The development of new molecular lasers is dependent upon our understanding of the V-V and V-R,T relaxation processes occurring in vibrationally excited gases. There have been many measurements of the relaxation rates of polyatomic molecules at room temperature and theories to explain these results, however a proper test of our understanding of these processes requires a knowledge of the temperature dependence of the relaxation rates. Though a number of such studies have been conducted using the ultrasonic absorption/dispersion technique, the proper interpretation of the raw data is open to question.⁽¹⁾⁽²⁾ The more reliable technique of laser induced fluorescence has been used to measure temperature dependences only in a few cases, and then on hydrogen containing molecules.

We are currently studying the vibrational relaxation of SO_2 over the temperature range 210 K to 500 K. Sulphur dioxide has three infrared active vibrational modes, the ν_1 stretch at 1151 cm^{-1} , the ν_2 bend at 518 cm^{-1} , and the ν_3 stretch at 1361 cm^{-1} . Using a Q-switched CO_2 laser, we excite the ν_1 band and observe the fluorescence decay of the ν_3 band. Previous room temperature studies⁽³⁾⁻⁽⁵⁾ show a rapid equilibration of the ν_1 and ν_3 bands, followed by a slower equilibration with the ν_2 band. This suggests the possibility of an optically pumped laser operating on either the $\nu_1 \rightarrow \nu_2$ or $\nu_3 \rightarrow \nu_2$ transition. Observation of the temperature dependences of these rates will indicate the proper operating parameters for such a laser.

In addition to studying the relaxations of pure SO_2 , we are also studying the temperature dependence of the rare gas induced relaxation of

SO₂. The experimental results can be compared to a number of semiclassical and quantum calculations on this system.

In our preliminary studies, we have obtained results on the pure SO₂ system over a temperature range from 218 K to 365 K. The raw data has been analyzed assuming a kinetic system consisting of only two rates, the V-V equilibration of ν_1 and ν_3 , and the (slower) equilibration of the ν_1 , ν_3 pair with the $2\nu_2$ state. The $2\nu_2$ state is assumed to relax very rapidly to the ν_2 state, and thus is not significantly populated. From the observed decay rates, we are able to obtain the above noted microscopic rate constants. The temperature dependence of the slow rate corresponding to the ν_1 , ν_3 to $2\nu_2$ equilibration, agrees with an SSH theory calculation by Rao.⁽⁶⁾ However, the fast rate constant, corresponding to the ν_1 to ν_3 equilibration shows non-SSH behavior at low temperatures. Preliminary results suggest that the rate constant reaches a minimum at approximately room temperature, and increases at lower temperatures. Further experiments are underway to check these results and to determine the rare gas dependence of these rate constants.

*This research was also supported by the National Science Foundation under Grant NSF-CHE77-11384.

- (1) H. E. Bass, T. G. Wenter, and L. B. Evans, J. Chem. Phys. 54, 644 (1971).
- (2) F. D. Sheelds, J. Chem. Phys. 46, 1063 (1967).
- (3) D. R. Siebert, F. R. Grabiner, and G. W. Flynn, J. Chem. Phys. 60, 1564 (1974).
- (4) D. Siebert and G. W. Flynn, J. Chem. Phys. 62, 1212 (1975).
- (5) B. L. Earl, A. M. Ronn, and G. W. Flynn, Chem. Phys. 9, 307 (1975).
- (6) Y. V. C. Rao, Chem. Phys. Lett. 62, 107 (1979).

C. LASER EXCITED INFRARED FLUORESCENCE IN OXALYL FLUORIDE

(T. H. Allik, G. W. Flynn)

(Principal Investigator: G. W. Flynn (212) 280-4162)

Time-resolved laser excited fluorescence experiments have appeared in the literatures since the mid 1960's.⁽¹⁾ Although numerous articles have been written on the topic of vibrational relaxation in simple polyatomic molecules, little is understood concerning the energy transfer mechanism of molecules with "hundreds" of vibrational states. We have studied one such case, the molecule oxalyl fluoride, trans-C₂O₂F₂.

Oxalyl fluoride has twelve fundamental frequencies and the number of vibrational states alone below 2500 cm⁻¹ is > 5000.⁽²⁾ The molecule has a low lying torsional mode ν_7 , whose frequency is 127 cm⁻¹.⁽³⁾ Ab initio calculations for the barrier to internal rotation in C₂O₂F₂ suggest a value of 1830 cm⁻¹.⁽⁴⁾ An interesting situation occurs between approximately 2000 and 8000 cm⁻¹. The ν_7 mode is in the "quasicontinuum" whereas most of the other fundamentals are in discrete states. This is not the case for "simple" polyatomics!

The antisymmetric C-F stretching mode ν_{10} of oxalyl fluoride was excited with a Q-switch CO₂ laser operating at the R branch of the 9.6 μ band (energy = 3/4 mJ/pulse). Laser induced fluorescence was observed from: the antisymmetric carbonyl stretching mode ν_9 at 5.3 μ , the combination state $\nu_4 + \nu_{11}$ at 8.0 μ and states between 11-14 μ . Figure 1 shows the vibrational energy states and the density of vibrational states for COFCOF. In all three cases the fluorescence was observed to be quite similar with

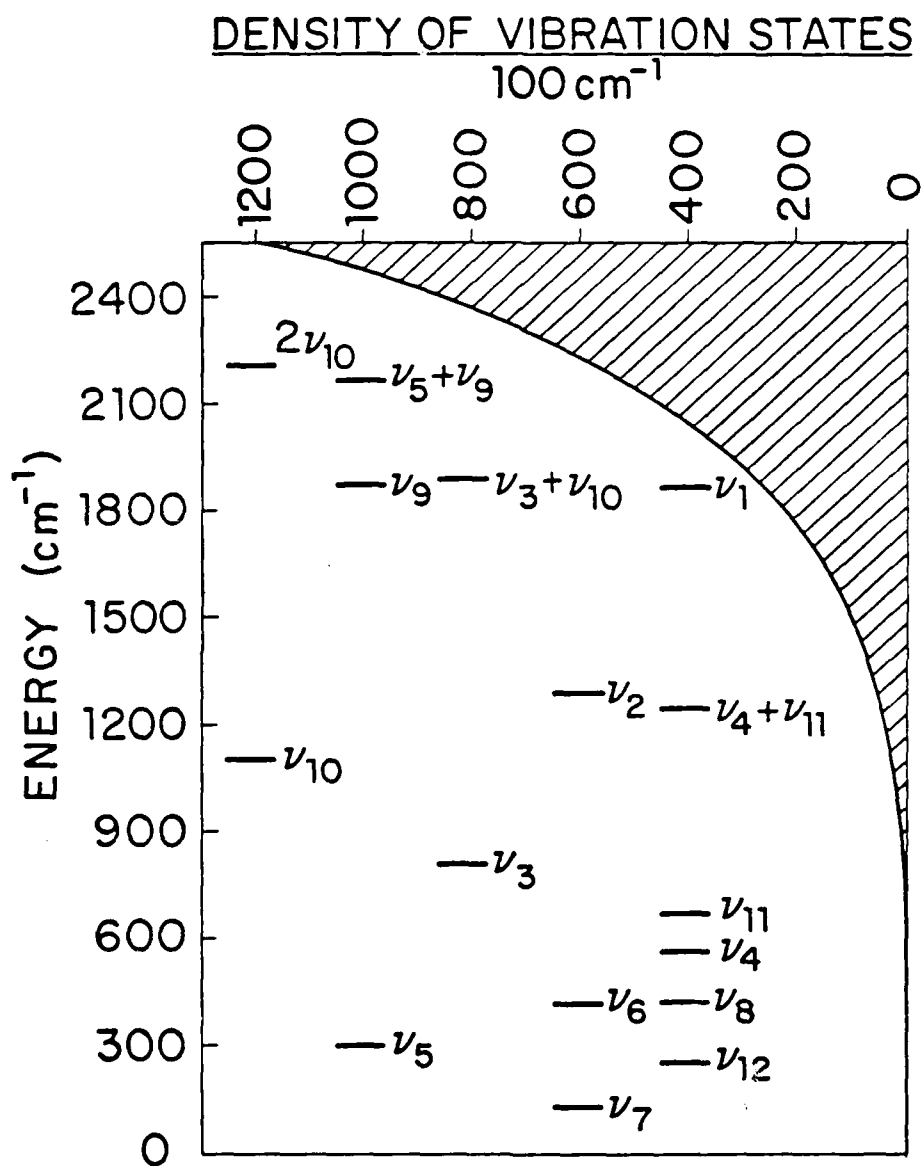


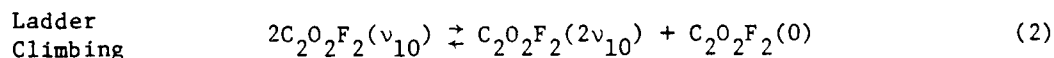
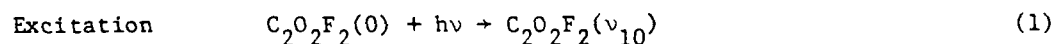
Figure 1

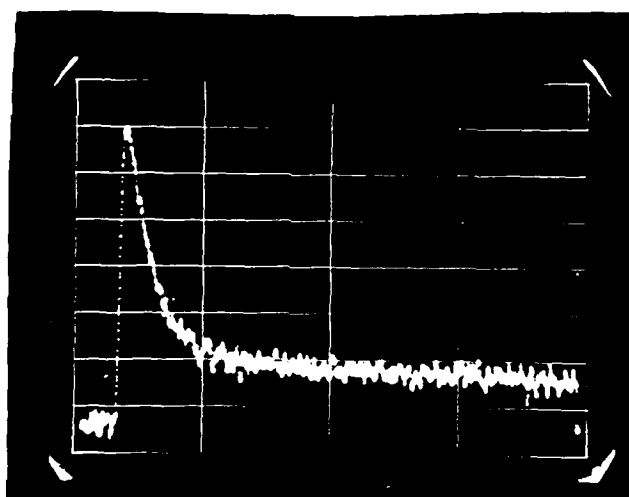
a fast rise followed by a double exponential decay. Figures 2, 3 and 4 show the fluorescence from the 5 and 8 μ states. The fast rise is within the laser pulse indicating an equilibration of energy in < 2 gas kinetic collisions. The slow decay is attributed to the decay of blackbody radiation from "hot" thermalized gas in the center of the cell. The fast decay rate for the 5.3 μ state was analyzed by fitting semilog plots of fluorescence intensity versus time. These rates were then measured as a function of $C_2O_2F_2$ pressure, over a range from 50 to 250 millitorr. Figure 5 shows a Stern-Vollmer plot of rate vs. pressure which provides the desired rate constant. The other states (8 μ and 11-14 μ) show the same order of magnitude decay rate.

Since we are not looking at fluorescence from the pump mode, the very fast rise time indicates that a rapid V-V equilibration is occurring. This fast V-V process can be either collisional or collisionless in nature. If it is collisional, the molecules are undergoing an extremely efficient energy exchange process. If it is collisionless, oxalyl fluoride is exchanging quanta between the modes intramolecularly!

The mechanism for the V-V energy transfer is however not yet clear. Two possible pathways may be occurring:

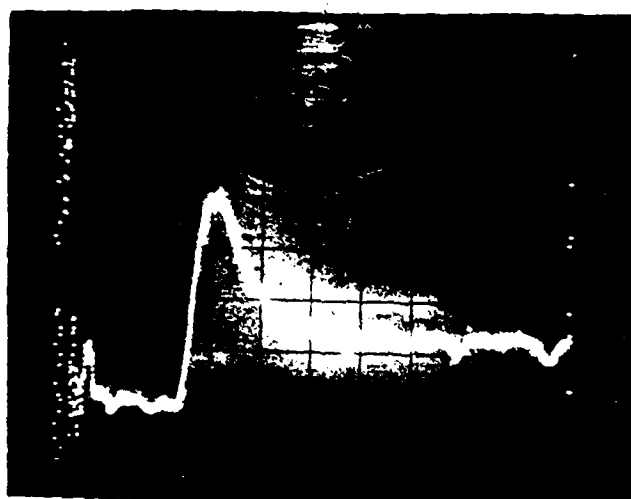
I. Fluorescence from a Combination State





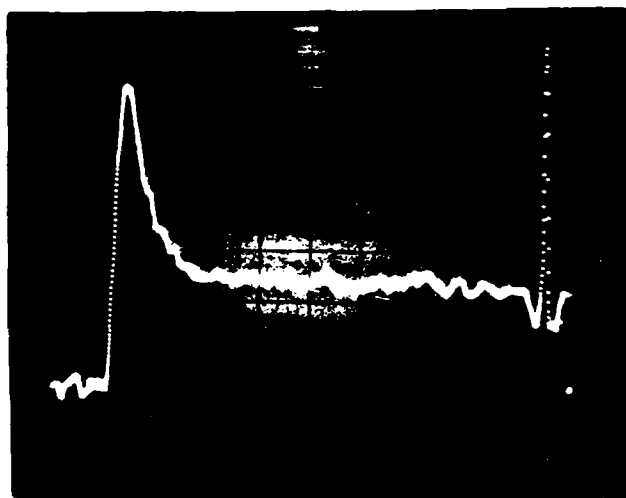
5.3 μ FLUORESCENCE
PRESSURE 0.057 TORR
102.4 μ SEC FULL SCALE
89 K SHOTS

FIGURE 2



5.3 μ FLUORESCENCE
PRESSURE 0.216 TORR
10.48 μ SEC FULL SCALE
144 K SHOTS

FIGURE 3



8.0 μ FLUORESCENCE
PRESSURE 0.167 TORR
40.98 μ SEC FULL SCALE
64 K SHOTS

FIGURE 4

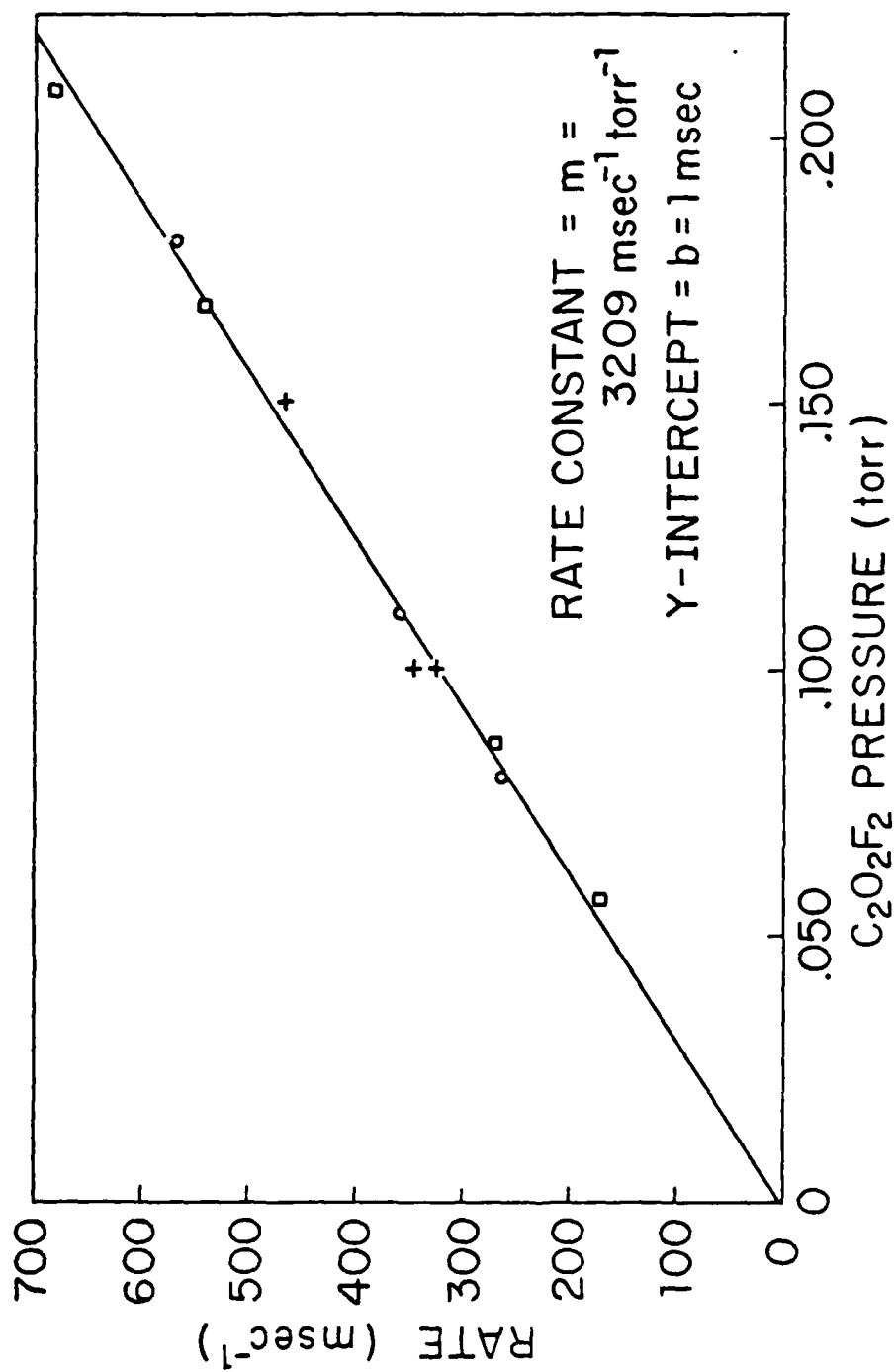
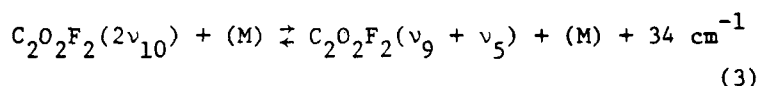
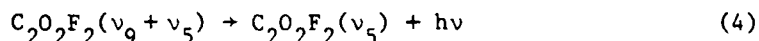


Figure 5

V-V Equilibration
(Collisional (M)
or Collisionless)



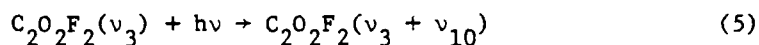
Fluorescence



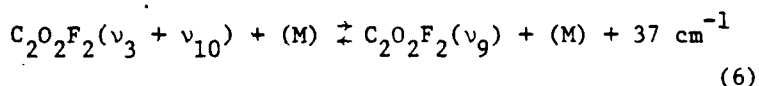
or

II. Hot Band Absorption

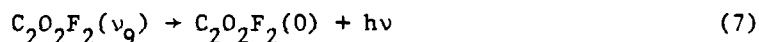
Hot Band
Excitation



V-V
Equilibration



Fluorescence



Nevertheless, the cold gas filter technique⁽⁵⁾ should be able to differentiate between the two. These experiments are currently underway and should yield interesting results.

The fast decay, V-T rate, which corresponds to approximately 8 gas kinetic collisions, can be attributed to the presence of the large number of low lying modes. These modes provide a near resonant path for the initial excitation to be converted into translation, with the maximum defect of 127 cm^{-1} .

As seen in the case of acetylene fluoride,⁽⁶⁾ the relaxation of molecules with a dense vibrational manifold having states within kT of the ground state appears to be extremely fast. These systems, where discrete states

exchange energy with states in the quasicontinuum, provide good models for relaxation of more complex molecules.

- (1) For a brief history, see J. T. Yardley, "Introduction to Molecular Energy Transfer" (Academic Press, New York, 1980), Chapter 3.
- (2) Assuming a harmonic oscillator with a 3 cm^{-1} anharmonicity in ν_7 .
- (3) J. L. Hencher and G. W. King, J. Molec. Spectrosc. 16, 168 (1965).
- (4) J. Tyrrell, J. Am. Chem. Soc. 98, 5456 (1976).
- (5) R. McNair, S. Fulghum, G. Flynn, M. J. Feld, and B. Feldman, Chem. Phys. Lett. 48, 241 (1977).
- (6) Columbia Radiation Laboratory Progress Report #29, March 21, 1979, pp. 65-66.

D. COLLISION ASSISTED LASER EXCITATION OF SF_6 IN A SUPERSONIC NOZZLE*

(M. I. Lester, D. R. Coulter, L. M. Casson, R. B. Bernstein, G. W. Flynn)

(Principal Investigator: G. W. Flynn (212) 280-4162)

Previous experiments have shown⁽¹⁾ that internal energy can be deposited in a beam of SF_6 by irradiation with a low-power cw CO_2 laser in the "collisional region" at the nozzle exit.^{(2),(3)} Greatly enhanced excitation has now been achieved by irradiating inside the nozzle.⁽⁴⁾ Both arrangements take advantage of molecular collisions to overcome inherent weak absorption in polyatomic molecule beams. Collisions assist by broadening absorption lines, promoting rotational hole filling, and providing up-pumping through (V-V) energy transfer. Following irradiation, excited beam molecules move rapidly into the collision-free region, freezing much of the absorbed energy in vibrational modes.

Collisions, which are an inherent part of the excitation and supersonic expansion processes, may also lead to some relaxation of the absorbed energy. The partitioning of the absorbed energy in the molecular beam between internal and translational degrees of freedom can be examined as a function of collision rate. Further, the laser experiments can be compared to the expansion of a thermally equilibrated system prepared by bulk heating of the nozzle source. The extent to which laser excitation with collisions assisting in the absorption process produces a non-equilibrium distribution which differs from bulk heating can thus be determined.

The previous apparatus⁽¹⁾ has been provided with an infrared-transparent, capillary nozzle beam source.⁽⁵⁾ The nozzle is a triangular cross-section, 10 mm long capillary formed by clamping a flat ZnSe plate on a polished block

of stainless steel containing a "V" shaped channel (0.2 mm deep x 0.3 mm wide). The flowing gas within the capillary is irradiated ("double pass") by a cw CO₂ laser at 10.6 μ m [P(16), 5.5-8.5W; area ca. 1 cm²] focused with a 0.4m f.l. lens at any given point along the capillary upstream or downstream of the exit. The electron bombardment ionizer-quadrupole mass filter monitors the number density n of SF₆ in the beam and provides time-of-flight (TOF) measurements of velocity distributions. The energy flux (power, W) carried by the beam is measured with the pumped liquid He-cooled bolometer.⁽¹⁾ For many different irradiation positions, mass spectrometer and bolometer measurements of the mechanically chopped (25 Hz) molecular beam were recorded (via lock-in detection) with and without cw laser excitation. TOF measurements were made at fewer positions of laser irradiation; thus velocity distributions were interpolated at intermediate positions. Separate bolometer experiments have shown that laser scatter along the capillary axis is undetectable except when the laser irradiates the exit surface of the nozzle.

For the heated nozzle experiments, the ZnSe plate of the infrared-transparent capillary nozzle beam source is replaced with an identical plate of highly polished copper. The entire capillary nozzle assembly (copper plate, stainless steel block and clamp) is resistively heated using heating tape. The nozzle temperature is monitored with a chromel-alumel thermocouple which is positioned within the copper plate. Mass filter, bolometer and TOF measurements were recorded as a function of nozzle temperature in the range from 290 to 550 K. Since heating and cooling of the nozzle may take several hours, accurate measurements require that the AC components of the bolometer and mass filter be stable on this time-scale.

Fig. 1 shows the following results from the laser excitation experiments plotted vs. laser irradiation position: the relative change in bolometer

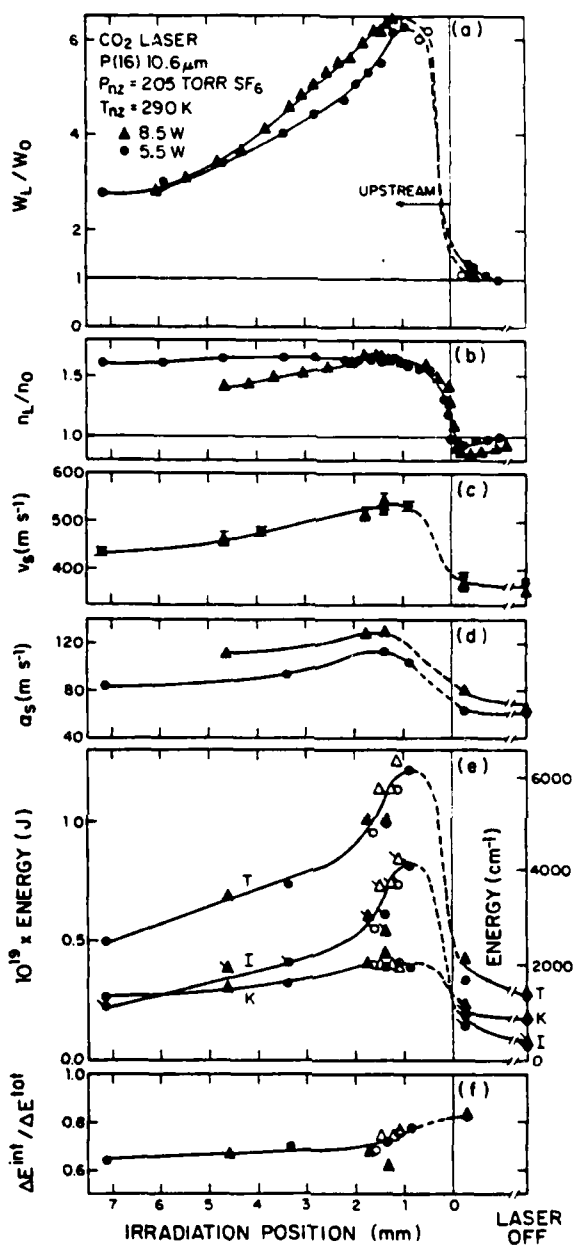


Figure 1: Plotted as a function of laser irradiation position along the infrared-transparent nozzle are: (a) the relative change in bolometer (W_L/W_0) and (b) mass filter (n_L/n_0) signals (open circles: bolometer data corrected for "laser scatter"(1)); (c) the stream velocity v_s and (d) the width parameter α_s from TOF velocity analysis; (e) the calculated average total (T), internal (I) and kinetic (K) energy per beam molecule (open points indicate use of interpolated velocity distributions); and (f) the ratio of the increment in I (i.e., ΔE^{int}) to that in T (ΔE^{tot}) due to laser excitation.

(W_1/W_0) and mass filter (n_L/n_0) signals upon laser excitation, and the TOF results (v_s, α_s) . (All of the results shown are for a pressure of 205 Torr of SF_6 in the oven.) Irradiating the beam downstream of the exit yielded small effects similar to those observed with the original nozzle.^{(1),(4),(5)} Ir-radiation inside the nozzle induced a large enhancement (ca. sixfold) in bolometer output accompanied by an increase in velocity of the beam molecules and an increase in their number density. These effects are seen to be maximized ca. 1 mm upstream of the exit. Laser irradiation of pure Ar or of SF_6 at wavelengths far from resonance yielded no enhancement of bolometer signal. Under all irradiation conditions with or without SF_6 in the capillary the temperature rise of the stainless steel nozzle was merely a few degrees, even over the course of many minutes of continuous irradiation.

The total, translational and internal energy per molecule in the beam, calculated from the laser excitation data as in Ref. (1), are also shown in Fig. 1. Irradiation inside the nozzle yields an increase in both the average kinetic energy (K) and the average internal energy (I). At the optimal irradiation position the increment in average total energy (T) due to laser excitation is ca. 9.5×10^{-20} J molec⁻¹ (4760 cm^{-1} , 0.6 eV), equivalent to ca. five $10.6 \text{ }\mu\text{m}$ photons. Of this absorbed energy ca. 80% is retained as internal excitation.

Normal heating experiments yielded similar qualitative trends as observed with laser excitation. As the nozzle was heated, both the velocity of the beam molecules and their number density increased. At the highest temperatures, the velocity distributions determined from TOF were comparable in magnitude to those observed at the maximum excitation conditions with the laser. However, in contrast to the sixfold enhancement of bolometer signal detected with laser excitation, thermal heating produces a bolometer signal increase (W_{550K}/W_{290K})

of approximately a factor of two.

The distribution of energy in the beam molecules between translational and internal degrees of freedom following thermal heating of the nozzle is calculated as above. The results at room temperature and at the maximum nozzle temperature of 550K are shown in Table I. Also displayed are the energy distributions obtained under optimum laser excitation conditions. Note that the contribution to kinetic energy (K) are similar for laser excitation and thermal heating at 550K. However, the internal energies are dramatically different! Laser excitation yields a SF_6 vibrational temperature (T_{VIB}) of $\sim 740\text{K}$ whereas thermal heating produces a nominal vibrational temperature of 310K. The vibrational temperatures achieved by thermal heating are much lower than the nozzle temperature indicating substantial relaxation during the supersonic expansion process. Saturation of the bolometer during the laser experiments may also have occurred. If so, this would mean that the laser pumped molecules have an even higher internal temperature. This point is presently under investigation.

Table I
Energy Distributions in the SF_6 Molecular Beam

	THERMAL 290K	THERMAL 550K	LASER EXCITATION 1 MM UPSTREAM
KINETIC (K)	920	1770	2000
INTERNAL (I) (T_{VIB})	410 (260K)	680 (310K)	4100 (740K)
TOTAL (T)	1330	2450	6100

All energies in cm^{-1}

The laser results may be interpreted via a collision-assisted absorption and up-pumping mechanism. During expansion the pressure and thus collision rate decreases along the capillary. As the point of irradiation is moved "up stream," the collision frequency in a given irradiation volume increases, resulting in increased absorption.⁽¹⁾ The high internal excitation achieved by irradiating inside the nozzle also implies that many vibrational states are collisionally coupled to the ν_3 pumped state of SF_6 . However, when the collision frequency is further increased, V-T relaxation and energy transfer to the walls limits the energy retained in SF_6 vibration. The increase in kinetic energy with laser excitation indicates that at least some V-T relaxation has occurred before SF_6 molecules reach the collision-free region of the molecular beam. This observation is consistent with expectations based upon the time scale for relaxation in the bulk gas phase⁽⁶⁾ at a pressure in the range of 50-75 Torr, comparable to that estimated for the SF_6 in the capillary immediately upstream of the nozzle exit. Irradiating far upstream (in the high pressure region) should simulate bulk heating, yielding equilibration among all degrees of freedom.

As demonstrated in Table I, laser excitation inside the nozzle produces a level of excitation and a partitioning of the absorbed energy which differs significantly from thermal heating of the nozzle. Thus, laser excitation even with some collisions can provide a distinctly non-equilibrium distribution of energy between internal and translational energies. Further, the present results suggest that thermal heating even to temperatures at which SF_6 would thermally decompose, would not produce vibrational excitation at the level achieved with laser irradiation inside the nozzle.

The present excitation technique provides a highly energetic molecular beam whose energy content can be rapidly modulated, synchronously with the

laser. Problems such as surface reactions and thermal decomposition associated with conventional heated-oven sources are avoided. This excitation method should be of general applicability to many molecules and is of potential use in reactive scattering studies of vibrationally excited species⁽⁷⁾ and multiphoton excitation diagnostics.⁽⁸⁾

*This research was also supported by the National Science Foundation under Grant NSF-CHE77-11384 and by the Department of Energy under Contract DE-AS02-ER-78-S-02-4940. Partial equipment support was provided by the National Science Foundation under Grant NSF-CHE77-24343.

- (1) D. R. Coulter, F. R. Grabiner, L. M. Casson, G. W. Flynn, and R. B. Bernstein, *J. Chem. Phys.* 73, 281 (1980).
- (2) Confirmation of this result comes from the electron diffraction observations of CO₂ laser irradiated jets of SF₆ by L. S. Bartell, S. R. Goates, and M. S. Kacner, *Chem. Phys. Lett.* 76, 245 (1980).
- (3) Somewhat related experiments on energy deposition in SF₆ jets by CO₂ laser irradiation have been reported by A. A. Vostrikov, S. G. Mironov, A. K. Rebov, and B. E. Semyakin, *Sov. J. Technical Phys.* 49, 2680 (1979).
- (4) M. I. Lester, D. R. Coulter, L. M. Casson, G. W. Flynn, and R. B. Bernstein, *J. Phys. Chem.* 85, 751 (1981).
- (5) B. J. C. Wu and G. A. Laguna, *J. Chem. Phys.* 71, 2991 (1979).
- (6) J. I. Steinfeld, I. Burak, D. G. Sutton, and A. V. Nowak, *J. Chem. Phys.* 52, 5421 (1970); R. D. Bates, J. T. Knudtson, G. W. Flynn, and A. M. Ronn, *Chem. Phys. Lett.* 8, 103 (1971); W. D. Breshears and L. S. Blair, *J. Chem. Phys.* 59, 5824 (1973); J. D. Lambert, D. G. Parks-Smith, and J. L. Stretton, *Proc. Roy. Soc. A* 282, 380 (1964).
- (7) U. Agam, M. Eyal, and F. R. Grabiner, *Chem. Phys. Lett.* 68, 35 (1979).
- (8) P. A. Schulz, A. S. Sudbo, E. R. Grant, Y. R. Shen, and Y. T. Lee, *J. Chem. Phys.* 72, 4985 (1980).

E. EXCIMER LASER-INDUCED PHOTOFRAGMENTATION AND VIBRATIONAL ENERGY DISPOSAL IN MOLECULES*

(J. O. Chu, G. W. Flynn)

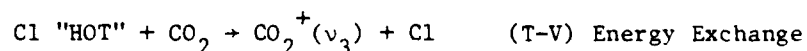
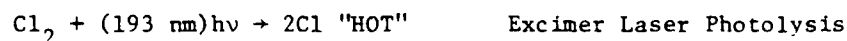
(Principal Investigator: G. W. Flynn (212) 280-4162)

In contrast to the numerous studies of collisional vibrational relaxation of neutral molecules,⁽¹⁾ there have been few investigations of the reverse process of collisional vibrational excitation. This can in part be attributed to the expected small excitation cross sections for such energy exchange events. In addition, bulb techniques must be abandoned in favor of molecular beams in order to obtain collisional energies above the endothermic threshold. On the other hand, beam experiments involving neutral collision partners suffer from difficulties associated with resolving individual vibrational-rotational transitions. Only one report of a molecular beam experiment has been made in which a single vibrationally excited state under single-collision conditions has been resolved.⁽²⁾

A new bulk phase technique has recently been developed⁽³⁾ for studying the process of translational to vibrational (T-V) energy transfer and translationally enhanced reactive events. The method involves excimer laser photolysis of bound molecules to produce translationally "hot" (or superthermal) atoms (or radical fragments) in a gas sample, followed by direct time-resolved detection of infrared fluorescence from vibrationally excited product species. This technique essentially provides a sensitive and direct probe of the translational-to-vibrational, rotational (T-V,R) energy transfer dynamics that occur during each highly energetic collisional event. Furthermore, infrared luminescence detection of T-V excited products

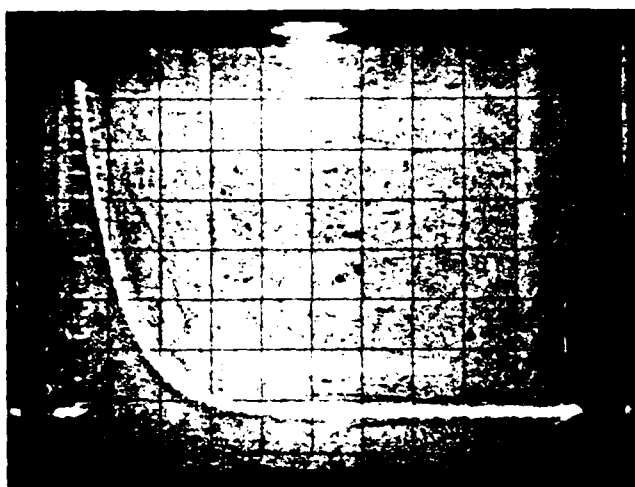
can readily be made wavelength state specific, and subsequent vibrational (possibly rotational) distributions can be obtained from the direct wavelength-resolved emission profile. In the case of generating "hot" highly reactive radical fragments, dynamical competition between the direct T-V energy transfer and the reactive exchange reactions can be studied in detail.

We have initiated a series of experiments to study the efficiency of vibrational excitation by energetic heavy atom fragments. In particular we have begun a study of the Cl_2/CO_2 and ICl/CO_2 systems. Schematically the experiments can be represented by



In the ICl/CO_2 system, laser photodissociation probably produces excited "hot" Cl ($^2\text{P}_{1/2}$) atoms which also undergo rapid reaction with ICl to produce Cl_2 .⁽⁴⁾ We have clearly observed vibrational excitation of CO_2 in these experiments (see Fig. 1) and are in the process of analyzing data. In the ICl/SO_2 system, we have also observed a definite (T-V) energy transfer contribution in addition to the $\text{SO}(\nu = 3,4)$ near resonant transfer to $\text{SO}_2(\nu_3)$, see Fig. 2.

In addition to producing translationally energetic fragments, laser photodissociation can also produce fragments with excess vibrational energies. By studying the energy disposition produced in the vibrationally excited fragments, we can probe and observe the photodissociation process. In our



$$P_{OCL_2}/P_{CO_2} = 1$$

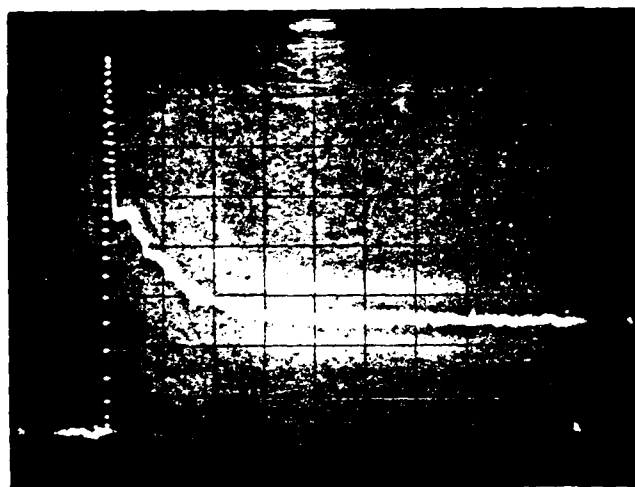
$$P_{TOTAL} = 1.0 \text{ TORR}$$

$$N \text{ SHOTS} = 800$$

$$\text{TIME BASE} = 20 \text{ MSEC} \\ (\text{FULL SCALE})$$

FILTER: 4.0-4.7 BAND PASS

LASER ENERGY: 5 MJ/PULSE.



$$P_{ICL}/P_{CO_2} = 1$$

$$P_{TOTAL} = 1.0 \text{ TORR}$$

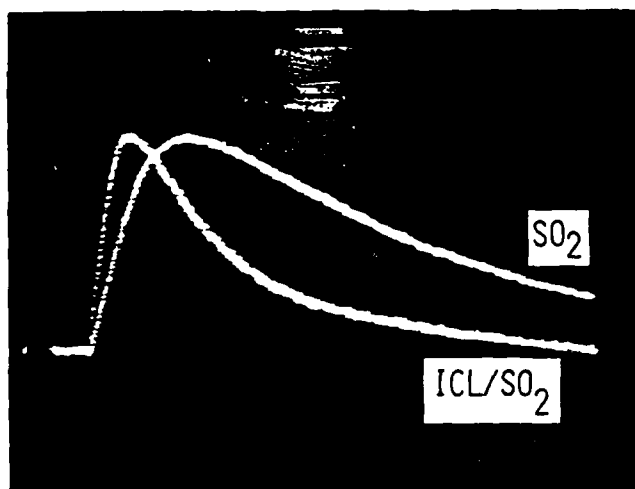
$$N \text{ SHOTS} = 900$$

$$\text{TIME BASE} = 0.1 \text{ MSEC} \\ (\text{FULL SCALE})$$

FILTER: 4.0-5.0 BAND PASS

LASER ENERGY: 1 MJ/PULSE

FIGURE 1. $CO_2(v_3)$ FLUORESCENCE CURVES



CURVE SO_2

$P_{\text{SO}_2} = 0.2 \text{ TORR}$

N SHOTS = 1024

TIME BASE = 2MSEC
(FULL SCALE)

FILTER: 7.0-8.0 BAND PASS

LASER ENERGY: 2MJ/PULSE

CURVE ICL/SO_2

$P_{\text{ICL}}/P_{\text{SO}_2} = 1$

$P_{\text{TOTAL}} = 0.4 \text{ TORR}$

N SHOTS = 1024

TIME BASE = 2MSEC
(FULL SCALE)

FILTER: 7.0-8.0 BAND PASS

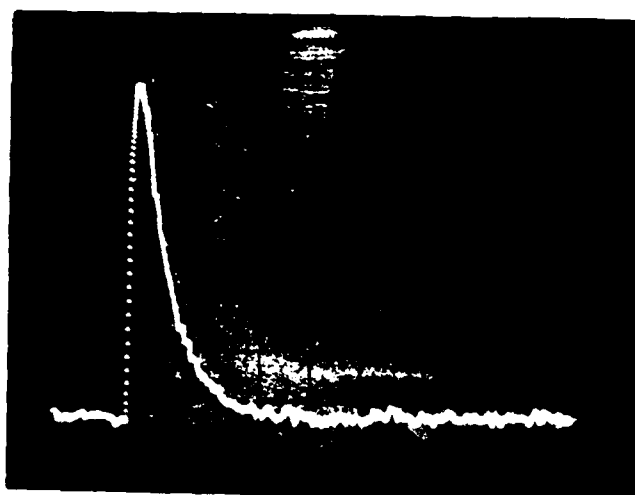
LASER ENERGY: 2MJ/PULSE

FIGURE 2. $\text{SO}_2(\nu_3)$ FLUORESCENCE CURVE.

experiments, we have obtained preliminary results on the vibrational energy disposal in the photofragmentation of $(\text{HCN})_3$. In particular, infrared emission has been observed from different vibrational modes of HCN produced via photofragmentation, see Fig. 3.

A schematic of the experimental apparatus is shown in Fig. 4. A pulsed Lumonics TE-860S excimer laser operated either at 193 nm (ArF) or 248 nm (KrF) was used. All experiments were performed at low fluences ($< 3 \text{ mJ/cm}^2$) in order to avoid multiple photon events. Infrared emission from the system is observed with either a InSb, AuGe or a HgCdTe infrared detector. These detectors only viewed the emission through the appropriate infrared filters. The output from the detector is amplified and then digitized with a transient Bromiation model 8100 recorder. Digitized signals are summed in a signal averager (Nicolet 1170/Northern 575A) and then stored in a PDP 11-34 computer. A conventional glass vacuum flow system is used to provide a fresh gas sample before each laser pulse. All gas samples are used after multiple freeze-pump-thaw cycles.

We have obtained preliminary results on the vibrational energy disposal in the photofragmentation of $(\text{HCN})_3$ via infrared emission detection of the different vibrational modes of HCN. Results have also been obtained in the study of the relaxation process for electronically excited SO_2 molecules produced via excimer laser pumping (see Fig. 5). In addition laser photodissociation has been used to obtain heavy Cl atoms with substantial excess translational energies. These energetic Cl atoms are found to produce vibrational excitation of stable CO_2 molecules during collision encounters. The relative efficiency of heavy vs light "hot" atoms in producing vibrationally excited molecules is being investigated.



HCN (ν_3) FLUORESCENCE CURVE

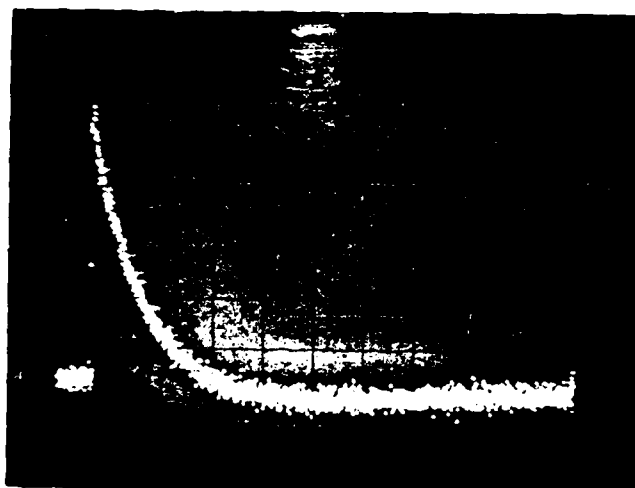
$P_{\text{HCN}} = 0.5 \text{ TORR}$

$N \text{ SHOTS} = 750$

TIME BASE = 0.1 MSEC
(FULL SCALE)

FILTER: 3.0-4.0 BAND PASS

LASER ENERGY: 1MJ/PULSE



HCN (ν_1) FLUORESCENCE CURVE

$P_{\text{HCN}} = 1.5 \text{ TORR}$

$N \text{ SHOTS} = 600$

TIME BASE = 0.04 MSEC
(FULL SCALE)

FILTER: 4.6 LONG PASS AND
1.0-6.0 MLAR

LASER ENERGY: 7MJ/PULSE

FIGURE 3. HCN FLUORESCENCE CURVES

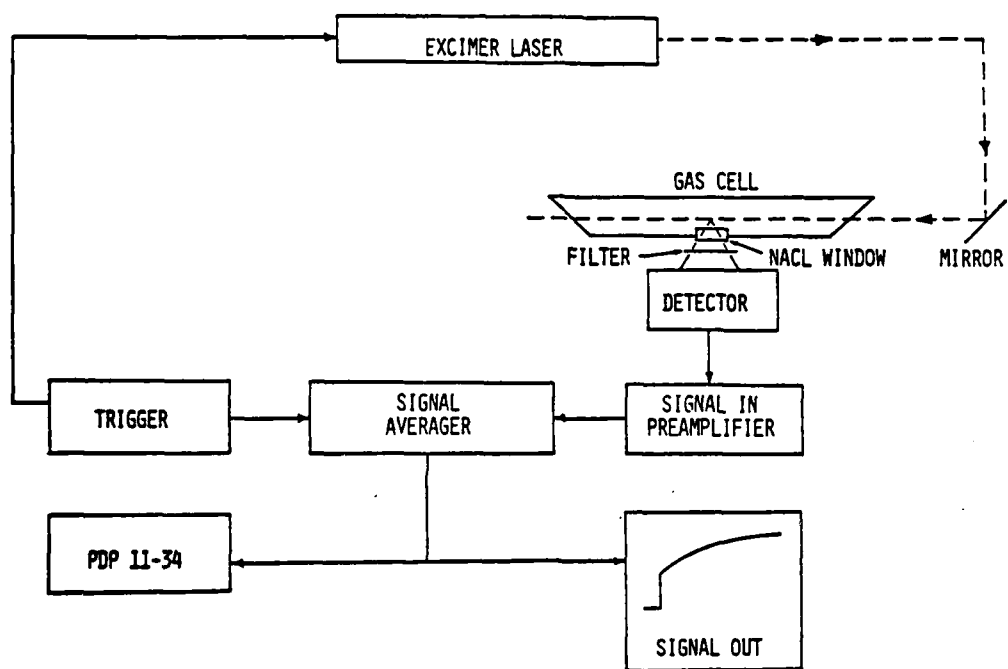
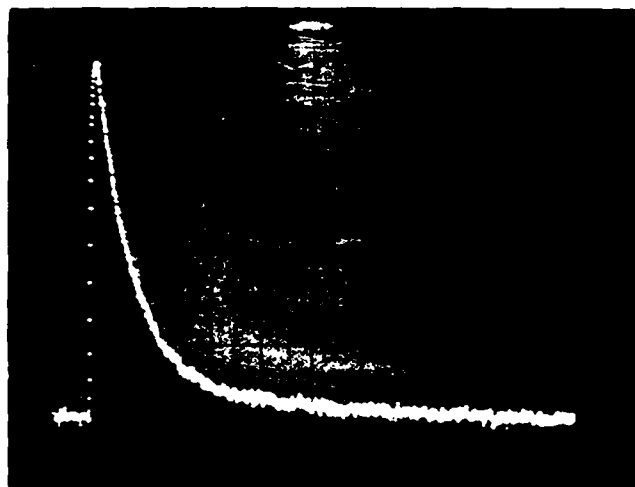


Figure 4: Experimental Apparatus Diagram



$P_{\text{SO}_2} = 1.0 \text{ TORR}$

$N \text{ SHOTS} = 1000$

$\text{TIME BASE} = 4 \text{ MSEC}$
(FULL SCALE)

$\text{FILTER: } 7.0\text{-}8.0 \text{ BAND PASS}$

$\text{LASER ENERGY: } 6 \text{ MJ/PULSE}$
(248NM KRF)

FIGURE 5. (ELECTRONIC RELAXATION) $\text{SO}_2(\nu_3)$ FLUORESCENCE CURVE

*This research was also supported by the Department of Energy under Contract DE-AS02-ER-78-S-02-4940, and by the National Science Foundation under Grant NSF-CHE77-11384.

- (1) E. Weitz and G. W. Flynn, *Ann. Rev. Phys. Chem.* 25, 275 (1974).
- (2) P. J. Dagdigan, *Chem. Phys.* 52, 279 (1980).
- (3) C. R. Quick, R. E. Weston, and G. W. Flynn, "Vibrationally Excited Molecules Produced by Hot Atom Photofragment Projectiles," manuscript in preparation; F. Magnolita, D. J. Nesbitt, and S. R. Leone, "Excimer Laser Photolysis Studies of Translational to Vibrational Energy Transfer," manuscript in preparation.
- (4) H. Okabe, Photochemistry of Small Molecules, (Wiley, New York, 1978), p. 191.

F. PHOTOPHYSICS AND PHOTOCHEMISTRY IN LOW TEMPERATURE SOLID MATRICES*

(P. Beeken, M. Mandich, G. W. Flynn)

(Principal Investigator: G. W. Flynn (212) 280-4162)

Investigation of trapped molecular species is a growing area of interest for both molecular physicists and spectroscopists alike. In the rare gas matrix, molecules are isolated in small cages where, unable to translate and collisionally interact, they may be studied under a variety of excitation conditions. A knowledge of the species of interest as well as an understanding of the interactions with the host lattice can be obtained.

Experiments involving the transfer of electronic to vibrational energy ($E \rightarrow V$) have been an active area of interest for several years in the gas phase.⁽¹⁾⁻⁽³⁾ $E \rightarrow V$ studies can lead to a better understanding of photochemical mechanisms, to the development of new pumping systems for molecular lasers, and can provide tests of theoretical data for nonadiabatic energy transfer theories.⁽²⁾ Because of the many careful investigations in the gas phase, the $\text{Br}_2\text{-CO}_2$ system would be an excellent place to begin an inquiry into $E \rightarrow V$ transfer in the matrix.

There are many questions to be asked concerning $E \rightarrow V$ energy transfer in the rare gas solid. One very important consideration is the fate of the halogen Br_2 after excitation with green light. When Br_2 is excited with green light in the gas phase it may dissociate into the constituent atoms. In the solid, however, the molecule is held in a rigid cage and cannot undergo the same process. We need, therefore, to investigate the

various relaxation pathways available to bromine in the matrix and proceed to look for possible transfer to other molecules such as CO_2 .

Mixtures of freeze-pump-thawed Br_2 (Alfa Ventron 99.998%) and the inert gas are mixed in a glass and stainless steel vacuum line and sprayed on a cold window using a pulsed deposition technique. A typical backing pressure of 400 torr is used within a 10 ml expansion volume to deposit, with 10 to 12 valve cycles, roughly 50 ml-torr of gas. The matrix is maintained on a CsI window held at temperatures varying upwards from 12K by an Air Products Displex 202A closed cycle Helium refrigerator fitted with a cowling to permit the mounting of windows transparent to excitation and fluorescence frequencies (see Figure 1).

Two sources of excitation are used in these studies: a Chromatix CMX4 linear flash pumped dye laser, and a Moletron DL200 N_2 pumped dye laser. The principal dyes used in this series of investigations were obtained from Exciton Corporation and are LD490, Coumarin 500, Rhodamine 6G, and Fluorescein. The laser intensity was measured with a Moletron J3-02DW joulemeter while fluorescence is gathered by a variety of detectors. Visible fluorescence is obtained by an RCA C31034A photomultiplier and far red to near IR light is seen by an Hamamatsu R316 S-1 phototube. Spectra were resolved using a boxcar integrator and an Instruments SA monochromator with a grating ruled with 600 grooves/mm and blazed at 700 nm. IR fluorescence beyond the range of the phototube is measured with an InSb detector using various interference filters to resolve the wavelength. Time dependent signals are taken using a transient recorder signal averager combination.

Argon Matrix: The emission spectrum of Br_2 (1:500 mixture) from a 500 nm excitation appears in Fig. 2 and Fig. 3. It should be noted that the asymmetry of the isotopic triplets is indeed a real phenomenon and is not an

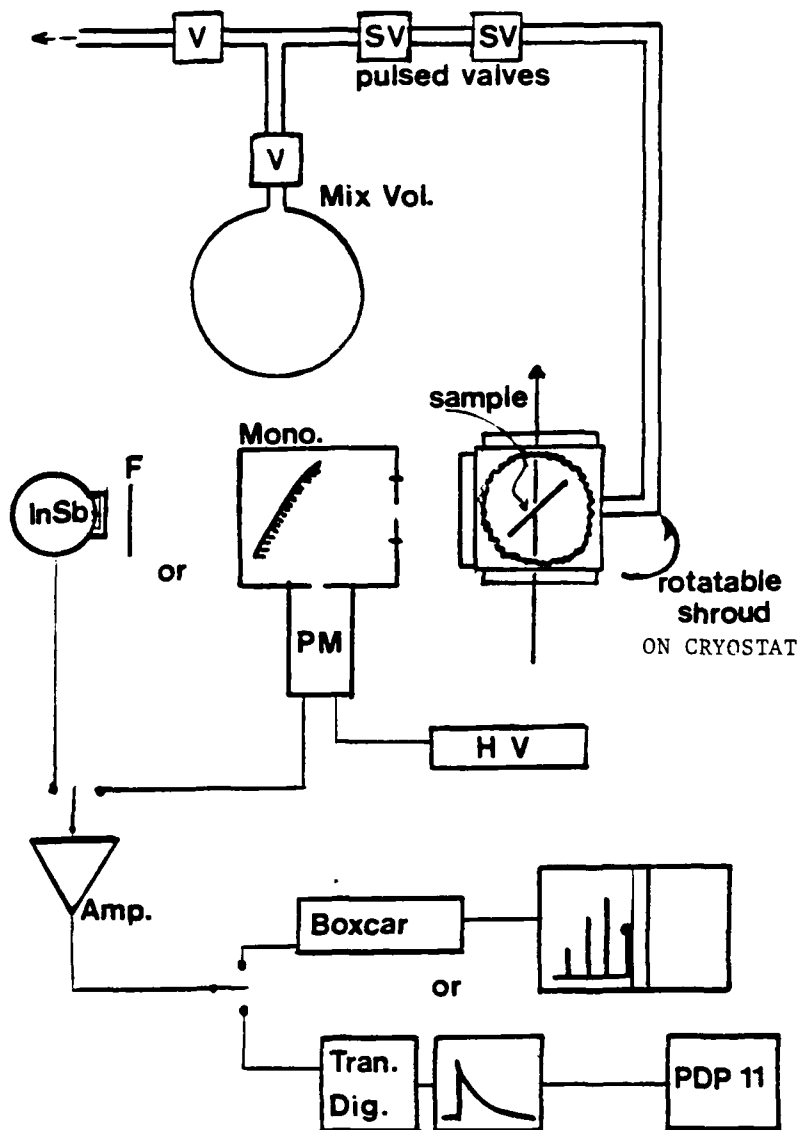


Figure 1: Schematic of Experimental Apparatus.
V = Manual Valve; SV = Solenoid Valve; Mono = Monochromator; PM = Photomultiplier; HV = High Voltage Power Supply; InSb - Indium Antimonide IR Detector; F = Filter; Tran. Dig. = Transient Digitizer/Signal Averager.

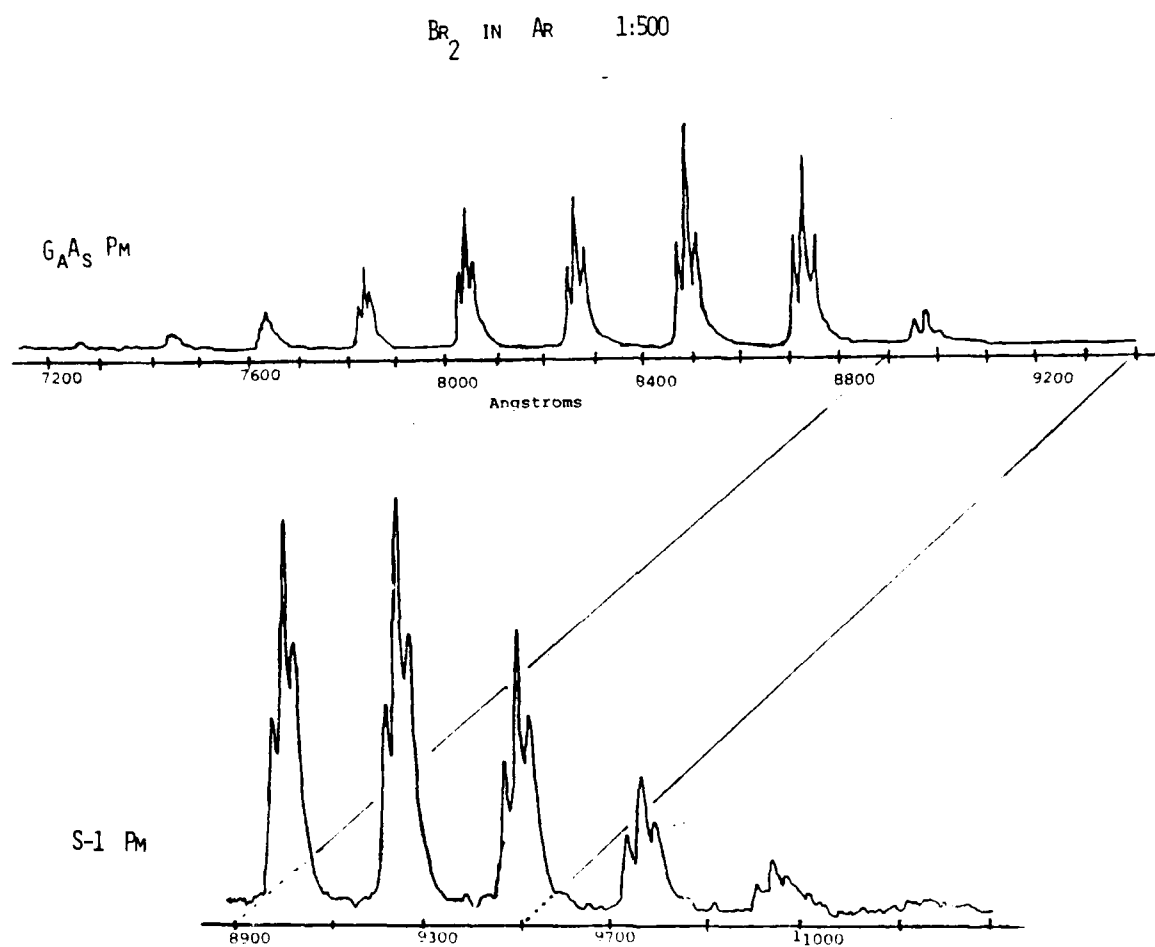
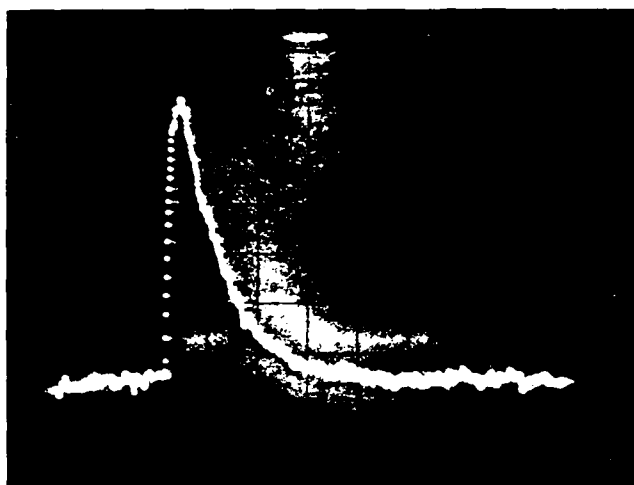
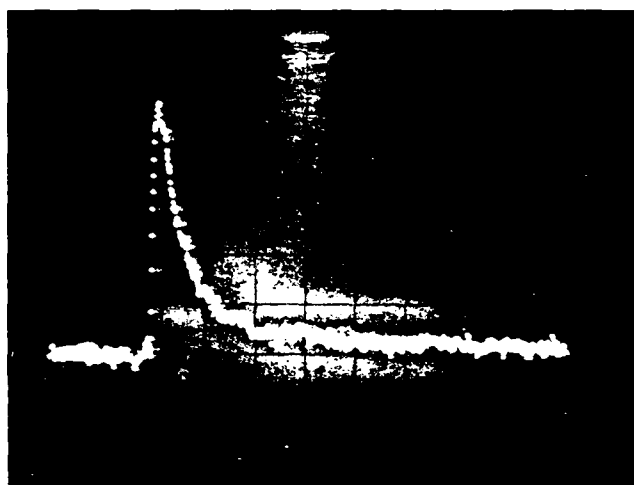


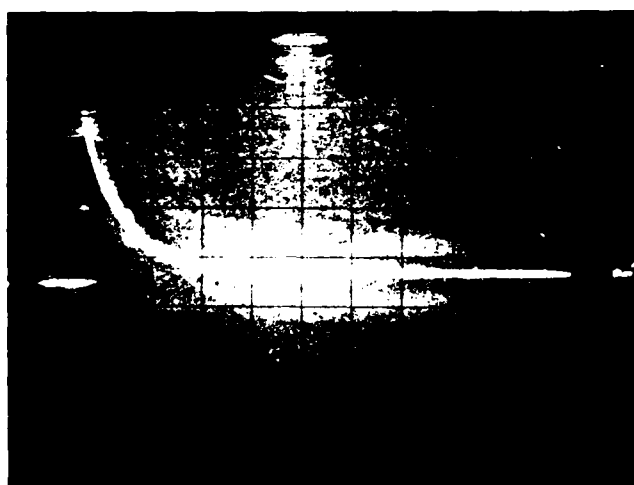
Figure 2: Spectrum of Br_2 in Ar.



Br₂: Ar 1:500
 Decay 73. \pm 4. msec⁻¹
 Taken with an S-1 PM at 970 Å



Br₂: Ar 1:500
 Slow Decay 10. \pm 2. msec⁻¹
 Fast Decay 104. \pm 9. msec⁻¹
 Taken with an S-1 PM at 9510 Å



Br₂: Ar 1:500
 Slow Decay .14 \pm .05 msec⁻¹
 Fast Decay 13.9 \pm .5 msec⁻¹
 Taken with an InSb detector
 above 1.0 microns

Figure 3: Typical Fluorescence Curves for Br₂ in Ar.

artifact of the recording process. This is a point which will be alluded to later in the discussion. The time dependence of the various peaks, including different regions of the triplets, have been measured and appear in Table I. The lifetimes of the various emissions did not vary, within experimental error, as both temperature and concentration were changed. A sample fluorescence appears in Fig. 3. IR emission is also observed above 1.0 microns but was not quite intense enough to resolve with the monochromator. The IR emission is not seen when a red excitation source was used.

Krypton Matrix: Although no spectrum has been obtained from the Br_2/Kr mixture (1:1000) the time dependence of the signals reveal no anomalous behavior with respect to the Ar data aside from a slight shift in lifetime. As it was with the Ar sample the time characteristics show no appreciable sensitivity to changes in temperature. Work is currently in progress to obtain the emission profile and gather frequency dependent lifetimes.

Xenon Matrix: It is in this matrix that the Br_2 sample (1:1000) shows a significant deviation from the Ar data. The spectrum's most significant feature (Fig. 4) is the complete loss of the triplet structure so pronounced in the Ar spectrum. In addition, the time dependent information illustrated in Table I show a considerable deviation from the expected trend in going from Ar to Kr. The one aspect common to the previous studies is that the lifetimes are indeed independent of temperature.

Other work has been reported on spectroscopy of bromine in rare gas matrices.⁽⁴⁾⁽⁵⁾ A red (614 nm) excitation source was used to obtain a lifetime of 7.3 μsec as well as an emission and excitation profile of Br_2 .⁽⁴⁾ In a series of studies on trapped halogen molecules the emission spectra were assigned to transitions from the ground vibrational level of the

TABLE I

<u>Host</u>	<u>Matrix Ratio</u>	<u>InSb Detector</u> (using a 1.1 μ long pass filter)		<u>S-1 PM</u> (using a monochromator)	
		<u>Slow Lifetimes</u>	<u>Fast Lifetimes</u>	<u>Slow Lifetimes</u>	<u>Fast Lifetimes</u>
Ar	500	12.5 msec	62.5 μ sec	--	--
	1000	12.5 msec	62.5 μ sec	8.3 μ sec (7.3 ⁴) (@ 778 nm)	64.8 μ sec (@ 976 nm)
	10000	14.3 msec	63.0 μ sec	--	--
Kr	1000	10.0 msec	142.0 μ sec	--	--
Xe	1000	8.3 msec	4.0 μ sec	4.5 (@ all wavelengths)	

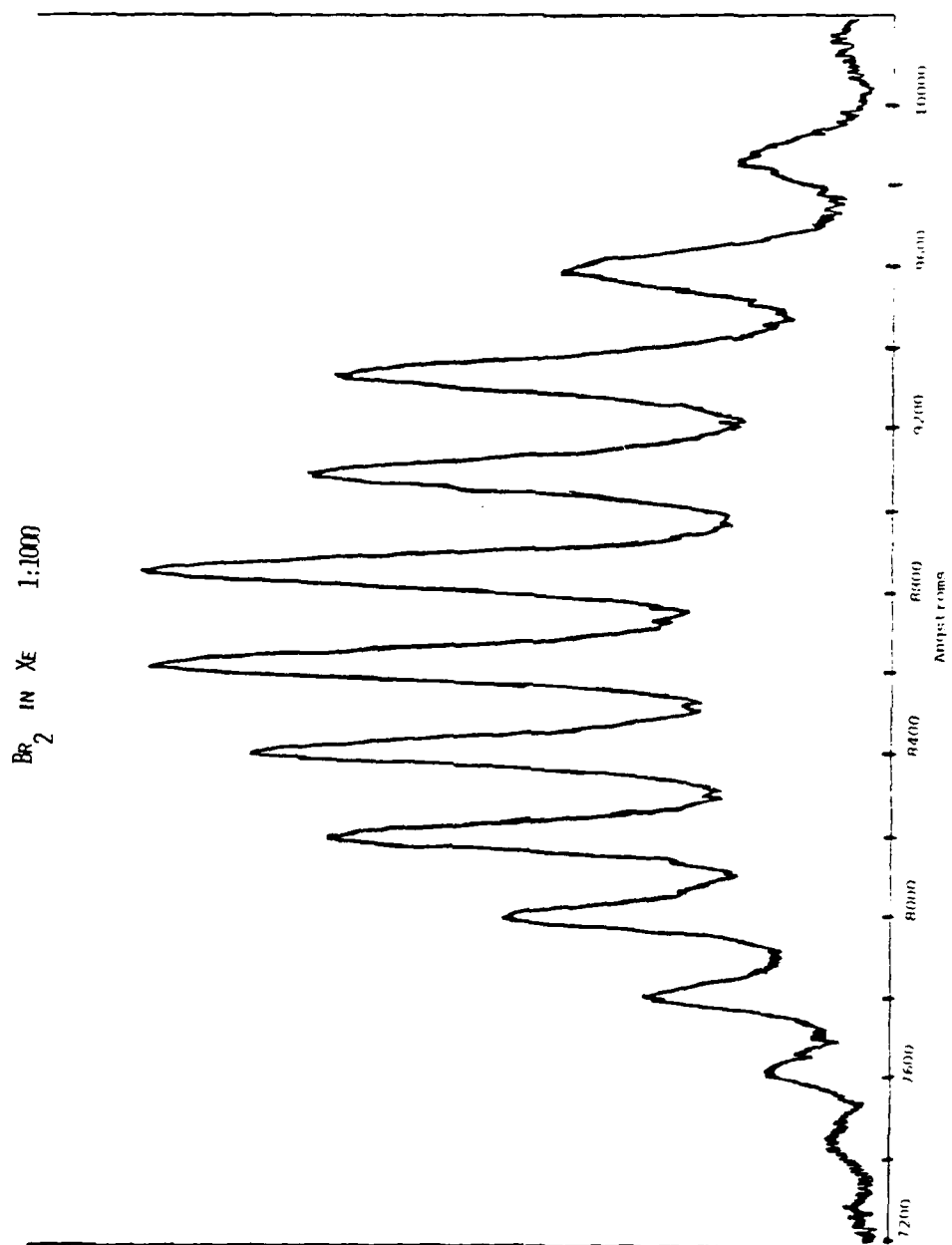


Figure 4: Spectrum of Br_2 in Xe.

excited electronic state to the various vibrational levels of the ground electronic well. The work concluded by assigning the emission solely to the $B^3\pi(0^+u)$ state (see Fig. 5). In a similar study isolated samples of Cl_2 were irradiated with a source that would correspond to a gas phase dissociation limit.⁽⁶⁾ Here the investigators reported that the $^3\pi(2u)$ was the only source of the emission in the trapped chlorine. We have investigated the trapped halogen, Br_2 , under conditions which closely resemble the Cl_2 work; we irradiate with a source which corresponds to the gas phase dissociation limit of Br_2 . When we examined the time resolved data, we found toward the red of the isotopic triplets two exponential decays. The blue side of the triplet yields only one decay. Closer examination of the spectra does suggest that there is a new resonance growing into the emission profile toward the red peak of the triplet. Toward the IR this peak resolves itself separately from the isotopic lines.

We examined lifetimes of bromine further to the infrared, although the sensitivity of our detection system would not allow us to use a monochromator. We did discover a decay rate very close to the slow decay measured in the visible/near IR region of the spectrum. The Franck-Condon profiles⁽⁷⁾ as given in Fig. 6 suggest that emission from the IR would reflect solely the lifetime of the A state while emission in the visible could most likely be due to B state. The region sampled in between, therefore, should exhibit characteristics of both emissions. Our emission profile coupled with the time dependent data obtained from the trapped bromine strongly suggests that, indeed, two states are responsible for the emission.

When bromine is isolated in xenon quite an unusual profile is obtained and very short lifetimes are observed (see Table I and Figure 4 for the

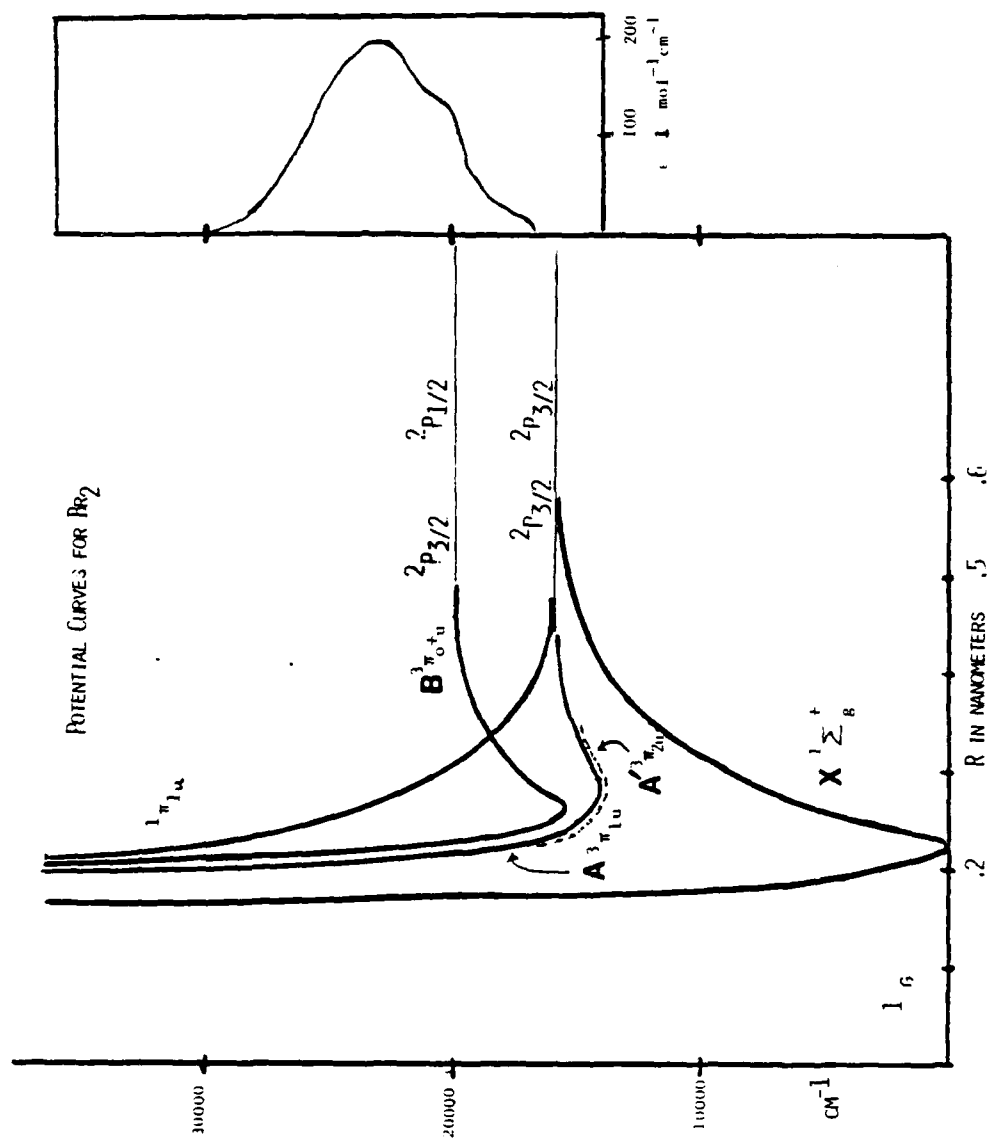


Figure 5: Bromine Potential Diagram with gas phase absorption coefficient.

FRANCK-CONDON PROFILE OF Br_2

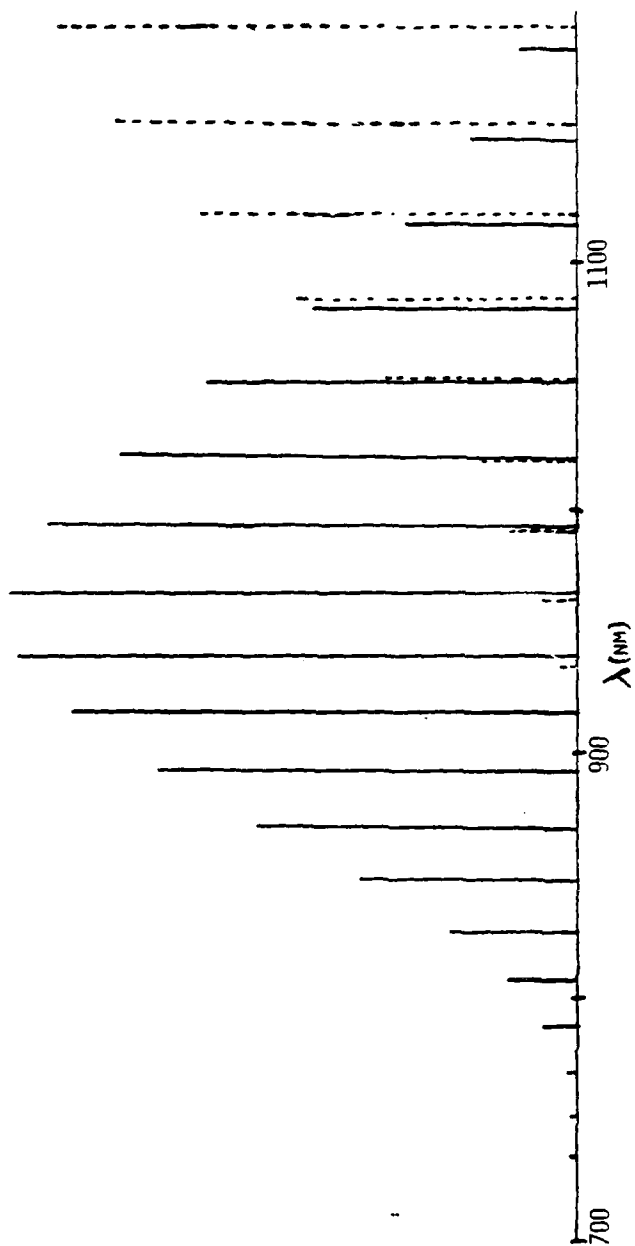


Figure 6: Franck Condon Profile of Br_2 . — $\text{B } 3\pi 0^+u$ State. - - - - $\text{A } 3\pi 1u$ State.

spectrum). The lifetime in the IR region, as well as elsewhere, yielded an unexpected deviation from the trend seen in going from Ar to Kr to Xe. The most obvious feature of the spectra is the complete loss of the structure so readily obtained in the Ar sample and the loss of a second decay. We believe that the lifetime seen in the IR is the lifetime observed further into the visible region of the spectrum.

The primary problem at this point is to try to determine what pathways are available to Br_2 if it cannot dissociate as it would in the gas phase. The Ar data suggests that the sample may indeed dissociate within the cage and reform in an excited state. Previous work⁽⁴⁾ has shown through selective isotopic excitation that very little electronic to electronic energy transfer occurs even between the nearly resonant isotopic neighbors. This implies that if the bromine molecule were excited into one electronic state, it would not be likely to transfer the excitation to another state of another Br_2 . The dissociation/recombination idea is strongly supported by a lack of a rise time in any of the molecular fluorescence signals. In Xe the excited Br_2 may be forming an excimer of the form $\text{Br}_2\text{-Xe}$ which would broaden the emission profile while leaving the resonance spacings close to the value expected for Br_2 . The close interaction of the bromine and xenon might then account for the extremely short lifetime.

Bromine under green excitation yields an emission profile from different emitting states. The spectra coupled with lifetime studies indicates that the primary source of the emission is from the $\text{B}^3\pi(0^+u)$ and $\text{A}^3\pi(1u)$ states. The data strongly suggest that the mechanism for production of population in all these states may be a dissociation/recombination reaction, where the new molecule can reform in a variety of excited states. A different mechanism of interaction is indicated by the results from the

Xe spectra; the excited molecule may be forming an excimer with its host. With an increased understanding of Br_2 in these assorted rare gas hosts we can begin to evaluate possibilities of transfer of energy to other species within the same matrix material.

Our initial impetus for pursuing the investigation into the nature of the excited bromine was to study a potential mechanism for electronic to vibrational energy transfer in a rare gas matrix. The $\text{Br}_2\text{-CO}_2$ system has been well characterized in the gas phase and our ultimate goal is to investigate the possibility for transfer of the electronic excitation to vibrational degrees of freedom.

*This research was also supported by the National Science Foundation under Grant NSF-CHE77-11384 and by the Department of Energy under Contract DE-AS02-ER-78-S-02-4940.

- (1) A. Hairi and C. Wittig, J. Chem. Phys. 67, 4454 (1977).
- (2) P. Houston, "Electronic to Vibrational Energy Transfer from Excited Halogen Atoms," to appear in Adv. in Chem. Phys.
- (3) R. Peterson, C. Wittig, and S. Leone, J. App. Phys. 47, 1051 (1976).
- (4) V. E. Bondybey, S. S. Bearder, and C. Fletcher, J. Chem. Phys. 64, 5243 (1976).
- (5) B. S. Ault, W. Howard, and L. Andrews, J. Mol. Spec. 55, 217 (1975).
- (6) V. E. Bondybey, C. Fletcher, J. Chem. Phys. 64, 3615 (1976).
- (7) J. Coxon, J. Quant. Spec. Radt. Transf. 12, 639 (1972).

IV. ENERGY TRANSFER AND RELAXATION IN ALKALI METALS

A. NUCLEAR SPIN POLARIZATION OF Xe by OPTICAL PUMPING*

(B. Suleman, T. McClelland, N. D. Bhaskar, W. Happer)

(Principal Investigator: W. Happer (609) 452-5584)

We have successfully polarized Xe¹²⁹ by spin exchange with optically pumped rubidium. The polarization was detected by adiabatic reversal of the xenon spins, as described in the preceding progress report. Work on this project is continuing at Princeton University.

*This research was also supported by the Air Force Office of Scientific Research under Grant AFOSR-79-0082.

B. SPECTROSCOPY OF THE 5D STATE OF CESIUM*

(A. Sharma, N. D. Bhaskar, W. Happer)

(Principal Investigator: W. Happer (609) 452-5584)

We have discovered that the cesium atoms within our glass sample cells lase continuously on many transitions in the infrared spectral region, e.g. 7P to 6S at 3.095μ and 2.93μ ; 7S to 6P at 1.469μ and 1.359μ ; 7P to 5D at 1.376μ and 1.360μ . The atoms are excited with cw laser radiation at $4593\overset{\circ}{\text{A}}$ and $4555\overset{\circ}{\text{A}}$ and the lasing occurs without any feedback mirrors. We believe this is the first reported example of mirrorless cw lasing. Work on this project is continuing at Princeton University.

*This research was also supported by the Army Research Office (Durham) under Contract DAAG29-80-C-0043.

C. INFRARED ABSORPTION OF ALKALI MOLECULES*

(A. Vasilakis, N. D. Bhaskar, W. Happer)

(Principal Investigator: W. Happer (609) 452-5584)

We have completed our studies of the newly discovered infrared absorption bands of dense alkali vapors of Cs, Rb, K and Na. All elements show very similar structure between 1μ and 2μ , structure which may be due to absorption from triplet molecules. Preliminary attempts to observe these bands in fluorescence failed to show any signal. We will soon repeat these experiments with a much better infrared detector, intrinsic germanium with a sensitivity at least 200 times better than the PbS detector we used in our first experiments. We have also constructed a high pressure alkali-vapor jet which will allow us to attain much better solid angles of viewing than in our earlier experiments. This work is continuing at Princeton University.

*This research was also supported by the Army Research Office (Durham) under Contract DAAG29-80-C-0043.

D. GROUND STATE POLARIZATION BY TWO-PHOTON OPTICAL PUMPING OF ATOMIC VAPORS*

(N. Tran, N. D. Bhaskar, W. Happer)

(Principal Investigator: W. Happer (609) 452-5584)

We have detected strong two photon excitation of rubidium according to the scheme discussed in the previous progress report. Substantial (i.e. 10% to 20%) spin polarization is also detected. However, our analysis of the data is complicated by the occurrence of strong excimer absorption which also leads to spin polarization of a comparable order of magnitude. This work is continuing at Princeton University.

*This research was also supported by the Naval Air Development Center, Warminster, PA.

E. TEMPERATURE AND DENSITY VARIATION OF THE INFRARED BANDS OF CsXe;
CESIUM POLYXENIDE BANDS*

(R. Novak, N. D. Bhaskar, W. Happer)

(Principal Investigator: W. Happer (609) 452-5584)

This work has been completed and the results have been published.⁽¹⁾

*This research was also supported by the Army Research Office (Durham) under Contract DAAG29-80-C-0043.

- (1) R. Novak, N. D. Bhaskar, and W. Happer, J. Chem. Phys. 71, 4052 (1979).

F. FARADAY ROTATION AND MAGNETIC CIRCULAR DICHROISM OF ALKALI-NOBLE GAS SYSTEMS*

(M. Islam, W. Happer)

(Principal Investigator: W. Happer (609) 452-5584)

Extensive measurements of the magnetic circular dichroism of the CsAr excimer bands and Cs₂ dimer bands have been made during the past year. We have been able to gain for the first time unambiguous information about the angular momentum and angular momentum coupling schemes of the electronic states of excimer molecules.

*This research was also supported by the Army Research Office (Durham) under Contract DAAG29-80-C-0043.

G. PARTICULATE FORMATION IN CESIUM-DEUTERIUM GAS CELLS*

(J. Camparo, J. Pietras, N. D. Bhaskar, W. Happer)

(Principal Investigator: W. Happer (609) 452-5584)

We have used spin exchange magnetic resonance spectroscopy to unambiguously identify free hydrogen atoms, free deuterium atoms and free electrons in cells containing mixtures of hydrogen or deuterium and cesium vapor which is optically pumped by the 4593\AA second resonance line of the cesium atom. The results will be published in a May 1981 issue of Physical Review Letters. This work is continuing at Princeton University.

*This research was also supported by the Air Force Office of Scientific Research under Grant AFOSR-79-0082.

H. SPIN DESTRUCTION IN COLLISIONS BETWEEN CESIUM ATOMS*

(J. Camparo, J. Pietras, N. Bhaskar, W. Happer)

(Principal Investigator: W. Happer (609) 452-5584)

This work has been completed and the results were published.⁽¹⁾

Closely related work on "light narrowing," a narrowing of the magnetic resonance lines of optically pumped alkali vapors by intense pumping light has also been completed and a paper summarizing the results will be published in Physical Review in May or June of 1981.

*This research was also supported by the Air Force Office of Scientific Research under Grant AFOSR-79-0082.

(1) N. D. Bhaskar, J. Pietras, J. Camparo, and W. Happer, Phys. Rev. Letters 44, 930 (1980).

I. SPIN EXCHANGE AND RELAXATION IN Na-NOBLE GAS MIXTURES*

(B. Suleman, N. D. Bhaskar, T. McClelland, W. Happer)

(Principal Investigator: W. Happer (609) 452-5584)

The spin destruction rates of sodium in xenon have been measured and found to be even greater than the rates of rubidium in xenon. Van der Waals molecules, NaXe, are also found to play an important role in the relaxation. Interim results have been published⁽¹⁾ and work on this project is continuing at Princeton University.

*This research was also supported by the Air Force Office of Scientific Research under Grant AFOSR-79-0082.

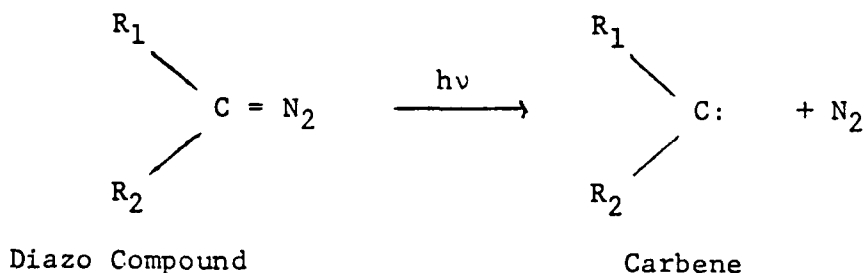
V. PICOSECOND ENERGY TRANSFER AND PHOTOFRAGMENTATION SPECTROSCOPY

A. PICOSECOND LASER STUDIES OF PHOTODISSOCIATION AND ENERGY RELAXATION IN SHORT-LIVED FRAGMENTS*

(C. Dupuy, G. M. Korenowski, M. McAuliffe, W. M. Hetherington III, K. B. Eisenthal)

(Principal Investigation: K. B. Eisenthal (212) 280-3175)

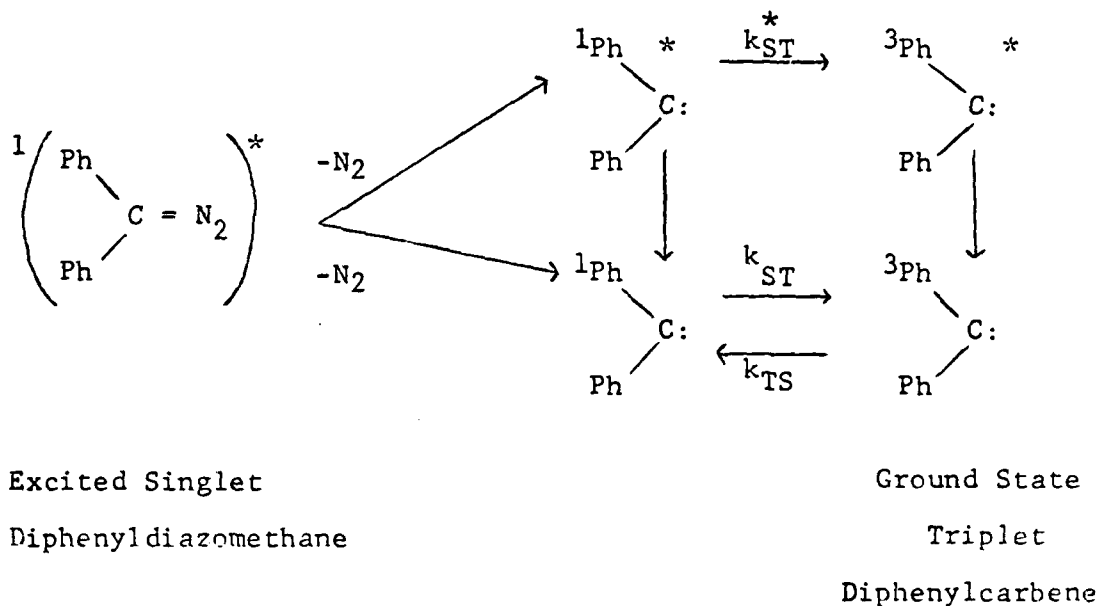
Molecules of the diazo family $>C \equiv N_2$ are of widespread utility in microelectronics and semiconductor fabrication, and in the general use of photosensitive materials for information recording and lithography.⁽¹⁾⁽²⁾ For many molecules of this type the dominant channel for electronic energy relaxation following ultraviolet photoexcitation (or electron beam excitation) is bond rupture generating nitrogen and an important short lived and reactive intermediate called a carbene.⁽³⁾⁽⁴⁾ We can write the photodissociation as




where R_1 and R_2 represent the groups attached. There has been a long standing and lively interest in the structural and chemical properties of carbenes due to their novel reactions and their distinctive electronic structures.⁽³⁾⁻⁽¹⁸⁾ The lowest lying singlet and triplet states, either of which can be the ground state as determined by the attached groups R_1 and R_2 , are close in energy.⁽³⁾⁽⁴⁾ This proximity of singlet and triplet, each having a different chemistry,⁽³⁾⁽⁴⁾ makes the kinetics⁽¹⁵⁾ of interconversion a key aspect of the properties of

these important chemical intermediates.

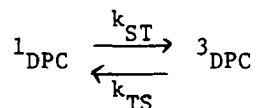
In order to elucidate the dynamics of the photodissociation of the parent diazo compound and the subsequent energy relaxation and reaction of the carbene generated, an ultraviolet picosecond laser pulse is used for photoexcitation. The parent molecule was diphenyldiazomethane. It was dissolved in 3-methyl pentane in acetonitrile at 25°C and irradiated at 266 nm. The sequence of energy decay steps following photoexcitation of diphenyldiazomethane, ultimately leading to diphenyl carbene in its triplet ground state can be written as:



where Ph is the phenyl group . In our initial work⁽¹⁹⁾ we established that a low yield of the excited state triplet carbene $^3\text{DPC}^*$ is produced on one photon excitation of the parent compound. Knowing the energy of the exciting photon and the energy of $^3\text{DPC}^*$ we conclude that the energy of the carbon-nitrogen bond in diphenyldiazomethane, heretofore unknown, is less than 2eV.⁽²⁰⁾

In our work reported here⁽²⁰⁾ we have used a streak camera to detect the rise time of the $^3\text{DPC}^*$ to be < 15 ps. Thus the bond rupture and excited state interconversion, $^*k_{\text{ST}}$, in the carbene must occur in less than 15 ps. To obtain the kinetics of formation of the ground state triplet carbene, ^3DPC , we used a laser induced fluorescence method. Measurement of the triplet fluorescence intensity from $^3\text{DPC}^*$ as a function of the time separation between the excitation and probe pulses yielded a value of 110 ps for the rise time of ^3DPC (Fig.1). Since we independently measured the lifetime of $^3\text{DPC}^*$ to be 4 ns, we conclude that the formation route of ^3DPC , which occurs in 110 ps, cannot be from $^3\text{DPC}^*$. The ground state triplet must therefore come primarily from ^1DPC . The value of k_{ST}^{-1} is thus 110 ps.

From our collaborative work with Professor N.J. Turro we know the value of the reverse process, namely k_{TS} , is $4.1 \times 10^6 \text{ sec}^{-1}$. We therefore find that the equilibrium constant for the process



is

$$K = \frac{9.1 \times 10^9 \text{ sec}^{-1}}{4.1 \times 10^6 \text{ sec}^{-1}} = 2.2 \times 10^3$$

We calculate the free energy difference at 25°C to be 4.6 kcal/mole. After correcting for the entropy difference arising from the multiplicity differences of the singlet and triplet states we find an energy separation between the ground triplet and first singlet state to be 3.9 kcal/mole.

*This research was also supported by the National Science Foundation under Grant NSF-CHE79-23291 and by the Air Force Office of Scientific Research under Grant AFOSR-77-3407B (expired 9/30/80) and AFOSR-81-0009.

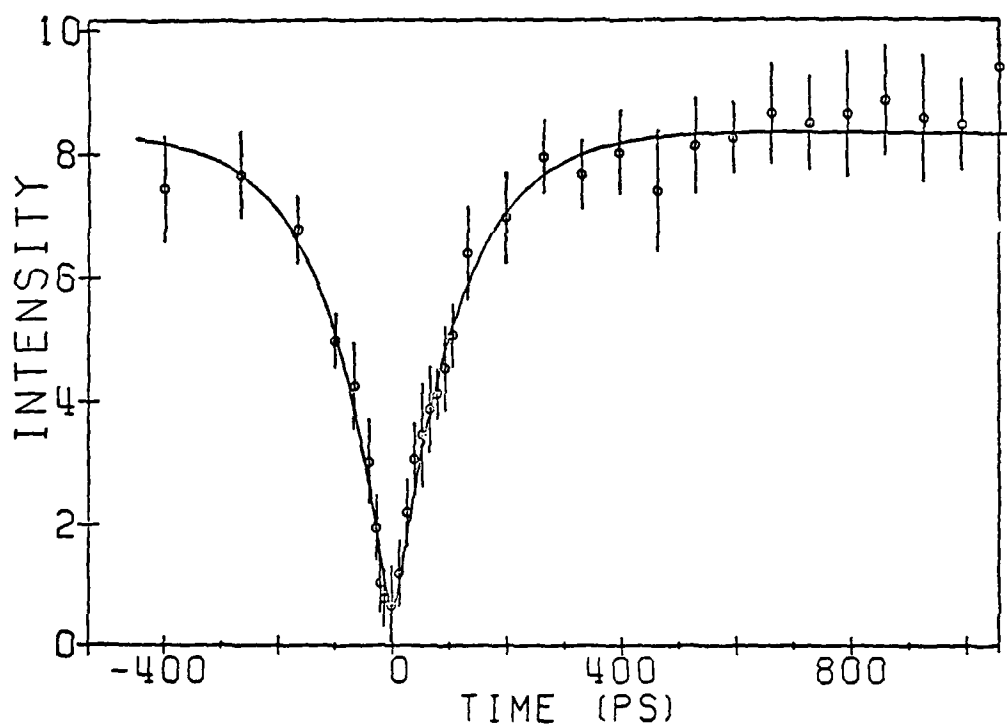


Figure 1: Formation kinetics of ^3DPC . The laser induced fluorescence signal as a function of the time delay between excitation and probe pulses. The solid curve is a calculated fit.

- (1) W. S. Deforest, "Photoresist Materials and Processes", McGraw Hill, New York, 1975.
- (2) M. S. Dinaburg, "Photosensitive Diazo Compounds", Focal Press, New York, 1964.
- (3) R. A. Moss and M. Jones Jr., "Carbenes", Vol. 2, Wiley, New York, 1975.
- (4) W. Kirmse, "Carbene Chemistry", Vol. 1, 2nd Edition, Academic Press, New York, 1971.
- (5) G. Herzberg and J. W. C. Johns, Proc. Roy. Soc. A295, 107 (1966).
- (6) G. Closs, C. A. Hutchison, Jr., and B. E. Kohler, J. Chem. Phys. 44, 413 (1966).
- (7) I. Moritani, S. I. Murahashi, M. Nishino, K. Kimura, and H. Tsubomura, Tetrahedron Letters 373 (1966).
- (8) A. M. Trozzolo, Accounts Chem. Res. 329 (1968).
- (9) W. Ware and P. J. Sullivan, J. Chem. Phys. 49, 1445 (1968).
- (10) P. F. Zittel, G. B. Ellison, S. V. O'Neill, E. Herbst, W. C. Lineberger, and W. P. Reinhardt, J. Am. Chem. Soc. 98, 3731 (1976).
- (11) J. Metcalfe and E. A. Halevi, J. Chem. Soc. Perkin II, 634 (1976).
- (12) J. F. Harrison, R. C. Liedtke, and J. F. Liebman, J. Am. Chem. Soc. 101, 7162 (1979) and references therein.
- (13) D. Bethell, G. Stevens, and P. Tickle, J. Chem. Soc. Chem. Commun. 792 (1970).
- (14) G. L. Closs, Topics Stereochem. 3, 193 (1968).
- (15) G. L. Closs and B. E. Rabinow, J. Am. Chem. Soc. 98, 8190 (1976).
- (16) L. B. Harding and W. A. Goddard III, J. Chem. Phys. 67, 1777 (1977).
- (17) H. D. Roth, Accounts Chem. Res. 10, 85 (1977).
- (18) R. K. Lengel and R. N. Zare, J. Am. Chem. Soc. 100, 7495 (1978).
- (19) K. B. Eisenthal, N. J. Turro, M. Aikawa, J. A. Butcher, Jr., C. Dupuy, G. Hefferon, W. Hetherington, G. M. Korenowski, and M. J. McAuliffe, J. Am. Chem. Soc. 102, 6563 (1980).
- (20) C. Dupuy, G. M. Korenowski, M. McAuliffe, W. M. Hetherington, and K. B. Eisenthal, Chem. Phys. Lett. 77, 272 (1981).

B. PICOSECOND LASER STUDIES OF THE DYNAMICS OF CHAIN RELAXATION*

(M. K. Crawford, Y. Wang, K. B. Eisenthal)

(Principal Investigator: K. B. Eisenthal (212) 280-3175)

The dynamics of chain molecules in solution is currently a subject of great interest and activity.⁽¹⁾⁻⁽⁸⁾ In the present study we have used intramolecular electron transfer between the two end groups of a chain molecule to probe chain dynamics. We have shown in earlier work⁽⁹⁾ that intramolecular exciplex formation in nonpolar solvents is governed by the rate of conformational changes. Thus by monitoring the fluorescence decay of the initially excited group and the rise of the exciplex fluorescence various chain relaxation processes can be examined.

In the present study anthracene and N,N-dimethylaniline are located at each end of the chain molecule consisting of three CH₂ groups. A-(CH₂)₃-DMA. It is therefore the end to end relaxation mode that we are studying in this molecule. Using a picosecond laser pulse to excite the anthracene part we monitor the fluorescence decay of anthracene and the exciplex fluorescence rise with a picosecond streak camera (Fig. 1). In nonpolar solvents we have found that the end to end relaxation of a four bond chain is exponential, i.e. the rate of relaxation is independent of time. This is the first experimental observation of the dynamics of end to end motion in short chain molecules. There have been a number of theoretical and computer simulation treatments of the end to end motions of polymer chains, some as short as ten bonds. (10)-(12) We are presently engaged in analyzing these theories in terms of our experimental findings.

*This research was also supported by the National Science Foundation under Grant NSF-CHE79-23291 and by the Air Force Office of Scientific Research under Grant AFOSR-77-3407B (expired 9/31/80) and AFOSR-81-0009.

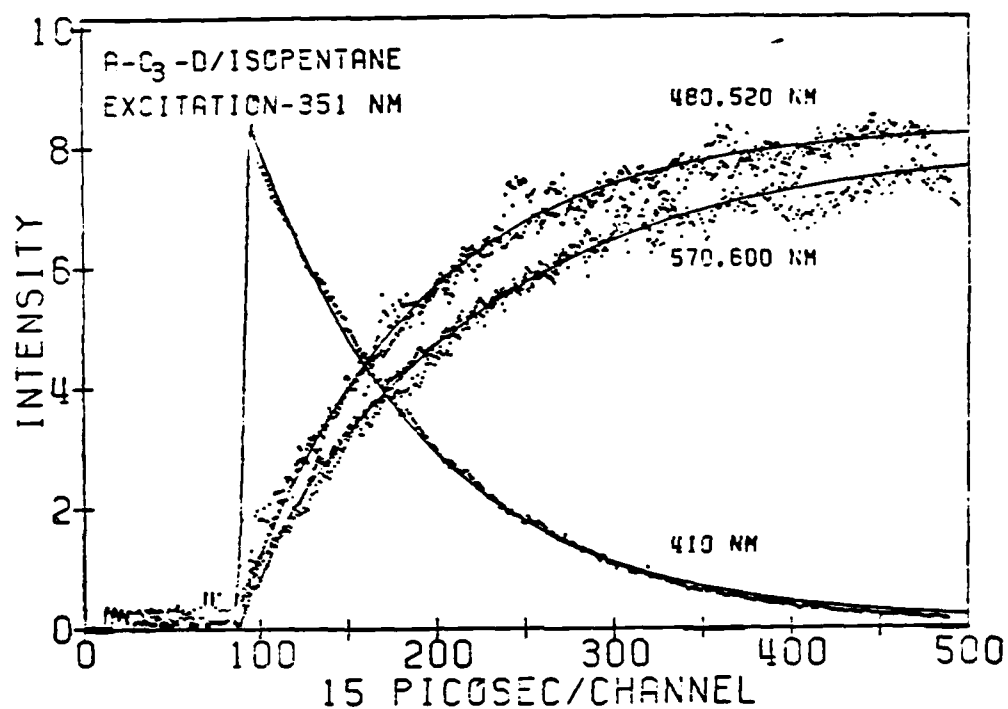


Figure 1: Decay of the anthracene moiety measured at 410 nm and the formation of the exciplex measured at two wavelengths, 480 nm and 520 nm. The dots are experimental points and the curves are theoretical calculations.

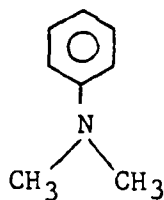
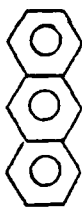
- (1) D. C. Rapaport, J. Chem. Phys. 71, 3299 (1979); M. Bishop, M. H. Kalos and H. L. Frisch, J. Chem. Phys. 70, 1299 (1979).
- (2) M. Fixman, J. Chem. Phys. 69, 1527, 1538 (1978).
- (3) G. T. Evans, Molecular Phys. 38, 1201 (1979); J. Chem. Phys. 72, 1504 (1980).
- (4) M. D. Barkley and B. H. Zimm, J. Chem. Phys. 70, 2991 (1979).
- (5) A. Baumsartner, J. Chem. Phys. 72, 871 (1980).
- (6) R. S. Adler and K. F. Freed, J. Chem. Phys. 72, 2032 (1980); J. Chem. Phys. 72, 4186 (1970).
- (7) A. Szabo, K. Schulten, and Z. Schulten, J. Chem. Phys. 72, 4350 (1980).
- (8) M. R. Pear and J. H. Weiner, J. Chem. Phys. 72, 3939 (1980).
- (9) Y. Wang, M. K. Crawford, and K. B. Eisenthal, J. Phys. Chem. 84, 2696 (1980).
- (10) D. C. Rapaport, J. Chem. Phys. 71, 3299 (1979).
- (11) M. Fixman, J. Chem. Phys. 69, 1527, 1538 (1978).
- (12) A. Szabo, K. Schulten, and Z. Schulten, J. Chem. Phys. 72, 4350 (1980).

C. ELECTRONIC ENERGY RELAXATION BY CHARGE TRANSFER PROCESSES*

(M. K. Crawford, Y. Wang, K. B. Eisenthal)

(Principal Investigator: K. B. Eisenthal (212) 280-3175)

Charge transfer (CT) interactions between an excited state molecule and surrounding molecules provide an extremely important and common pathway for electronic energy relaxation.⁽¹⁾⁻⁽⁸⁾ In nonpolar media a new and transient species called an excited CT complex is produced, whereas in polar media the formation of ions can be observed.⁽⁷⁾ From our previous studies⁽⁹⁾ on the system anthracene which in its excited state acts as an electron acceptor A^* and N,N-dimethylaniline as the donor D, we have found that an electron jump from D to A^* over a reaction distance of 8 Å in less than 10^{-11} sec (10 ps).

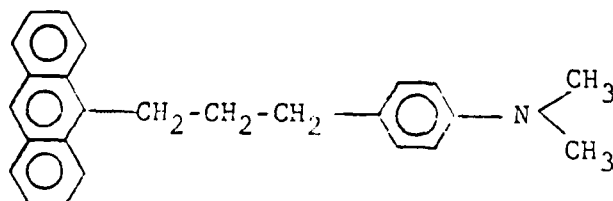


Excited
Anthracene

N,N-dimethylaniline

Excited CT Complex

By connecting the anthracene and N,N-dimethylaniline with three CH_2 groups we have imposed geometric restrictions on the relative orientational motions of A and D while still maintaining their close proximity (< 4 Å).



In this way we have been able to determine the role of geometry on the electron transfer process.⁽¹⁰⁾⁽¹¹⁾ We have found that in nonpolar media the formation of the excited CT complex for the A-(CH₂)₃-D takes nanoseconds to achieve versus picoseconds (10⁻¹¹ sec) for the free A and D. We have therefore learned that there are specific geometries required to effect electron transfer. For the molecule A-(CH₂)₃-D the formation time is determined by rotations of A and D about the CH₂ groups into the appropriate electron transfer conformation.

The issue we then proceeded to examine was the role of the solvent dielectric constant on the electron transfer process and its interplay with the geometric restrictions in the A-(CH₂)₃-D molecule. To this end we have studied A-(CH₂)₃-D in the strongly polar solvent acetonitrile ($\epsilon \approx 37$) using picosecond fluorescence as a probe method. Following picosecond laser excitation of the anthracene moiety at 351 nm (third harmonic of a Nd: phosphate glass system) the decay kinetics of the excited anthracene singlet was monitored at 411 nm and the formation kinetics of the excited CT complex was monitored in the 500-600 nm region (Fig. 1).

Although the CT complex is formed "instantaneously", we find that the excited anthracene moiety, which is monitored at 411 nm, has a lifetime of 7 ± 1 ps (Fig. 2). Since the CT rise is faster than the anthracene decay we conclude that these observed emissions correspond to independent processes.

The very fast CT rise suggests that only those molecules in a favorable ground state conformation at the time of excitation lead to the excited complexes. For those molecules in unfavorable extended conformations a new non-radiative decay channel is responsible for the observed 7 ps lifetime of the excited anthracene moieties. This channel, which becomes accessible in highly polar acetonitrile, is direct formation of ion pairs. For extended molecules,

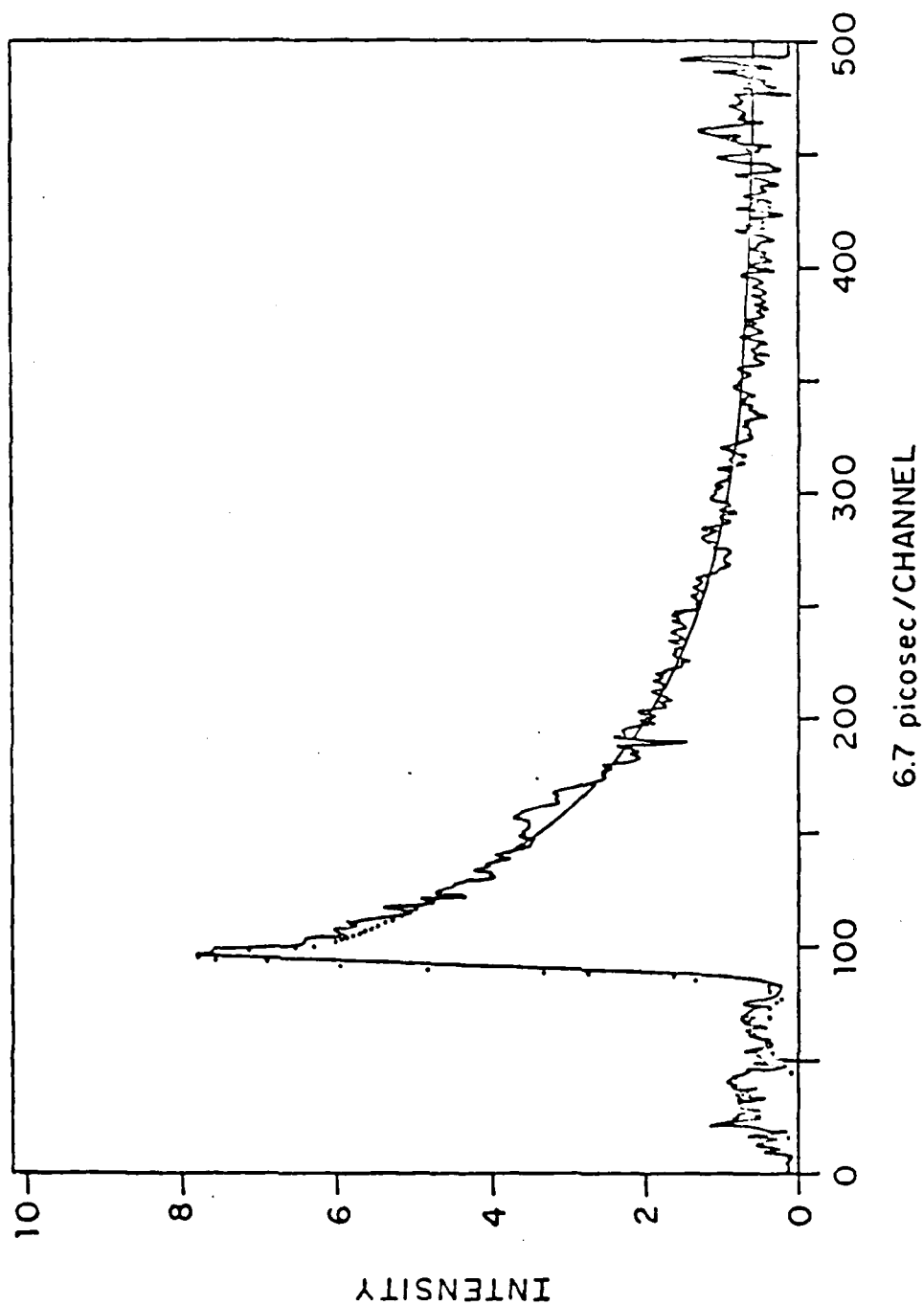


Figure 1: Fluorescence of the excited CT complex in acetonitrile (2.5×10^{-3} M).
The smooth curve is a theoretical fit to the experimental decay.

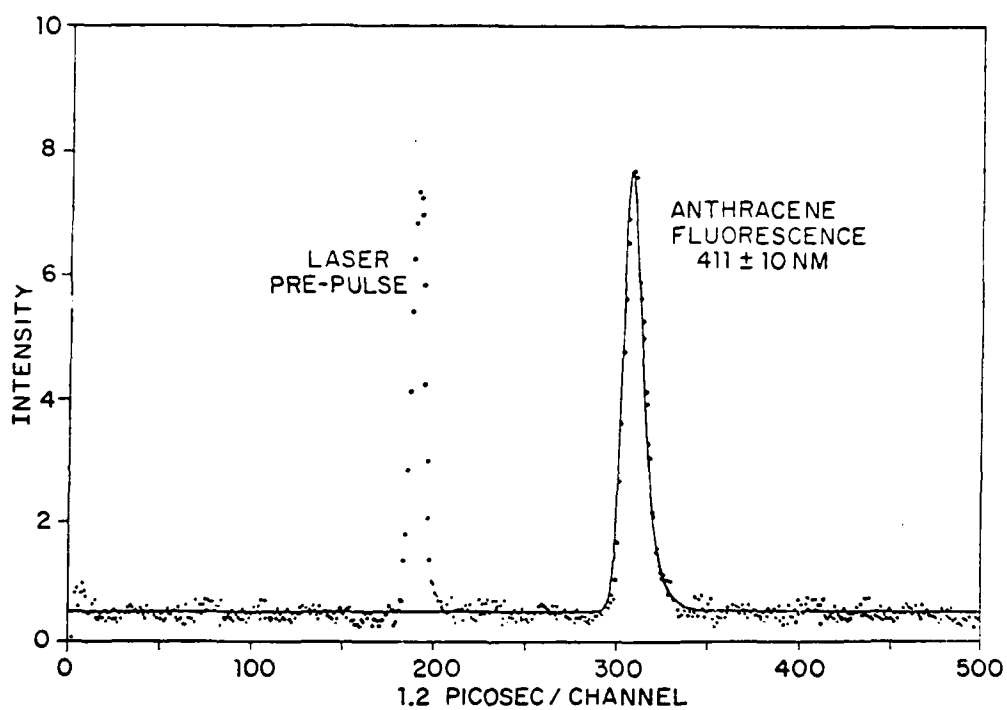
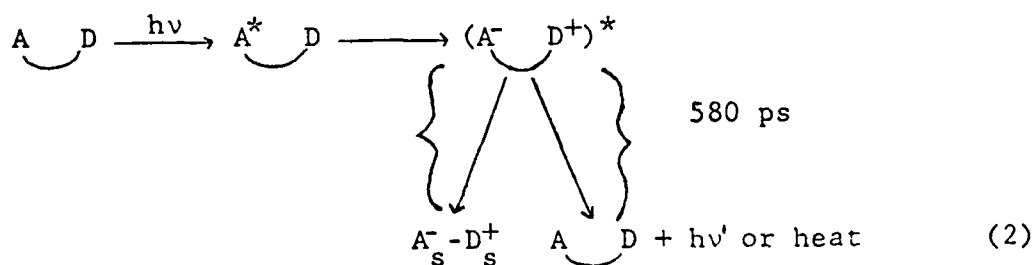
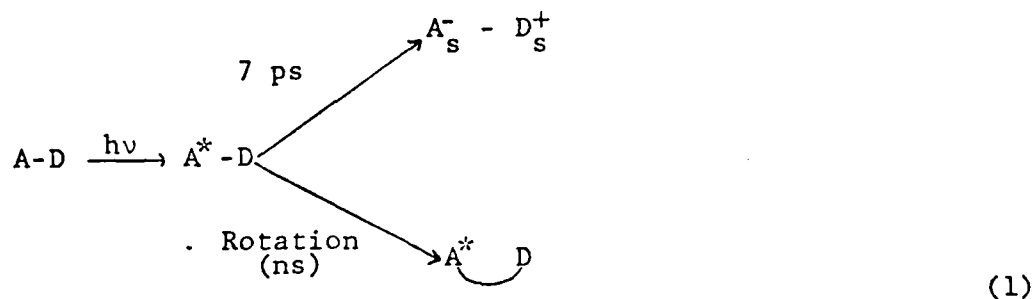


Figure 2: Anthracene moiety fluorescence in acetonitrile. The laser pre-pulse is both a pulse width display and a time marker for signal averaging. Solid curve is a theoretical fit to the experimental points.

the excited anthracene decays directly to the ion pair since the internal rotational motions necessary for the formation of excited CT complexes are too slow to compete. The appearance of this new channel for energy dissipation in polar solvents is a result of solvent stabilization of the ion pair. On the other hand, in the nonpolar solvents, e.g. 2-methylbutane, it is probable that the energy of $A^{\cdot-}-(CH_2)_3-D^+$ is higher than that of $A^{\cdot+}-(CH_2)_3-D$ in extended conformations. The following scheme summarizes the results in very polar media:



where $\text{A} \text{---} D$ represents the sandwich conformation, A-D , an extended conformation, $\text{A}_s^- - \text{D}_s^+$ the solvent stabilized extended ion pair, and $(\text{A}^- \text{---} D^+)^*$ the excited CT complex.

We are extending our studies to other systems to test our conclusions on the nature of dielectric and geometric effects on charge transfer phenomena in liquids.

*This research was also supported by the National Science Foundation under Grant NSF-CHE79-23291 and by the Air Force Office of Scientific Research under Grant AFOSR-77-3407B (expired 9/30/80) and AFOSR-81-0009.

- (1) Th. Förster and K. Kasper, Z. Electrochem. 59, 977 (1955).
- (2) J. Ferguson, J. Chem. Phys. 28, 765 (1958).
- (3) H. Leonhardt and A. Weller, Ber. Bunsenges, Phys. Chem. 67, 791 (1963).
- (4) H. Beens and A. Weller, Acta. Phys. Pol. 34, 593 (1968).
- (5) D. Rehm and A. Weller, Z. Phys. Chem. N.F. 69, 183 (1970).
- (6) M. Ottolenghi, Acc. Chem. Res. 6, 153 (1973).
- (7) N. Mataga and M. Ottolenghi, Molecular Association 2, 1 (1979).
- (8) N. Mataga and N. Nakashima, Spec. Lett. 8, 275 (1975).
- (9) T. J. Chuang and K. B. Eisenthal, J. Chem. Phys. 59, 2140 (1973);
J. Chem. Phys. 62, 2213 (1975).
- (10) T. J. Chuang, R. J. Cox, and K. B. Eisenthal, JACS, 96, 6828 (1974).
- (11) Y. Wang, M. K. Crawford, and K. B. Eisenthal, J. Phys. Chem. 84, 2696 (1980).

VI. GENERATION AND CONTROL OF RADIATION

A. SPONTANEOUS AND INDUCED COHERENT RADIATION GENERATION AND CONTROL IN ATOMIC VAPORS*

(K. P. Leung, R. Kachru, E. Whittaker, T. W. Mossberg, S. R. Hartmann)

(Principal Investigator: S. R. Hartmann (212) 280-3272)

Because of the inherent doppler-free nature of the photon echo we were able to investigate the sub-doppler regime of the sodium D line where we saw for the first time the effect of velocity changing collisions.⁽¹⁾ Our first experiments used He gas to perturb the Na resonance and were reported in last year's progress report. In the absence of velocity changing collisions, the broadening cross section σ_{eff} is independent of the photon-echo laser-excitation-pulse-separation-time τ . We found instead that σ_{eff} had the form $\sigma_{\text{eff}} = \sigma_0 + \alpha\tau^2$. It has been shown that in the collision kernel approximation the general expression for σ_{eff} is given by⁽²⁾

$$\sigma_{\text{eff}} = \sigma_0 + (\sigma_\infty - \sigma_0) \left[1 - \frac{1}{\tau} \int_0^\tau dt \tilde{g}(kt) \right] \quad (1)$$

where $\sigma = \sigma_0$ at $\tau = 0$, $\sigma = \sigma_\infty$ at $\tau = \infty$, k is the wave vector associated with the resonance line and \tilde{g} is the Fourier transform of the collision kernel $g(v)$. The collision kernel gives the probability that a collision will result in a velocity change $\Delta\vec{v} \cdot \hat{v}$ where \vec{v} is the initial velocity. Since $g(v)$ is supposed to be an even function of v it follows that for small τ the cross section σ has the form $\sigma = \sigma_0 + \alpha\tau^2$. The constant α is equal to $(\sigma_\infty - \sigma_0) \frac{1}{6} k^2 \langle v^2 \rangle$ where $\langle v^2 \rangle$ is the second moment of the collision kernel.

We have extended our photon echo relaxation measurements to the other noble gases where we find similar evidence of velocity changing collisions.

We have used these results to measure σ_0 , the phase changing collision cross section, and we find reasonable agreement with more standard line broadening measurements.⁽³⁾ See Table I where we compare broadening constants in terms of FWHM with the results obtained by other workers. There are serious problems associated with standard line broadening measurements and the echo technique which allows work at low perturber pressures is singularly free of them. Most notable among the advantages of the echo technique is the absence of optical pumping effects and the freedom from high frequency stability requirements.

We have just completed a series of two-pulse photon echo relaxation measurements on the Li D line perturbed by the noble gases. Here the effect of velocity changing collisions is more dramatic and the cross section has the interesting dependence on τ shown in Fig. 1. The solid lines are theoretical fits using a gaussian kernel for all perturbers except He where we use a Lorentzian. An argument based on the uncertainty principle insures that we have come close to the asymptotic limit where σ_{eff} becomes constant. These measurements are readily analyzed by writing (1) in the asymptotic form

$$\sigma_{\text{eff}} = \sigma_0 + (\sigma_{\infty} - \sigma_0) [1 - (\pi/2) g(0)/k\tau] \quad (2)$$

so that a plot of $\sigma_{\text{eff}}\tau$ vs τ should, for large enough τ , yield a straight line whose slope gives σ_{∞} and whose intercept gives $(\sigma_{\infty} - \sigma_0)(\pi/2)g(0)/k$. This plot is shown in Fig. 2. If we use the fit of Fig. 1 to determine σ_0 we obtain $g(0)$ from our knowledge of $(\sigma_{\infty} - \sigma_0)(\pi/2)g(0)/k$. We have obtained a simple interpretation for σ_0 and σ_{∞} which we find can be represented by

Table I

Comparison of the results obtained in the present experiment with previous work. The broadening constants represent the FWHM in units of 10^{-9} rad s $^{-1}$ cm 3 .

Broadening constants				
	This work	Previous work		Theory
		(a)	(b)	(c)
He D ₁	3.57(0.23)	3.55(0.09)	3.80(0.2)	3.76
D ₂	3.90(0.25)	4.30(0.03)	4.38(0.4)	3.94
Ne D ₁	2.27(0.15)	2.79(0.05)	2.28(0.2)	
D ₂	2.37(0.16)	2.53(0.03)	2.88(0.2)	
Ar D ₁	4.33(0.28)	5.56(0.04)	5.54(0.4)	
D ₂	4.31(0.27)	4.22(0.10)	4.54(0.4)	
Kr D ₁	4.51(0.29)	4.83(0.09)		
D ₂	4.33(0.29)	4.73(0.11)		
Xe D ₁	5.00(0.32)	5.83(0.12)	5.26(0.4)	
D ₂	5.08(0.33)	4.94(0.11)	4.64(0.5)	

^aR. H. Chatham, A. Gallagher, and E. L. Lewis, J. Phys. B: Atom. Molec. Phys. 13, L7 (1980).

^bN. Lwin, D. G. McCartan, and E. L. Lewis, J. Phys. B: Atom. Molec. Phys. 9, L161 (1976); Astrophys. J. 213 599 (1977).

^cA. D. Wilson and Y. Shimoni, J. Phys. B: Atom. Molec. Phys. 8, 2415 (1975).

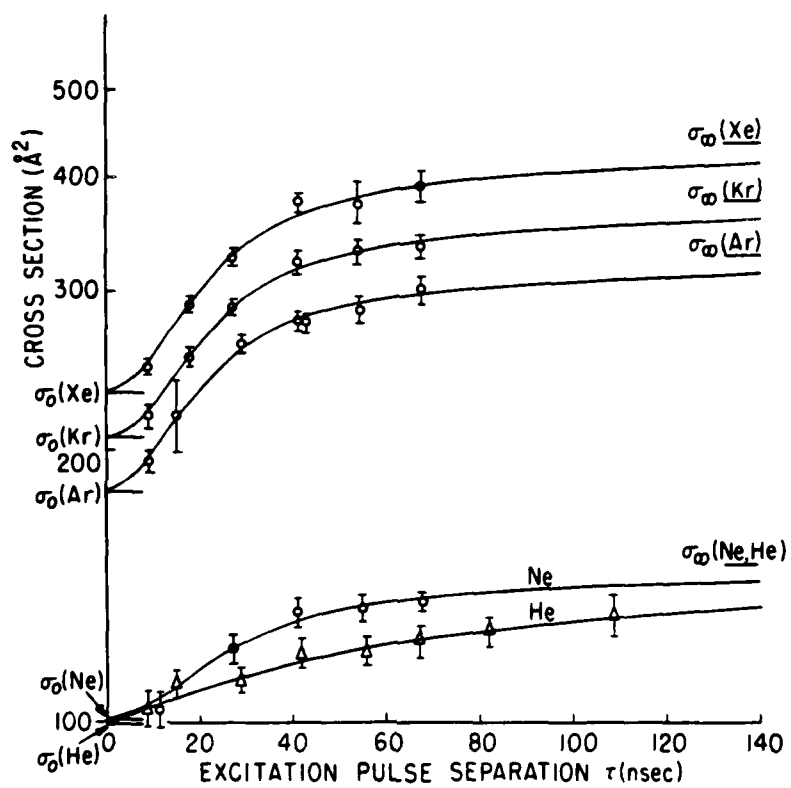


Figure 1

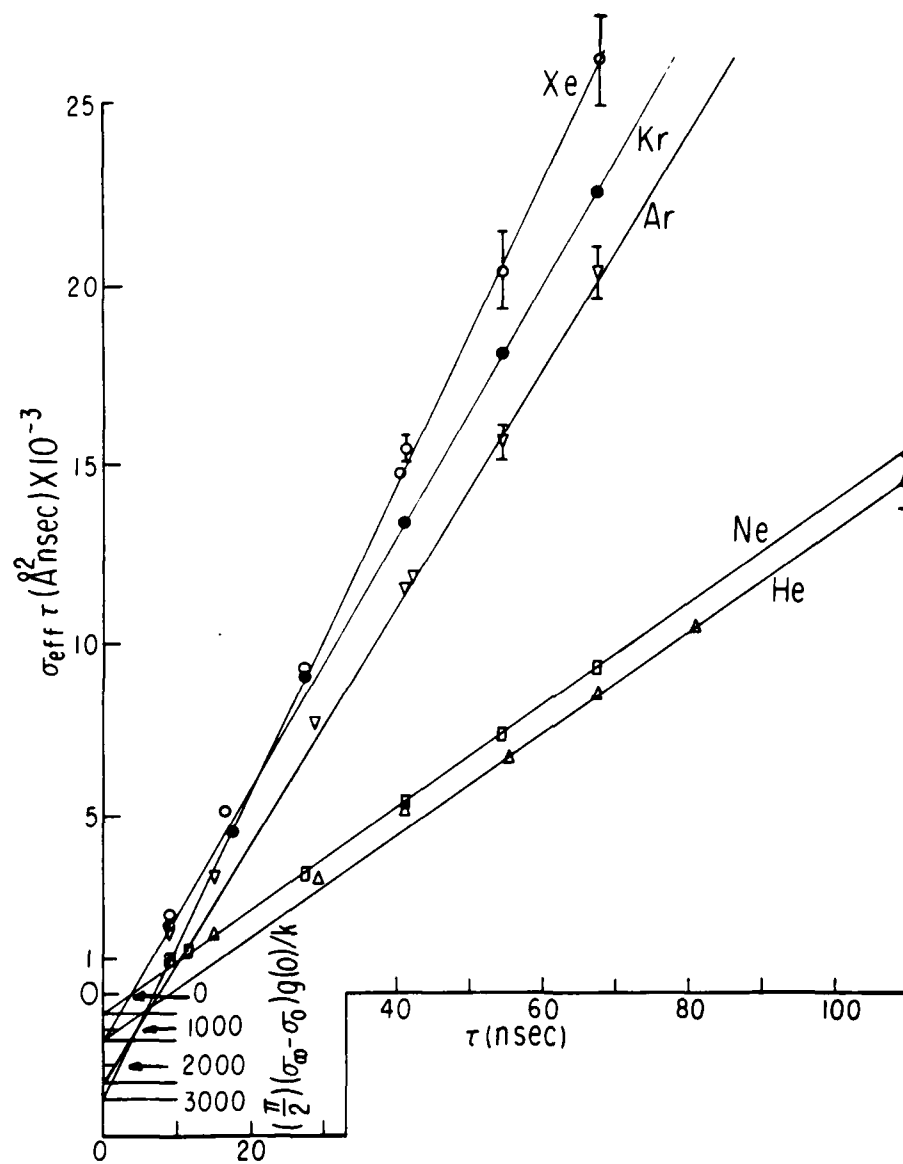


Figure 2

$$\sigma_l = \text{Re} \int_{S_l} (\vec{j}_k - \vec{j}) \cdot d\vec{s} / \vec{j}_k \cdot \hat{k} \quad (3)$$

where the index l is either 0 or ∞ . In this expression \vec{j} represents the amplitude of the dipole current density $\psi^* p \nabla \psi - \nabla \psi^* p \psi$ where p is the dipole moment operator. Then j_k corresponds to a plane wave current and j is the current when a plane wave is scattered by a perturber. For $l = \infty$ the area of integration S_∞ corresponds to an infinitesimal solid angle directed along \hat{k} and displaced infinitely far away. This yields σ_∞ as the average of the total scattering cross sections for the ground and excited states. For $l = 0$ velocity changes are not important and S_l encloses the perturber. Then σ_0 becomes identical with the phase changing cross section as obtained by Baranger.⁽⁴⁾

The wide variety of seemingly unrelated reordering phenomena which exists today has prompted us to develop a simple diagrammatic method for their analysis.⁽⁵⁾ With this method one treats ordinary two-pulse photon echoes, raman echoes,⁽⁶⁾ tri-level echoes,⁽⁷⁾ grating echoes,⁽⁸⁾ etc. on the same basis.

A new method of observing coherent transient has been developed. A probing laser pulse is used to modify the polarization properties and/or propagation direction of a coherent transient signal. The excitation pulses can then be blocked by spatial filters or passive polarization elements, and the echo can be observed without the use of fast optical shutters. This technique should prove widely applicable and especially important in the study of picosecond processes where sufficiently fast optical shutters are difficult to obtain. Preliminary experiments have been performed on the resonance lines of atomic Li and Tl which demonstrate the practicality of the technique.

Our previous measurements of stimulated echo relaxation in Na vapors have stimulated us to develop a picosecond capability in order to examine the behavior of the collision kernel at short times where our data base was deficient. We also will use this apparatus for examining two-pulse echo relaxation in the short time regime. This is especially important in the case of Li where our data to date does not show the τ^2 behavior for σ which is to be expected at short time. As of this writing we have produced subnanosecond pulses by using an actively mode locked dye laser pumped by a cw argon laser. A pulsed N_2 laser is being used to pump a dye laser to selectively amplify one of the picosecond pulses.

In a separate experimental setup we are developing a pulsed dye laser-amplifier system using a YAG laser as the pump source. With this system we plan to extend our measurement of Rydberg atom relaxation properties into regimes previously inaccessible because of lack of excitation power. The first experiment we plan to perform will be to extend our work in Na-vapor using the tri-level echo technique to beyond principle quantum numbers of 40. We expect to see a dramatic increase in collision cross section when S and D level spacing becomes small enough so that ℓ and n changing collisions become probable.

*This research was also supported by the Office of Naval Research under Contract N00014-78-C-0517.

- (1) T. W. Mossberg, R. Kachru, and S. R. Hartmann, Phys. Rev. Lett. 44, 73 (1980).
- (2) A. Flusberg, Opt. Commun. 29, 123 (1979).
- (3) R. Kachru, T. W. Mossberg, and S. R. Hartmann, J. Phys. B 13 L363 (1980).
- (4) M. Baranger, Phys. Rev. 111, 481 (1958).

- (5) T. W. Mossberg and S. R. Hartmann, Phys. Rev. A 23, 1271 (1981).
- (6) S. R. Hartmann, J. Quan. Elec. 11, 802 (1968).
- (7) T. W. Mossberg, A. Flusberg, R. Kachru, and S. R. Hartmann, Phys. Rev. Lett. 39, 1523 (1977).
- (8) T. W. Mossberg, R. Kachru, E. Whittaker, and S. R. Hartmann, Phys. Rev. Lett. 43, 851 (1979).

B. RELAXATION AND EXCITATION TRANSFER OF OPTICALLY EXCITED STATES IN SOLIDS*

(K. Chiang, E. Whittaker, T. J. Chen, S. R. Hartmann)

(Principal Investigator: S. R. Hartmann (212) 280-3272)

Measurements of photon echo modulation on the 3P_0 - 3H_4 transition of the Pr^{3+} ion in a crystal of LaF_3 proved to be singularly successful in obtaining spectroscopic and relaxation data for all aspects of the 3P_0 - 3H_4 transition. In particular, it is possible to obtain, in addition to the homogeneous optical linewidth, a complete description of the hyperfine Hamiltonians associated with both the 3P_0 and 3H_4 states as well as the associated nuclear transition linewidths.⁽¹⁾ As discussed in the last progress report, there are experimental difficulties connected with carrying out an echo modulation experiment on the 1D_2 - 3H_4 transition of Pr^{3+} in LaF_3 and the data which we presented reflected this fact. It was therefore decided to proceed in two separate ways. We would improve upon our experimental technique with the hope that we could make the technique successful in this application and we would separately perform a PENDOR experiment⁽²⁾ to unambiguously determine the 1D_2 excited state splittings which were in doubt. Both approaches were successful.

A PENDOR experiment works by exploiting the sensitivity of the three-pulse stimulated photon echo to hyperfine transitions induced by a resonant radiofrequency magnetic field. The resonance condition is detected by a change in the echo signal amplitude. The timing sequence is shown in Fig. 1. The first and second 90° laser excitation pulses were produced by a single N_2 laser pumped dye laser whose output is split, one half going into the first pulse and the other half directed to a white cell where it is delayed

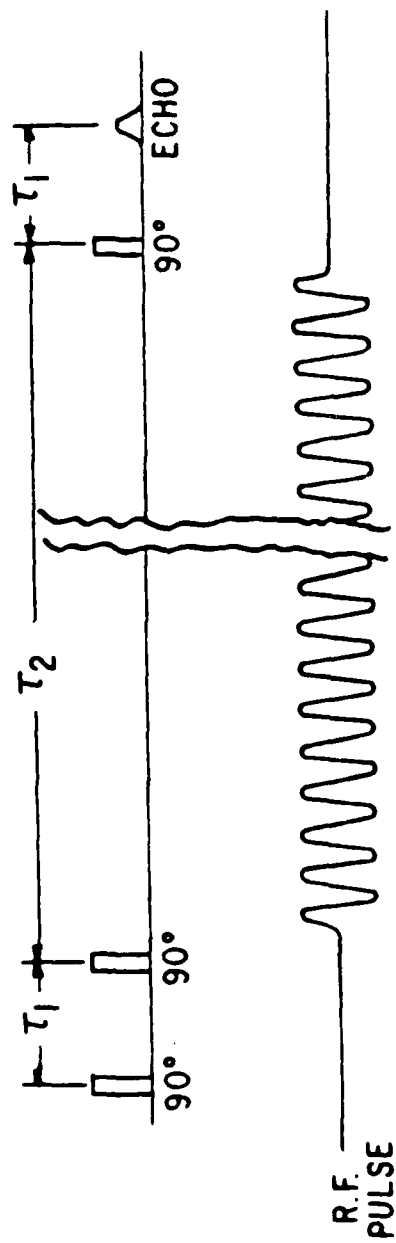


Figure 1: PENDOR experiment pulse timing.

to form the second pulse. The third 90° laser excitation pulse is produced by a separately triggered N_2 laser pumped dye laser. These lasers were the same as were described in the last progress report.

Stimulated photon echoes were produced on the transition connecting the lowest levels of the crystal-field split levels of the 3H_4 and 1D_2 states. These levels are electronic singlets that are further split into three doubly degenerate nuclear levels by the combined influence of the Pr^{3+} nuclear quadrupolar and second order magnetic dipolar interactions. Previously measured⁽³⁾ nuclear splittings for both the 3H_4 and 1D_2 states are small compared to the 10 Ghz bandwidth of the laser excitation pulses. Figure 2 shows the percentage decrease in the stimulated photon echo intensity as a function of the applied RF frequency. The dips at 3.7 Mhz and 4.65 Mhz correspond to the energy splittings in the 1D_2 state, and agree very well with Erickson's⁽³⁾ reported values of 3.7 Mhz and 4.7 Mhz. Our measured linewidths of 350 Khz (FWHM) are, however, larger than the 200 ± 50 Khz linewidth that he reported. In Fig. 2, the dotted and solid lines are Lorentzian and Gaussian fits, respectively, to the data points with a (FWHM) linewidth of 350 Khz. The quality of our data prevents our choosing one over the other, but since a large part of the inhomogeneity of the nuclear hyperfine levels is due to the perturbing effects of eleven ^{19}F neighbors, one would expect the linewidth to be Gaussian rather than Lorentzian.

Fourier analysis⁽¹⁾ of the $^3H_4-^3P_0$ transition has shown that the inhomogeneous linewidth of the nuclear transitions in the 3P_0 state is approximately 20 Khz while the inhomogeneous linewidth of the 3H_4 ground state is approximately 200 Khz. For the 3P_0 state, $J=0$, and the linewidths are due primarily to the static and quadrupolar interactions of the ^{141}Pr

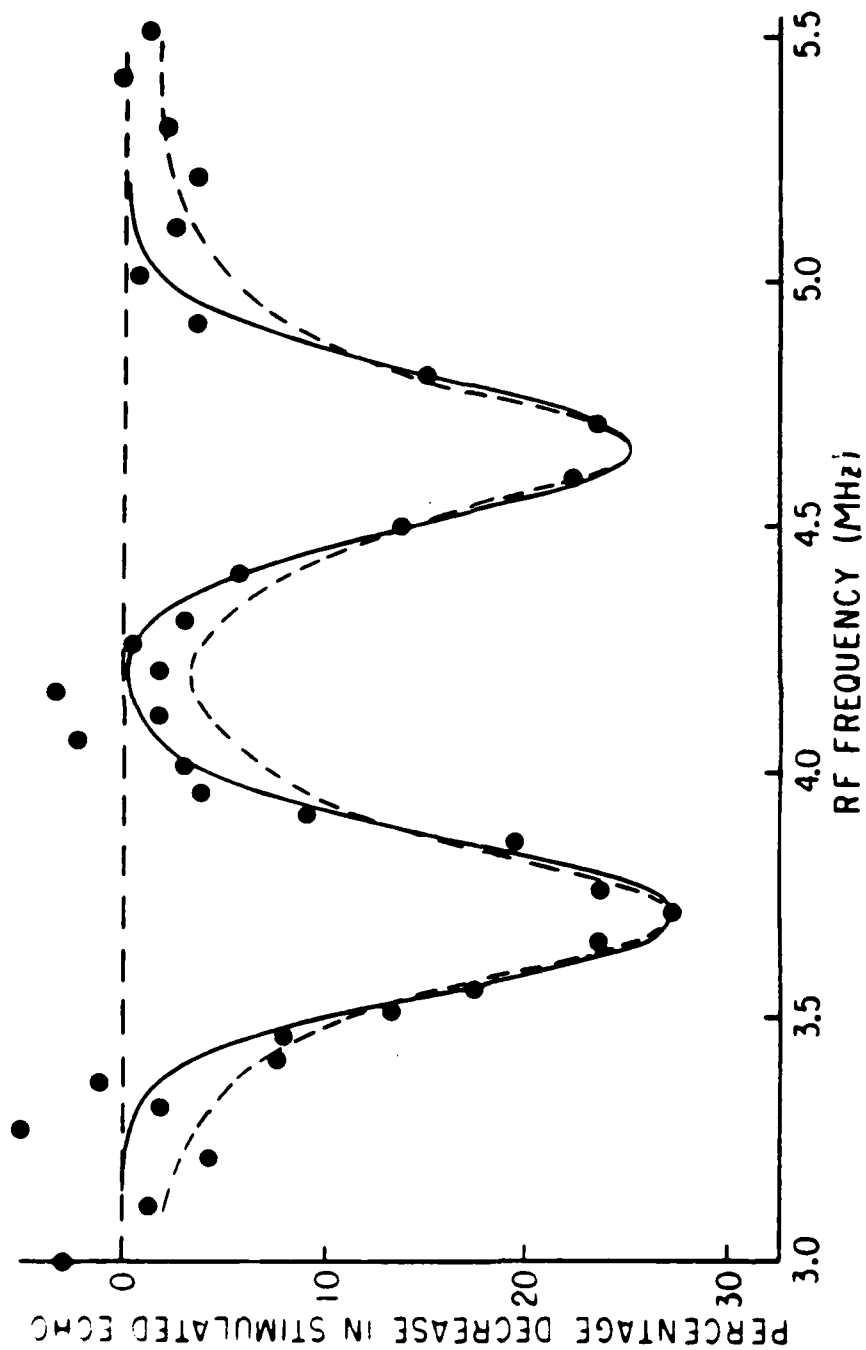


Figure 2: PENDOR resonance signal showing hyperfine splittings in the $1D_2$ excited state of $\text{Pr}^{3+}:\text{LaF}_3$.

nucleus with the neighboring ^{19}F nuclei and the electric field gradient at the ^{141}Pr site respectively. For the $^3\text{H}_4$ state, $J=4$, and the close spacing of the crystal field split levels of the $^3\text{H}_4$ multiplet gives rise to an enhanced moment that interacts strongly with the surrounding nuclear neighbors and leads to an increased linewidth. In like manner the $^1\text{D}_2$ levels would be expected to be broadened beyond the 20 KHz linewidth of the $^3\text{P}_0$ state. According to a second moment calculation, the contribution to the inhomogeneous linewidth with the unenhanced Pr-F nuclear dipolar interaction is 13 KHz. When we take into account the experimentally determined enhanced nuclear gyromagnetic ratio ~ 3 KHz/gauss for the $^1\text{D}_2$ state⁽⁴⁾ we obtain an inhomogeneous linewidth of approximately 40 KHz. The contribution from other sources such as lifetime broadening (~ 600 Hz) and phonon processes (~ 800 Hz)⁽³⁾ are negligible. Since we typically used rf pulses 20 secs long, the contribution to the linewidth due to the finite duration of the rf field is 8 KHz. The rather large measured linewidth that must be accounted for is possibly due to rf power broadening. These results will be published shortly.⁽⁵⁾

We have also taken several steps to improve the results of the echo modulation experiment on the $^1\text{D}_2$ - $^3\text{H}_4$ at the $\text{LaF}_3:\text{Pr}^{3+}$ system. The first step was to install intracavity etalons in the Hansch type dye lasers, thereby reducing laser bandwidth to 4 GHz, but increasing the power per unit bandwidth somewhat. This step enhanced our signal-to-noise by a factor of three. We also obtained crystal samples whose length was three times longer than our original samples. Since echo intensity is proportional to $(\alpha L)^2$, where α is the small signal absorptivity and L the interaction length, this step enhanced the signal by about a factor of ten. Despite

these improvements we found that the overall echo envelope decayed to less than the detection noise level beyond a pulse separation of one microsecond, for a sample doped with 1% Pr^{3+} . However, a dramatic improvement was noted when a Pr^{3+} sample with lower concentration was used. At 0.1% Pr^{3+} concentration, a measurable signal persists out to pulse separations of nine microseconds, when the sample is maintained at a temperature of 2.5K.

We have also made a number of improvements in the computer assisted data taking process, which, while not directly improving signal size, do effectively improve the quality of our measurements by increasing data taking efficiency. In particular, two new computer operated peripherals have been installed in the system. The first is a computer controllable electrical attenuator which is used to maintain the modulated signal within the linear range of the data acquisition electronics. The computer is thus able to adjust the signal level automatically. The second device is a pair of digitally programmable pulse generators, used to set the laser pulse separation and Pockel's cell gate. These devices are of a "random access" nature allowing the pulse separation to be varied over several orders of magnitude between a single laser shot. This allows us to periodically measure the echo magnitude at a single fixed reference time without suffering a loss in the data taking rate.

The reference measurement allows us to compensate for echo amplitude drift during the course of a single data taking run, as well as providing a normalization factor which facilitates averaging data sets from different runs. The result of all these improvements can be seen in the data presented in Fig. 3, which shows the echo envelope versus pulse separation for the

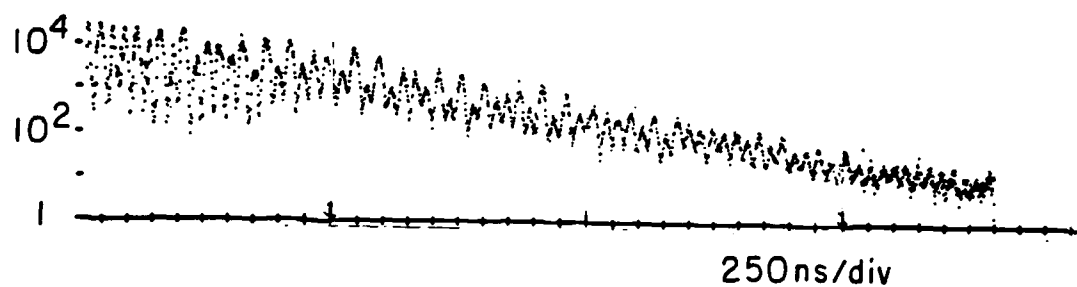


Figure 3: Photon echo amplitude versus pulse separation for the ${}^1\text{O}_2\text{-}{}^3\text{H}_4$ transition at $\text{Pr}^{3+}:\text{LaF}_3$.

$^1D_2 - ^3H_4$ transition of .01% $Pr^{3+}:LaF_3$. Each point is the average of 100 or more echoes from data sets taken on different days.

The high quality of this data allows us to extract a significant amount of spectroscopic information about the system under investigation. Fig. 4 shows the discrete Fourier transform⁽¹⁾ at the data shown in Fig. 3. Clearly shown are the resonances due to the hyperfine structure in the 3H_4 ground and 1D_2 excited states of Pr^{3+} in LaF_3 . These resonances are in close agreement with the values deduced in previous experiments⁽¹⁾⁽³⁾ including our PENDOR experiment outlined above. In addition to the resonance frequencies we are also able to deduce the inhomogeneous linewidths of the nuclear transitions. The values for the ground state result are in close agreement with our previous measurement. The deduced linewidths of < 100 Khz (our present resolution limit due to finite span of time domain data) is a new upper limit on the excited state linewidths, and are consistent with recently published theoretical discussions of the inhomogeneous nuclear linewidths.⁽⁶⁾

Development work over the last year has given us a very versatile apparatus for investigating photon echo phenomena in solids. We intend to pursue a vigorous program of study with this setup. In particular, we intend to carry out modulation experiments similar to the one described above in a variety of other ion-host systems, most likely beginning with $Er^{3+}:LaF_3$. In addition, we hope to utilize the excited state⁽⁷⁾ and tri-level echo⁽⁸⁾ techniques for the first time in solids. A particularly interesting set of levels for use in multilevel experiments would be the 3P_0 and 1S_0 levels in $Pr^{3+}:LaF_3$. Magnetic interactions between Pr^{3+} and neighboring nuclei have been shown⁽⁶⁾ to be the dominant line-broadening mechanism. These effects should be very small for an ion in a $^3P_0 - ^1S_0$

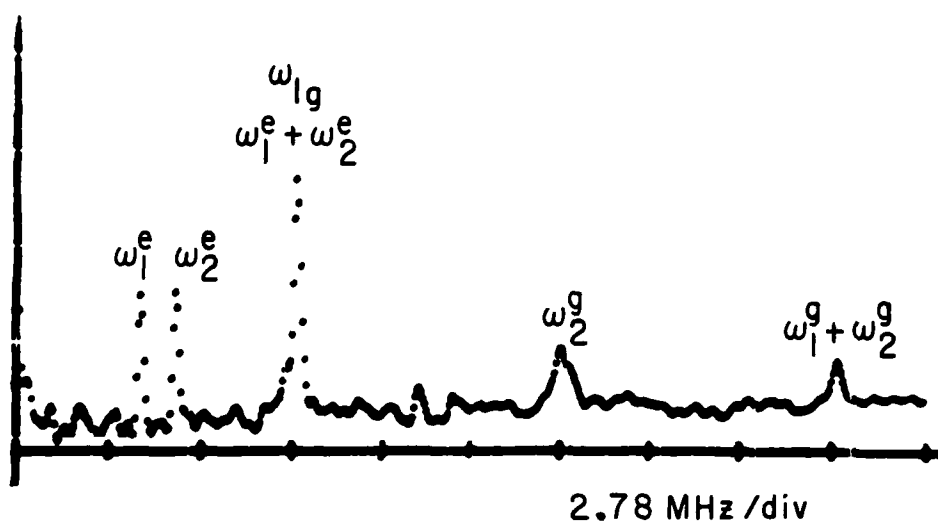


Figure 4: Discrete Fourier Transform of data shown in Fig. 3. The peaks at 3.72 MHz and 4.79 MHz are the excited state hyperfine resonances. The peak at 8.51 MHz is a sum frequency of the excited state resonances and obscures a ground state resonance at 8.48 MHz. Also present are ground state resonances at 16.7 MHz and 25.0 MHz.

superposition as both states are electronic singlets, having only nuclear quadrupole interactions. Use of the 1S_0 state is an exciting prospect, too, because of its close proximity to 4fSd configuration states, which may induce previously unseen effects on the photon echoes. These experiments should be under way in the near future.

*This research was also supported by the National Science Foundation under Grant NSF-DMR80-06966.

- (1) Y. C. Chen, K. Chiang, and S. R. Hartmann, Phys. Rev. B, 21, 40 (1980).
- (2) P. Hu, R. Leigh, and S. R. Hartmann, Phys. Lett. A 40, 164 (1972).
- (3) L. E. Erickson, Phys. Rev. B, 16, 4731 (1977).
- (4) R. M. McFarlane and R. M. Shelby, Opt. Lett. 6, 96 (1981).
- (5) K. P. Chiang, E. A. Whittaker, and S. R. Hartmann, Phys. Rev. B 23, (1981).
- (6) R. G. DeVoe, A. Wokoun, S. C. RAnd, and R. G. Brewer, Phys. Rev. B 23, 3125 (1981).
- (7) A. Flusberg, T. Mossberg, and S. R. Hartmann, Opt. Commun. 24, 207 (1977).
- (8) T. Mossberg, A. Flusberg, R. Kachru, and S. R. Hartmann, Phys. Rev. Lett. 39, 1523 (1977).

SIGNIFICANT ACCOMPLISHMENTS AND TECHNOLOGY TRANSITION REPORT

Significant Accomplishments

1. Solid State Electronics and Device Fabrication

We have fabricated Schottky barrier diodes with a silicon-aluminum-silicon structure by a laser irradiation process. This novel technique produces diodes with a large barrier height (> 0.95 eV) and good rectifying properties, and it is likely to be useful in multi-layer integrated-circuit applications.

By making use of the large diffusivity of aluminum in polysilicon, we have found a low temperature process for making a poly Si-Si diode. With our approach, both single-crystal and polycrystalline p-n junctions can be fabricated on the same IC chip giving added flexibility in the design of integrated structures.

2. Physical Properties of Solid State Devices

We have recently developed a theoretical model for the statistical fluctuations of dopant impurities in ion-implanted bipolar transistor structures and the minimum device dimensions for VLSI system reliability.

3. Energy Transfer, Photophysics and Photochemistry

The evolution of spin polarization due to collisions between ground-state atoms in $^2S_{1/2}$ states is dominated by spin exchange. Recently we have shown that collisions between alkali atoms also destroy the electronic spin at a rate which is about 1% of the spin exchange rate. This spin destruction is probably due to magnetic dipole spin-spin interactions, and it has important consequences for various optically pumped devices.

While investigating spin exchange collisions in dense, laser-pumped alkali vapors we noticed that a pronounced narrowing of the magnetic resonance linewidth occurred when the laser beam intensity increased. In all other experiments known to us, an increase in the optical intensity causes the magnetic resonance linewidth to broaden. More careful experimental and theoretical studies of this light narrowing phenomenon showed that it was due to the interplay of the optical pumping with the peculiar properties of spin exchange collisions. The phenomenon may be of importance in some optically pumped devices.

By combining picosecond transient absorption and emission methods we have succeeded in developing a model for the interplay between solvent polarity and geometric structure on excited state electron transfer processes. We have found that in low dielectric solvents the electron transfer between two organic molecules separated by three methylene groups can only occur for very limited configurations. However in the high dielectric solvent rapid electron transfer to ion radical states occurs indicating that geometric factors are no longer crucial. We have used these studies to establish that the dynamics of short chain molecules, or polymer segments, can be obtained from measurements of these electron transfer processes.

Technology Transition Reports

1. Multifrequency heterodyne techniques developed by M. C. Teich under JSEP support (Research Unit 12) are currently under consideration for possible application in over-water pilot rescue missions where the use of a light-chopping mechanism is interdicted because of its interruptive nature (Naval Weapons Center).

2. The Neyman Type-A characterization of photomultiplier fluorescence noise developed by M. C. Teich under JSEP support (Research Unit 13) is being used to design the star scanner for the optical guidance system in the NASA/JPL Galileo orbiter mission scheduled to explore Jupiter in 1988.

PERSONNEL

Faculty

N. D. Bhaskar, Assistant Professor of Physics
K. Eisenthal, Professor of Chemistry
G. W. Flynn, Professor of Chemistry, Director
W. Happer, Professor of Physics
S. R. Hartmann, Professor of Physics
W. Hwang, Assistant Professor of Electrical Engineering
T. Mossberg, Assistant Professor of Physics
P. Prucnal, Assistant Professor of Electrical Engineering
I. I. Rabi, University Professor Emeritus
M. C. Teich, Professor of Engineering Science
P. Thaddeus, Adjunct Professor of Physics
E. Yang, Professor of Electrical Engineering

Research Associates and Physicists

Dr. R. Bohn	Dr. A. Kerr
Dr. R. Cohen	Dr. M. Wu

Graduate Research Assistants

J. Ahl	M. Lester
T. Allik	K. Leung
P. Beeken	M. Mandich
T. Brown	T. McClelland
J. Camparo	A. Sharma
T. Chen	P. Siegel
K. Chiang	B. Suleman
J. Chu	N. Tran
M. Islam	A. Vasilakis
R. Kachru	E. Whittaker

Technical Research Assistants

Mr. I. Beller

Physics Department Electronics Engineering and Construction Shop*

Mr. J. Packer

Physics Department Machine Shop*

Mr. E. Jauch

Administration

Ms. I. Moon

Ms. P. Pohlman

Ms. V. Ricketts

*The Machine Shop and Electronics Shop facilities are available for the
Columbia Radiation Laboratory.

JSEP REPORTS DISTRIBUTION LIST

DEPARTMENT OF DEFENSE

Director
National Security Agency
ATTN: Dr. T.J. Beann, R-5
Fort George G. Meade, MD 20755

Defense Documentation Center
ATTN: DDC-DDA
Cameron Station
Alexandria, VA 22314

Dr. George Gamota
Director for Research
Deputy Under Secretary of Defense
for Research and Engineering
(Research and Advanced Technology)
Room 3D1067, The Pentagon
Washington, DC 20301

Defense Advanced Research
Projects Agency
ATTN: Dr. R. Reynolds
1400 Wilson Boulevard
Arlington, VA 22209

DEPARTMENT OF THE ARMY

Commander
US Army Armament R&D Command
ATTN: DRDAR-TSS #59
Dover, NJ 07801

Director
US Army Ballistics Research Lab.
ATTN: DRDAR-BL
Aberdeen Proving Ground
Aberdeen, MD 21005

Commander
US Army Communications Command
ATTN: CC-OPS-PM
Fort Huachuca, AZ 85613

Commander
US Army Materials and Mechanics
Research Center
ATTN: Chief, Applied Sciences Div.
Watertown, MA 02172

Commander
US Army Material Development and
Readiness Command
ATTN: Technical Library, Room 7S 35
5001 Eisenhower Avenue
Alexandria, VA 22333

Commander
U.S. Army Missile Command
Redstone Scientific Information Ctr.
ATTN: DRSMI-RPRD (Documents)
Redstone Arsenal, AL 35809

Commander
US Army Atmospheric Sciences Lab.
ATTN: DELAS-DM-A (Tech Writing Sec.)
White Sands Missile Range, NM 88002

Commander
US Army R&D Command
ATTN: DRSEL-FI-M (Mr. John Walker)
Fort Monmouth, NJ 07703

Director
TRI-TAC
ATTN: TR-4F Mrs. Bruller
Fort Monmouth, NJ 07703

Director
US Army Electronics R&D Command
Night Vision & Electro-Optics Lab.
ATTN: DELNV-L (Dr. Rudolf G. Buser)
Fort Belvoir, VA 22060

Director
US Army Electronics R&D Command
ATTN: DELEN-D (Electronics
Warfare Laboratory)
White Sands Missile Range, NM 88002

Executive Secretary, TCC/JSEP
US Army Research Office
P.O. Box 12211
Research Triangle Park, NC 27709

Commander
Harry Diamond Laboratories
ATTN: Mr. John E. Rosenberg
2800 Powder Mill Road
Adephi, MD 20763

HQDA (DAMA-AR2-A)
Washington, DC 20310

Director
US Army Electronics Technology and
Devices Laboratory
ATTN: DELET-E (Dr. Jack A. Kohn)
Fort Monmouth, NJ 07703

Director
US Army Electronics Technology and
Devices Laboratory
ATTN: DELET-ER (Dr. S. Kronenberg)
Fort Monmouth, NJ 07703

Director
US Army Electronics R&D Command
Night Vision & Electro-Optics Labs.
ATTN: Dr. Ray Balcerak
Fort Belvoir, VA 22060

Commander
US Army Research Office
ATTN: DRXRO-MA (Dr. Paul Boggs)
P.O. Box 12211
Research Triangle Park, NC 27709

Commander
US Army Missile Command
Research Directorate
ATTN: DRDMI-TRD (Dr. Charles Bowden)
Redstone Arsenal, AL 35809

Commander
US Army Missile Command
Advanced Sensors Directorate
ATTN: DRDMI-TER (Dr. Don Burlage)
Redstone Arsenal, AL 35809

Director
US Army Electronics R&D Command
Night Vision & Electro-Optics Labs.
ATTN: Mr. John Dehne
Fort Belvoir, VA 22060

Commander
US Army Missile Command
Physical Sciences Directorate
ATTN: DRDMI-TER (Dr. Michael D. Fahren)
Redstone Arsenal, AL 35809

Commander
US Army Satellite Communications Agency
Fort Monmouth, NJ 07703

Commander
US Army Missile Command
Physical Sciences Directorate
ATTN: DRDMI-TRC
(Dr. William L. Gamble)
Redstone Arsenal, AL 35809

Commander
US Army White Sands Missile Range
ATTN: STEKS-ID-D (Dr. Al L. Gilbert)
White Sands Missile Range, NM 88002

Commander
US Army Communications R&D Command
ATTN: DRDCO-TCS-CP (Mr. David Harrell)
Fort Monmouth, NJ 07703

Commander
US Army Communications R&D Command
ATTN: DRDCO-COM-RF
(Mr. R.A. Kulinsky)
Fort Monmouth, NJ 07703

Commander
US Army Communications R&D Command
ATTN: DRDCO-TCS-BC (Mr. E. Lierfeldt)
Fort Monmouth, NJ 07703

Director
US Army Electronics Technology and
Devices Laboratory
ATTN: DELET-M (Mr. V. Gelnovatch)
Fort Monmouth, NJ 07703

Commander
US Army Electronics R&D Command
ATTN: DRDEL-SA (Dr. W.S. McAfee)
Fort Monmouth, NJ 07703

Director
US Army Electronics R&D Command
Night Vision & Electro-Optics Labs.
ATTN: DELNV
Fort Belvoir, VA 22060

US Army Resch. Dev. & Stdzn GP-CP
National Defence Headquarters
Ottawa, Ontario, Canada K1A 0K1

Commander
US Army Communications R&D Command
ATTN: DRDCO-COM-RM-L
(Dr. Felix Schwing)
Fort Monmouth, NJ 07703

Director
US Army Electronics Technology
and Devices Laboratory
ATTN: DELET-L (Dr. E.T. Hunter)
Fort Monmouth, NJ 07703

Director
US Army Electronics R&D Command
Night Vision & Electro-Optics Labs.
ATTN: Dr. Randy Longshore
Fort Belvoir, VA 22060

Commander
US Army Research Office
ATTN: DRXRO-EL (Dr. James Nicks)
P.O. Box 12211
Research Triangle Park, NC 27709

Director
US Army Communications R&D Command
Night Vision & Electro-Optics Labs.
ATTN: Dr. William E.
Fort Belvoir, VA 22060

Commander
Harry Diamond Laboratories
ATTN: DELMD-RJ-A (Mr. J. Salerno)
2800 Powder Mill Road
Adelphi, MD 20783

Director
US Army Electronics R&D Command
Night Vision & Electro-Optics Labs.
ATTN: DELNV-IRTD (Dr. John Pollard)
Fort Belvoir, VA 22060

Commander
US Army Research Office
ATTN: DRXRO-EL
(Dr. William A. Sander)
P.O. Box 12211
Research Triangle Park, NC 27709

Director
US Army Electronics Technology
and Devices Laboratory
ATTN: DELET-ES (Dr. A. Tauber)
Fort Monmouth, NJ 07703

Director
Division of Neuropsychiatry
Walter Reed Army Institute of Res.
Washington, DC 20012

Commander
USA ARRADCOM
ATTN: DRDAR-SCF-CC (Dr. N. Coleman)
Dover, NJ 07801

Director
US Army Signals Warfare Lab
ATTN: DELSW-OS
Vint Hill Farms Station
Warrenton, VA 22186

Director
US Army Electronics Technology
and Devices Laboratory
ATTN: DELET-ED (Dr. E.H. Poindexter)
Fort Monmouth, NJ 07703

Commander
US Army Research & Standardization
Group (Europe)
ATTN: Dr. F. Rothwarf
Box 45
FPO NY 09510

US Army Research Office
ATTN: Library (3 copies)
P.O. Box 12211
Research Triangle Park, NC 27709

Commander
US Army Communications R&D Command
ATTN: DRDCC-COM-RM (Mr. I. Kullback)
Fort Monmouth, NJ 07703

Dr. Sidney Ross
RCA GSD Engineering
Cherry Hill, NJ 08358

DEPARTMENT OF THE AIR FORCE

Mr. Clarence D. Turner
AFOSR/ES
Hanscom AFB, MA 01731

Dr. Carl E. Saur
AFWL (NTVEE)
Kirtland AFB, NM 87117

Dr. E. Champagne
AFWAL/AADC
Wright-Patterson AFB, OH 45433

Dr. R. P. Dolan
RADC/ESR
Hanscom AFB, MA 01731

Mr. W. Edwards, Chief
AFWAL/AAD
Wright-Patterson AFB, OH 45433

Professor R.E. Fontana
Head Department of Electrical Eng.
AFIT/ENG
Wright-Patterson AFB, OH 45433

Dr. Alan Garscadden
AFWAPL/POOC-3
Air Force Aeronautical Labs
Wright-Patterson AFB, OH 45433

USAF European Office of Aerospace
Research and Development
ATTN: Captain A.E. Mardigian
Box 14, FPO, New York 09510

Mr. Murray Kesselman (ISCA)
Rome Air Development Center
Griffiss AFB, NY 13441

Chief, Electronic Research Branch
AFWAL/AADR
Wright-Patterson AFB, OH 45433

Dr. Edward Altshuler
RADC/EEP
Hanscom AFB, MA 01731

Mr. John Mott-Smith (TOIT)
HO ESD (AFSC), Stop 36
Hanscom AFB, MA 01731

Dr. Richard Picard
RADC/ETSL
Hanscom AFB, MA 01731

Dr. J. Ryles
Chief Scientist
AFWAL/AS
Wright-Patterson AFB, OH 45433

Dr. Allan Schell
RADC/EE
Hanscom AFB, MA 01731

Mr. H.E. Webb, Jr. (ISCP)
Rome Air Development Center
Griffiss AFB, NY 13441

Dr. Howard Schlossberg
Air Force Office of Scientific Res.
(AFSC) AFOSR/NP
Bolling AFB, DC 20332

Dr. J. Bram
AFOSR/NV
Bolling AFB, DC 20332

Major Clarence Gardner
Air Force Office of Scientific Res.
(AFSC) AFOSR/NE
Bolling AFB, DC 20332

DEPARTMENT OF THE NAVY

Director
Office of Naval Research Branch
666 Summer Street
Boston, MA 02210

Commanding Officer
Office of Naval Research
Western Regional Office
1030 East Green Street
Pasadena, CA 91106

Naval Surface Weapons Center
ATTN: Technical Library
Code DX-11
Dahlgren, VA 22448

Dr. J. H. Mills, Jr.
Naval Surface Weapons Center
Code DF
Dahlgren, VA 22448

Dr. Gernot M. R. Winkler
Director, Time Service
US Naval Observatory
Massachusetts Avenue
34th St., NW
Washington, DC 20390

G. Gould
Technical Director
Naval Coastal Systems Center
Panama City, FL 32407

Naval Air Development Center
ATTN: Code - 301 G. Eck
Technical Library
Warminster, PA 18974

R. S. Alligier, Jr. B-209
Naval Surface Weapons Center
Silver Spring, MD 20910

Office of Naval Research
800 North Quinn Street
ATTN: Code 150
Arlington, VA 22217

Office of Naval Research
800 North Quinn Street
ATTN: Code 417
Arlington, VA 22217

Office of Naval Research
800 North Quinn Street
ATTN: Code 431
Arlington, VA 22217

Commanding Officer Naval Res. Lab.
ATTN: Dr. S. Teitler, Code 145
Washington, DC 20375

Commanding Officer Naval Res. Lab.
ATTN: Mrs. D. Erieh, Code 147
Washington, DC 20375

Commanding Officer Naval Res. Lab.
ATTN: Mrs. J. Erieh, Code 148
Washington, DC 20375

AD-A100 755

COLUMBIA RADIATION LAB NEW YORK

F/G 20/14

RESEARCH INVESTIGATION DIRECTED TOWARD EXTENDING THE USEFUL RAN--ETC(U)

MAR 81 6 W FLYNN

DAAG29-79-C-0079

NL

UNCLASSIFIED

3 OF 3

40 2
100755



END
DATE
FILMED
7-81
DTIC

Commanding Officer Naval Res. Lab.
ATTN: Mr. J. E. Davel, Code 5210
Washington, DC 20375

Commanding Officer
Naval Research Laboratory
ATTN: Mr. B. D. McCombe, Code 4800
Washington, DC 20375

Commanding Officer
Naval Research Laboratory
ATTN: Mr. J. E. Shore, Code 7503
Washington, DC 20375

Commanding Officer
Naval Research Laboratory
ATTN: Mr. J. R. Davis, Code 7550
Washington, DC 20375

Commanding Officer
Naval Research Laboratory
ATTN: Mr. W. L. Faust, Code 6510
Washington, DC 20375

Commanding Officer
Naval Research Laboratory
ATTN: Mr. J. D. Brown, Code 4701
Washington, DC 20375

Technical Director
Naval Underwater Systems Center
New London, CT 06320

Naval Research Laboratory
Underwater Sound Ref. Detachment
Technical Library
P.O. Box 8337
Orlando, FL 32856

Mr. J. C. French
National Bureau of Standards
Electronics Technology Division
Washington, DC 20234

Naval Ocean Systems Center
ATTN: Mr. P. C. Fletcher, Code 015
San Diego, CA 92152

Naval Ocean Systems Center
ATTN: Mr. W. J. Dejka, Code 8302
San Diego, CA 92152

Naval Ocean Systems Center
ATTN: Mr. H. M. Wieder, Code 922
San Diego, CA 92152

Naval Ocean Systems Center
ATTN: Mr. J. H. Richter, Code 532
San Diego, CA 92152

Naval Weapons Center
ATTN: Dr. G. H. Winkler, Code 381
China Lake, CA 93553

Naval Weapons Center
ATTN: Mr. M. H. Ritchie, Code 5515
China Lake, CA 93553

Dr. Donald E. Kirk
Professor & Chairman, Electronic Eng.
Soc-15
Naval Postgraduate School
Monterey, CA 93940

Dr. D. F. Fence
Naval Underwater Systems Center
New London Laboratory
ATTN: Code 34
New London, CT 06320

Dr. William C. Mehuron
Office of Research, Development,
Test & Evaluation
NOP-987
The Pentagon, Room 5D760
Washington, DC 20350

Dr. A. L. Siatkosky
Headquarters, U.S. Marine Corps.
ATTN: Code RD-1
Washington, DC 20380

Dr. H. J. Mueller
Naval Air Systems Command
AIR-310
Washington, DC 20361

Mr. Reeve D. Peterson
Naval Electronics Systems Command
NC #1
ATTN: Code 03R
2511 Jefferson Davis Highway
Arlington, VA 20360

Naval Sea Systems Command
NC #3
ATTN: Mr. J. H. Huth, Code 03C
2531 Jefferson Davis Highway
Washington, DC 20362

David Taylor Naval Ship Research and
Development Center
ATTN: Technical Library, Code 522.1
Bethesda, MD 20084

David Taylor Naval Ship Research and
Development Center
ATTN: Mr. G. H. Gleissner, Code 18
Bethesda, MD 20084

Mr. Martin Mandelberg
Coast Guard R&D Center
Avery Point
Groton, CT 06340

Naval Underwater Systems Center
New London Laboratory
ATTN: 101E (Dr. Edward S. Eby)
New London, CT 06320

OTHER GOVERNMENT AGENCIES

Dr. Ronald E. Nagarise
Director
Division of Materials Research
National Science Foundation
1800 G Street
Washington, DC 20550

Dr. Stephen Kahne
Director-ECSE
Devices and Waves Program
National Science Foundation
1800 G Street
Washington, DC 20550

Los Alamos Scientific Lab.
ATTN: Main Library
P.O. Box 1663
Los Alamos, NM 87545

Dr. Dean Mitchell
Program Director, Solid-State Physics
Division of Materials Research
National Science Foundation
1800 G Street
Washington, DC 20550

M. Lane Thornton
Deputy Director Institute for
Computer Sciences and Technology
National Bureau of Standards
Washington, DC 20234

Mr. Frederick F. Ponnelle
Deputy Director
Research and Technology Division
Office of Aeronautics and Space Techn.
NASA
Washington, DC 20546

Judson C. French, Director
Center for Electronics and
Electrical Engineering
A357 Technology Building
National Bureau of Standards
Washington, DC 20234

Dr. Jay Harris
Office of the Dean
School of Engineering
San Diego State University
San Diego, CA 92182

Mr. Harvey Ostrow
Chief, Sensing and Detection
Information Systems Office, Code R51
NASA HQ
600 Independence Avenue, SW
Washington, DC 20546

Mr. John Sos
Assistant Chief, Information
Processing Division
Code 560
Goddard Space Flight Center
Greenbelt, MD 20771

Mr. Charles Huxson
Aerospac Technologist
Langley Research Center
Hampton, VA 23061

Mr. John Gould
Chief, Design Techniques Branch
George C. Marshall Space Flight Ctr.
Marshall Space Flight Center, AL 35812

NON-GOVERNMENT AGENCIES

Director
Columbia Radiation Laboratory
Columbia University
538 West 120th Street
New York, NY 10027

Director
Coordinated Science Laboratory
University of Illinois
Urbana, IL 61801

Dean
Institute for Materials Research
Harvard University
Science Hall
Cambridge, MA 02138

Director
Electronics Research Center
University of Texas
P.O. Box 7728
Austin, TX 78712

Director
Electronics Research Laboratory
University of California
Berkeley, CA 94720

Director
Electronics Sciences Laboratory
University of Southern California
Los Angeles, CA 90007

Director
Microwave Research Institute
Polytechnic Institute of New York
333 Jay Street
Brooklyn, NY 11201

Director
Research Laboratory of Electronics
Massachusetts Institute of Technology
Cambridge, MA 02139

Director
Stanford Electronics Laboratory
Stanford University
Stanford, CA 94305

Director
Edward L. Ginzton Laboratory
Stanford University
Stanford, CA 94305

Dr. Lester Eastman
School of Electrical Engineering
Cornell University
316 Phillips Hall
Ithaca, NY 14850

Dr. Carlton Walter
ElectroScience Laboratory
The Ohio State University
Columbus, OH 43212

Dr. Richard Sacks
Department of Electrical Eng.
Texas Tech University
Lubbock, TX 79409

Dr. Roy Gould
Mail Station 104-44
California Institute of Technology
Pasadena, CA 91125

Director
School of Electrical Engineering
Georgia Institute of Technology
Atlanta, GA 30332

Dr. John F. Walkup
Department of Electrical Engineering
Texas Tech University
Lubbock, TX 79409

Mrs. Renate D'Arcangelo
Editorial Office
250 Aiken Computation Laboratory
Division of Applied Sciences
31 Oxford Street
Cambridge, MA 02138

EN
DAT